MEMBRANE SEPARATION OF CHIRAL PHARMACEUTICAL PRODUCTS

ZHOU ZHENGZHONG
(*B. CHEM. ENG. (Hons) NUS***)**

A THESIS SUBMITTED

FOR THE DEGREE OF DOCTOR OF PHILOSOPHY

IN CHEMICAL AND PHARMACEUTICAL ENGINEERING

SINGAPORE-MIT ALLIANCE

NATIONAL UNIVERSITY OF SINGAPORE

2011

Acknowledgement

I would like to take this opportunity to thank all those people who have helped me in my work and life, not limited to the four years of PhD studies. I wish to express my gratitude to my family members especially my parents for their support and understanding; and my heartfelt thanks to my supervisors Prof. Chung and Prof. Hatton for their mentoring. They are always approachable and give valuable feedbacks whenever I have questions; also, their working ethics, positive spirit and persistent attitude, etc. influenced and shaped me to become a qualified researcher.

I would also like to thank Dr. Xiao Youchang and Dr. Cheng Jiuhua for teaching me the necessary experimental and sharing their working experience, Dr. Li Yi, Dr. Yang Qian and Dr. Widjojo for the fruitful discussions, and Dr. Teoh May May for guiding me the simulation. Thanks are also due to Prof. Donald Paul and Prof. Andrew Zydney for their suggestions and comments on my work, and Prof. Saif Khan and his research group for help on micro fluid study. I also wish to thank all my group members who have helped me in one way or another and made my PhD study an enjoyable journey.

I also want to thank Singapore-MIT Alliance for giving me the opportunity to pursue my PhD and providing the scholarship and funding for the study; and the Department of Chemical and Biomolecular Engineering for the fundamental studies and experimental facilities. Besides, thanks are also due to the NUS (Grant No.R-279-000-249-646) for the funding.

Last but not least, I also wish to thank Ms. Chng Mei Lin, Ms. Lin Huey Yi, Ms. Alyssa Tay, Ms Vivian Tan and all other lab technicians for their helps on lab matters such as safety management, equipment usage and consumable purchasing, etc.

Table of contents

Summary

The production of enantiomerically pure drugs is crucial to the current pharmaceutical industry due to the contrasting pharmacological effects associated with the different enantiomeric forms of a drug. Apart from the more complicated direct synthesis, various resolution techniques are also developed, among which the membrane process, due to its advantages such as lower energy consumption and higher productivity, is chosen to be investigated in depth by fabricating superior membrane and designing innovative membrane systems in this study.

The first part of this study was inspired by and was actually a continuation of our previous publications by Dr. Xiao et al who studied the effects of membrane pore size on chiral separation using the beta-cyclodextrin (β-CD) and acetylated β-CD functionalized cellulose membranes. To have a more complete picture of chiral separation, we investigated here the effects of spacer arm lengths of the β-CD by reacting the β-CD with ethylenediamine (EDA), diaminopropane (PDA) and diaminobutane (BDA) before functionalization. The enantioselectivity, in racemic tryptophan resolution, increased with decreasing spacer arm length, i.e. $\alpha_{BDA\text{-}\beta\text{-}CD} < \alpha_{PDA\text{-}\beta\text{-}CD} < \alpha_{EDA\text{-}\beta\text{-}CD}$, while the highest selectivity of 1.20 was obtained when a mixture of chiral selectors were grafted to the membranes. Further improvement of enantioselectivity, to ~1.3-1.5, was realized by substituting the hydroxyl groups on the aminated cyclodextrins with benzoate groups. The effects of membrane preparation and functionalization protocol, chiral separation operating conditions and more importantly, different driving forces were investigated in the subsequent studies using the chitosan functionalized cellulose acetate membranes. The tryptophan enantiomeric excesses obtained using the same membrane in

concentration gradient, hydraulic pressure and electric field driven processes are 94%, 66% and -19%, respectively. This reverse in the enantioselectivity in the electric driven process was also observed in phenylalanine resolution and was mainly attributed to the orienting force exerted by the electric field and the tryptophan complexes formed with copper ions generated via electrolysis.

Besides the membrane itself, a novel membrane separation process is also critical to better resolution. A membrane process named selective permeation enhancement (SPE) was developed by injecting human serum albumin (HSA), which binds selectively to L-tryptophan, in the strip chamber of a dialysis permeation cell, resulting in a more enhanced permeation flux of L-tryptophan than that of D-tryptophan. Furthermore, the separation efficiency was enhanced by introducing a racemic mixture into the strip solution that decreased the flux of the more weakly bound D-tryptophan; and by integrating the SPE with affinity dialysis, the highest enantioselectivity of ~9.7 was obtained. Another membrane system that integrates stereoselective affinity dialysis and ion-exchange membrane partitioned free flow isoelectric focusing (FFIEF) was also studied. And it showed superior optical resolution efficiency over the normal affinity dialysis (AD) and affinity ultrafiltration (AUF) membrane processes under similar experimental conditions, i.e. by using the same sulfonated polyetherketone (SPEK) membranes and identical human serum albumin (HSA) to tryptophan ratio of 0.75. The separation factor is increased with increasing protein concentration while the permeation flux can be enhanced by increasing the operating current.

List of tables

List of figures

List of Abbreviations

AD	Affinity dialysis
API	Active Pharmaceutical Ingredients
AUF	Affinity ultrafiltration
BDA	Diaminobutane
BSA	Bovine serum albumin
EDA	Ethylenediamine
CA	Cellulose acetate
CE	Capillary Electrophoresis
CS	Chitosan
DS	Degree of substitution /sulfonation
FDA	Food and Drug Administration
FFIEF	Free flow isoelectric focusing
HPLC	High Performance Liquid Chromatography
HSA	Human serum albumin
IEC	Ion exchange capacity
IPA	Isopropanol
MWCO	Molecular Weight Cut-off
NMP	n-methyl pyrrolidone
PDA	Diaminopropane
Phe	phenylalanine
SP	Separation factor
SPE	Selective permeation enhancement
SPEK	Sulfonated polyetherketone
Trp	tryptophan
Ts -	P-toluenesulfonyl –
β-CD	β-Cyclodextrin

List of Symbols

A	Membrane area
C	Chemical concentration
d	Membrane thickness
d_p	Pore size
ee%	Enantiomeric excess
F	Feed
G	Gradient of concentration vs time graph
I	Current
J, j	Flux
k	Association constant
k’	Dissociation constant
K	Equilibrium constant
M	Molecular weight
P	Permeability coefficient
Q	heat
R	Solute rejection
r_s	Solute radius
t	time
V	Volume of permeation cell chamber
W	mass
α	Enantioselectivity
σ_p	Standard deviation
λ_p	conductivity
μ	mobility
ΔG	Binding energy
ΔΔG	Difference in binding energy

Subscripts

D	D-tryptophan
F	Feed
L	L-tryptophan
P	Permeate
1,2,3	Chamber numbers
cs	Chitosan

Chapter 1. Introduction & motivation

1.1. Chirality

An object is termed chiral if it cannot be superimposed onto its mirror image. For example, human hands are the most naturally observed chiral object as shown in Figure 1.1 [1]. In molecular level, a pair of chiral molecules is called enantiomers. Normally, the structure of an enantiomer contains at least one chiral center which is an atom bonding to four different neighboring groups. The physical and chemical properties of enantiomers are identical except in reactions with other chiral compounds. Different enantiomers may have different taste and odor because of the receptors in human body also contains chiral molecules which behave differently towards different enantiomers.

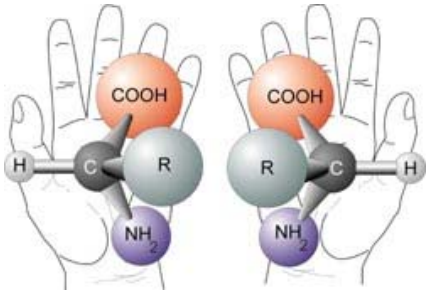

Figure 1.1. Illustration of chirality

1.2. Chiral pharmaceuticals

Most of the biochemical processes in living organism involve stereochemistry since the building units of life, such amino acids, proteins and enzymes are chiral in nature and only certain enantiomer can exist. For example, there are only L-amino acids and D-sugars in human body.

As most of the active pharmaceutical ingredients (API) in drugs are also chiral, their enantiomers would therefore interact with biological macromolecules, which are

stereoselective, differently, resulting in different pharmacological effect. Normally only one enantiomer is active while the other being either inactive or even a toxin. For example, ibuprofen is an anti-inflammatory drug used for the treatment of arthritis and fever, however, its R-form is teratogenic especially in first trimester. In view of this, the US Food and Drug (FDA) administration has required the detailed analysis of both enantiomers before the drug can be approved [2]. Hence it is important to develop single enantiomer drugs.

1.3. Current technologies for chiral separation

1.3.1. Need for chiral separation [2]

It is clear that, from the above discussion, the production of single enantiomer drugs is necessary. And in fact, more and more drugs have been marketed as single enantiomeric form in recent year. According to the Chiral Chemicals Report, the chiral chemical market is expected to grow at 13.57% compounded annually from 2005 to 2012 [3].

There are basically two approaches: one is the asymmetric synthesis by stereoselective processes which are usually catalyzed by metal complexes [4] and enzymes [5-7], and the second is chiral separation from the racemic mixtures via techniques such as crystallization, high pressure liquid chromatography (HPLC), capillary electrophoresis (CE) and membrane.

The asymmetric synthesis can be the most elegant if it can produce above 99% enantiomeric pure compounds in a cost effective manner. However, the catalysts such as Rhodium, Ruthenium (II) complexes [4] and enzymes [6] are expensive; moreover, the processes are usually complex and sometimes require extreme conditions such as -78 ºC

[8]. Most importantly, the products from these processes are not enantiomerically pure; there are numerous examples in the literature that the enantiomeric excesses range from 80% to 99% for most of the synthesized β-amino acids in the review [9]. Thus, a second step of chiral separation may be still required at the current stage.

1.3.2. Preferential crystallization [10, 11]

This is a crystallization process done by seeding a saturated racemic solution with a pure crystal of one enantiomer. The enantiomer can precipitate out and grow on the seed with the same chirality and enantiomer crystal of high purity can be obtained by this process; however, there are a few limitations. First, a pure seed must be available to start the crystallization; other separation techniques such as HPLC and CE may be needed to get the pure seed. Second, the racemic compound must be a conglomerate i.e. the two enantiomers of which show two different crystal structures, which is not common in nature (less than 20%) [12]. Therefore this process cannot be generally applied for chiral separation.

1.3.3. High Performance Liquid Chromatography (HPLC)

HPLC is the most widely applied technique in enantiomer resolution. Separation is achieved by the chiral stationary phases (CSP) which consist of chiral recognizing compounds that interact and form transient diastereomeric complexes with enantiomers differently. A three point interaction rule must be fulfilled for separation: there must be at least three simultaneous interactions between one enantiomer and the CSP, and the total interaction energies of the two enantiomers must be distinct. The type of interaction can

be either attractive or repulsive, including hydrogen bonding, ionic, dipole and steric interactions depending on the functional groups available.

In analytical application, HPLC can resolute enantiomers with high purity in relatively short time [13]. However, it is usually a batch process and not suitable for large scale production, where continuous processes are preferred. Besides, HPLC is not an economical process either, due to the costly chromatography column and the packing materials, the consumption of a large quantity of solvent, and more importantly the energy requirement for maintaining the high pressure.

Moving bed chromatography is a special continuous chromatography process, capable of separating larger quantity of chiral chemicals. Instead of eluting the solutes from one outlet, the chromatography column is moving in a reverse direction to the solvent flow while the feed is introduced in the column body, such that the products can be collected at two distinct outlets continuously. It is able to achieve higher yield (10% more), higher productivity (5 to 10 fold) and lower solvent consumption (5 to 10 fold) than a batch chromatography process [14, 15], making a more cost effective. The difficulties lie in the system design and control as much more system and operating parameters need to be optimized; furthermore, a point to note is that this system is not suitable for multi-component separation, although it may not be detrimental in our application here where a chiral system is usually binary.

1.3.4. Capillary Electrophoresis (CE)

This is a powerful technique for enantiomer resolution in analytical application developed in last decade. The working principle of CE is based on the difference in

mobility of the analytes in the capillary under a strong electric field. The separation principle is similar to that of HPLC but with different driving forces. A chiral selector, which interacts with enantiomers and drags the enantiomers to a different extent, is either added into the background electrolyte [16] or coated on the inner wall of the capillary [17]; the two enantiomers hence experiences different resistance due to their interactions with the chiral selector and elute out the capillary at different time, in such a way chiral separation is achieved by applying a suitable voltage.

CE is slowly replacing HPLC in analytical application mainly due to its higher flexibility, lower consumption of solvent and lower operating cost. However, it is not practical for preparative applications due to its low throughput, the scale of which is in the μl range only.

1.3.5. Membrane separation

Membrane technology is, in principle, particularly suited for large scale production of enantiomers as it presents various attractive features: continuous operation, easy to scale up and low energy consumption. A membrane can be made of polymers, inorganic materials or even liquid. There are mainly two types of separation mode depending on whether the chiral selector is immobilized in the membrane, making a chiral selective membrane, or dissolved in solution. Chiral selectors in membranes include cyclodextrins [18], crown ethers [19], proteins [20] and even recognition sites formed by molecular imprinting [21]. A chiral selective membrane can facilitate or slow down the transport of one enantiomer, thus separate the enantiomers in different proportion. With a non-chiral selective membrane, the chiral selectors, normally large molecules such as proteins and

enzymes, are added into the racemic feed solution and form complexes with one enantiomer which are then retained by the membrane by size exclusion [22, 23].

The amount of enantiomers processed by membrane separation is much larger than HPLC and CE. For example, Zydney and Romero performed chiral separation of 80ml of feed solution using a membrane area of only 5 cm^2 within a few hours [24], while Morbidelli et al used 8 columns of the size 12.5×1.0 cm to produce 0.72 g/day of α-ionone and 0.22 g/day of α-damascone [25] in a moving bed HPLC. Besides, the energy required in a membrane process is also lower. While the pressure in HPLC easily reaches above 100 bars, an pressure driving force less than 10 bars are sufficient in an ultra-filtration membrane process for chiral separation, and even zero transmembrane pressure for affinity dialysis membrane process. Also, another advantage of the membrane process is it can be easily scaled up by increasing the membrane area by inserting more membrane fibers or adding parallel membrane modules, etc.

However, the main drawback of this technology is its relatively lower purity. The above mentioned membrane technique [24] can give a purity of 95% by a two stage process, which is among the highest in membrane research, while the usual separation factor is less than 10 [20]; however, the HPLC can produce purity of 99.9% and 99.2% for S and R enantiomers of α-ionone for instance.

The comparison of the current technologies discussed is summarized in Table 1.1. An ideal process should have high throughput, high purity and low cost with a simple operation system. The asymmetric synthesis is more expensive and complex. The preferential crystallization method has only limited application, though it can produce large amount of pure product with low cost; separation methods are still needed for

chemical compounds other than conglomerates. Capillary electrophoresis, although shows high resolution power on enantiomers, is mainly used for analytical purpose due to its extremely low throughput. HPLC is the separation technology currently employed in industry due to its high purity, and the issue of low throughput is being tackled by moving bed technique; however, the system becomes more complex and its high cost is not reduced. The membrane technology has the attractive features such as high throughput, lower energy cost, simple operation and easily scalable, but its selectivity remains the major challenge currently to really compete with HPLC.

	Advantages	Disadvantages
Membrane separation	High throughput Energy saving Continuous process Easily scale up	Fouling; Challenging selectivity (increased by new chiral selectors, cascade, new model design)
Asymmetric synthesis	One stop process; chiral separation may not be required	Expensive and complex process
Preferential crystallization	Low cost, confirmed purity	Only applicable to conglomerates which is not common in drugs
Chromatography	High purity, reliable	Low throughput, expensive stationary phase and operation cost
Capillary electrophoresis	High flexibility low consumption of chemicals and solvents	Low throughput

Table 1.1. Comparison of advantages and disadvantages of chiral separation technologies

1.4. Project objectives & thesis organization

From the above discussion, we conclude that the membrane separation system can be the most suitable technology for large scale production of pure enantiomer pharmaceuticals only if its selectivity can be greatly improved and comparable to that of HPLC. Since

membrane chiral separation is still an emerging field, there are more areas to be explored and improved in searching for the solution of higher separation performance. Possible ways to improve chiral selectivity are: 1, synthesizing more specific and powerful chiral selectors of enhanced intrinsic selectivity; 2, optimizing the fabrication and functionalization of chiral selective membranes; 3, novel membrane system design. Hence, the objectives of this study are to achieve the improved separation performance by employing the above approaches and investigating their effects. And through this study, we have not only developed the new chiral selective membranes and membrane systems for enantiomer resolution, but gained more in-depth knowledge of the membrane chiral separation mechanisms and characteristics, which are significant contributions to the literature as well.

The dissertation is organized in the following manner; the Chapter 2 introduces the membrane preparation, chiral separation with various membrane systems and calculations for separation efficiency analysis.

Chapter 3-6 show the in depth study of chiral separation using various membrane systems. The chapter 3 is a study utilizing approaches 1 and 2. We have shown that by carefully designed chemical modification of the chiral selector β-cyclodextrin, its intrinsic selectivity can be increased, so is the overall membrane selectivity; also, the membrane structure design plays an important role: the spacer arm between the chiral selector and the membrane surface affects the chiral selectivity.

Chapter 4 and 5 present two cases on innovative system design and utilization for chiral separation via approach 3. The systems developed in these two studies (Selective Permeation Enhancement and Free Flow Iso-Electric Focusing) both show enhanced

chiral separation performance than normal membrane processes such as affinity ultra-filtration and dialysis, under similar experimental conditions. Besides, we have also designed and fabricated new membranes for the system described in chapter 5.

Chapter 6 employed the approaches 2 and 3: we have designed both a chiral selective membrane and the separation system, which is modified from the system developed in chapter 5. We have shown the interesting effects of the nature of driving forces on enantiomeric separation as well.

The thesis is then concluded in chapter 7 and a list of publication and presentation is attached in the appendix.

Chapter 2. Theoretical background

2.1. Membrane preparation by phase inversion

Phase inversion in the membrane formation process is a process by which a homogeneous polymer solution separates into two liquid phase (polymer rich and polymer lean) caused by a quenching media. The polymer rich phase then starts to be solidified, resulting in the formation of a solid polymer matrix [26]. Phase inversion can be induced by different techniques including solvent evaporation, thermal precipitation and immersion precipitation, etc. The membrane prepared in this study used immersion precipitation as the induce technique. It is done by casting a thin film on a substrate and then immersing the film into a coagulant bath containing a nonsolvent (a liquid that is miscible with the solvent of the dope but not able to dissolve the polymer) [27, 28].

2.2. Chiral separation with membrane systems

2.2.1. Three point contact model

The enantio-recognition is described by a three point contact model: the enantiomers should have at least three distinct interactions such as hydrogen bonding, hydrophobic/ hydrophilic interactions, steric hindrance, dipole-dipole interactions, etc. The strengths of each bonding should be different, and the total energies of interaction between the two enantiomers must be different for a good resolution. A simple schematic diagram is shown below: for a pair of enantiomers, we assume that the numbers 1-3 represent three distinct point of interaction sites which are not in the same plane, i.e. the two structures are not super imposable by flipping the other over, then only the molecule at the left can fit well to all the interaction sites of the selector on top. As a result, the left molecule

binds more strongly to the selector and absorbed, while the other molecule stays in the bulk; chiral separation is thus achieved.

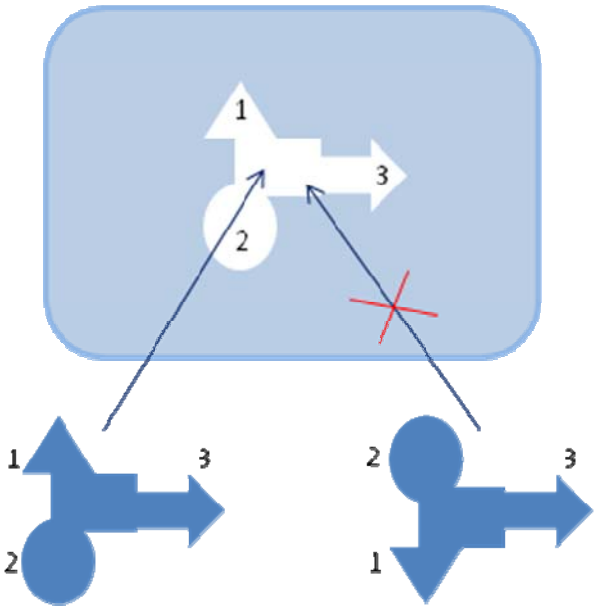

Figure 2.1. The schematic of a three point contact model.

Another special kind of interaction model is in situation where the chiral molecules are experiencing external field such as electric or magnetic field. A schematic is shown below for clear representation: if a pair of chiral molecules nearby an interacting surface are under the effect of two fields that are perpendicular to each other (for simplicity, the model works as long as the two field are non-parallel), field E orientates the molecules in a direction such that R_2 points to the right, and field F orientates R_3 to point outside the paper, the R_1 of D-type molecules then points to the interacting surface while the R_1 of the L-type points away, resulting in different bonding energies with the surface and hence chiral selectivity.

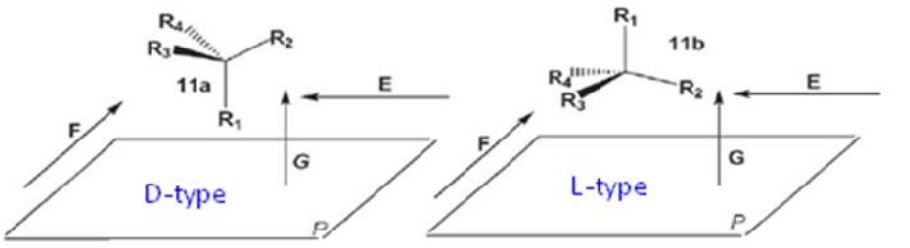

Figure 2.2. The Schematic of chiral recognition in presence of external field [29]

2.2.2. Chiral selector

Chiral selectors are molecules that exhibit different binding strengths towards a pair of enantiomers and they are the key component in a membrane system for chiral separation. The common examples are cyclodextrins and their derivatives [18, 30], proteins [22-23], DNA [31], enzymes [20] and crown ether derivatives [19], etc. In this thesis, the chiral selectors used are β-cyclodextrins, bovine serum albumin and human serum albumin.

Cyclodextrins

Cyclodextrins are a family of naturally occurring, water-soluble oligosaccharides forming a bucket-shaped macrocycle comprised of α-(+)-glucopyranose units. The common forms contain six to eight sugar units and are named α, β, and γ-CD, respectively. Their chiral recognition ability is realized through a three-point contact model: hydrophobic interactions in the CD cavity and hydrogen bonding with two secondary hydroxyl groups at the cavity opening [32]. The intrinsic selectivity of cyclodextrins is relatively low, thus they are often derivatized such that the binding of enantiomers can be more specific due to chemical interaction and steric hindrance.

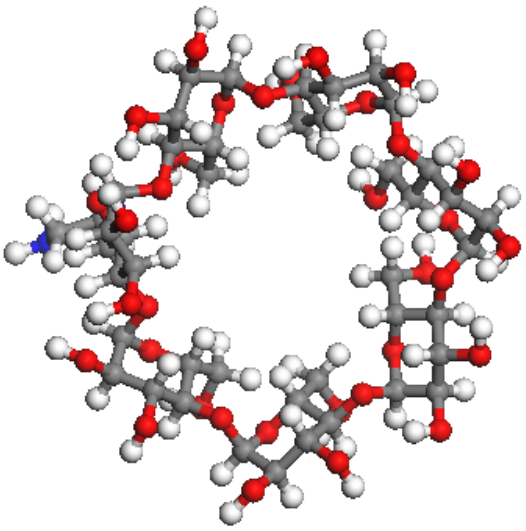

Figure 2.3. A sample of derivatized β-cyclodextrin drawn in material studio

Serum albumins

Serum albumin is the most abundant plamsma protein in mammals; its main functions are maintaining osmotic pressure, transporting hormones, fatty acids and drugs, etc [33]. Its chiral selectivity to L-tryptophan was first discovered more than 50 years ago [34]; the main selectivity is resulted from the predominant binding of L-tryptophan in a highly stereoselective manner towards one site, to which the D-tryptophan has 100-fold less affinity. The selectivity varies with pH and the optimum pH was found to be ~8.5; this implies that the presence of an ionizable group at the protein site can prevent the binding when both this group and the amino acids are similar charged. Also, the protein starts to unfold at lower pH as shown in Fig 2.5 [34-36], thus the binding site loses its stereo-specificity.

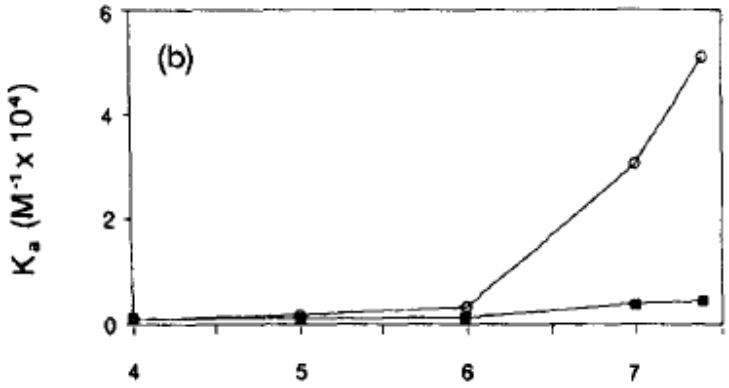

Figure 2.4. The effect of pH on equilibrium constants between human serum albumin and tryptophan enantiomers [35]

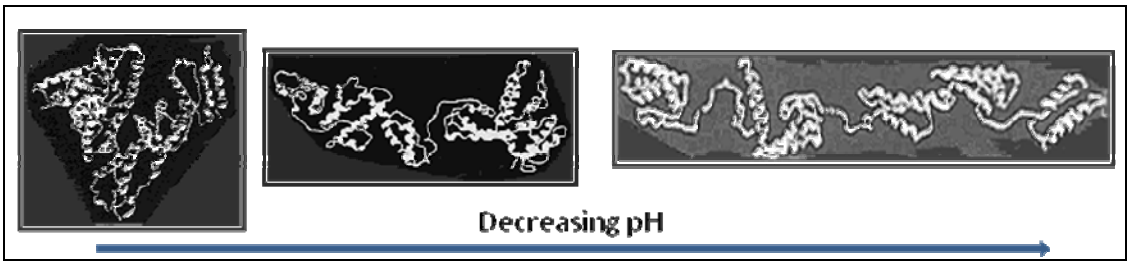

Figure 2.5. The diagram of bovine serum albumin [36]

The enantioselectivity of albumin has also been found to decrease with increasing temperature [35]: both the equilibrium binding constants of L-tryptophan and D-tryptophan decrease while the decrease associated with the L-tryptophan is to a much greater extent.

The most commonly used albumin proteins in chiral separations are bovine serum albumin (BSA) and human serum albumin (HSA), which are used in this study as well. They have similar selectivity (slightly lower for BSA), but with different dimensions: the hydrodynamic radius of BSA is 4-5nm while that of HSA is 7-8nm [37-38].

Compound	Temperature (°C)	Association constant, K_a $(M^{-1})^a$
L-Tryptophan	4	$8.2\ (\pm 0.9)\cdot 10^4$
	10	$7.8\ (\pm 0.8)\cdot 10^4$
	18	$4.7\ (\pm 0.7)\cdot 10^4$
	25	$3.2\ (\pm 0.7)\cdot 10^4$
	37	$2.4\ (\pm 0.3)\cdot 10^4$
	45	$2.0\ (\pm 0.2)\cdot 10^4$
D-Tryptophan	4	$3.8\ (\pm 1.1)\cdot 10^3$
	10	$3.7\ (\pm 1.2)\cdot 10^3$
	18	$3.7\ (\pm 0.3)\cdot 10^3$
	25	$3.7\ (\pm 1.3)\cdot 10^3$
	37	$3.6\ (\pm 1.2)\cdot 10^3$
	45	$3.0\ (\pm 1.0)\cdot 10^3$

Table 2.1. The temperature effect on association constants

2.2.3. Separation mechanisms in membrane systems

2.2.3.1. Chiral separation with chirally selective membranes

Chirally selective membranes can be divided into two classes: membrane made from polymer materials with stereoselective behavior and membranes functionalized with chiral selectors. Polymers such chitosan [39-40] and cellulose acetate butyrate [41] do demonstrate chiral selectivity due to the abidance of chiral centers in the polymer chains. However, not all polymers with chiral centers show chiral selectivity, such as regenerated cellulose and cellulose acetate, etc. It depends on the actual position of the point of bonding /interaction between the polymer and the enantiomers. The detail is still unclear, though the molecular simulations can help better understanding of the mechanism. In this study, the chitosan polymer was treated as a chiral selector and functionalized on cellulose acetate, rather than a polymeric membrane material.

Another kind of chirally selective membrane without chiral selector is made from helical polymeric structures such as polypeptide [42]. These materials mimic the helix of a DNA

structure which is chiral in nature; the separation can be achieved by two ways: first, an enantiomer can only be inserted inside one helix with a fixed rotations while its isomer fit in a helix having the other direction as shown in Figure 2.6; in the second manner, the small enantiomers migrating in-between the polymer chains rotate in a certain direction such that one migrate in the favorite direction and the other in a hindered manner.

Figure 2.6. Schematic diagram of interaction between enantiomers and helical structure (modified from [43]).

The more common chirally selective membranes are prepared by immobilizing various chiral selectors such as cyclodextrins [18] on the membrane surface or/and matrix. The chiral selectivity is solely resulted from the different interaction between the chiral selector and the enantiomers. One special case is the molecular imprinted membranes where the membrane is first prepared by mixing one of the enantiomer in the polymer dope before membrane casting. The enantiomer is then removed from the membrane matrix afterwards and leaves a void space that only fit with this particular enantiomer, which can be treated as a special chiral selector as well. A crosslinker can also be mixed together in the polymer dope prior to membrane preparation to enhance the performance [21].

In the common case, the kinetic mechanism is as shown in Figure 2.7: first, the enantiomer is adsorbed onto the membrane surface and the more preferentially bound

enantiomer is adsorbed in a greater concentration; second, the enantiomers diffuse in the membrane matrix from one surface to the other side, the more preferentially bound enantiomer experiences a stronger resistance force and diffused more slowly than the weakly bound enantiomer; third, the desorption from the other membrane surface also favors the weakly bound enantiomers. And thermodynamically, a greater amount of the more strongly bound enantiomer is absorbed in the membrane, resulting in a higher concentration of the more weakly bound enantiomer permeating through the membrane. Thus, generally, for a membrane with immobilized chiral selectors, the more weakly bound enantiomer is preferentially permeated through the membrane.

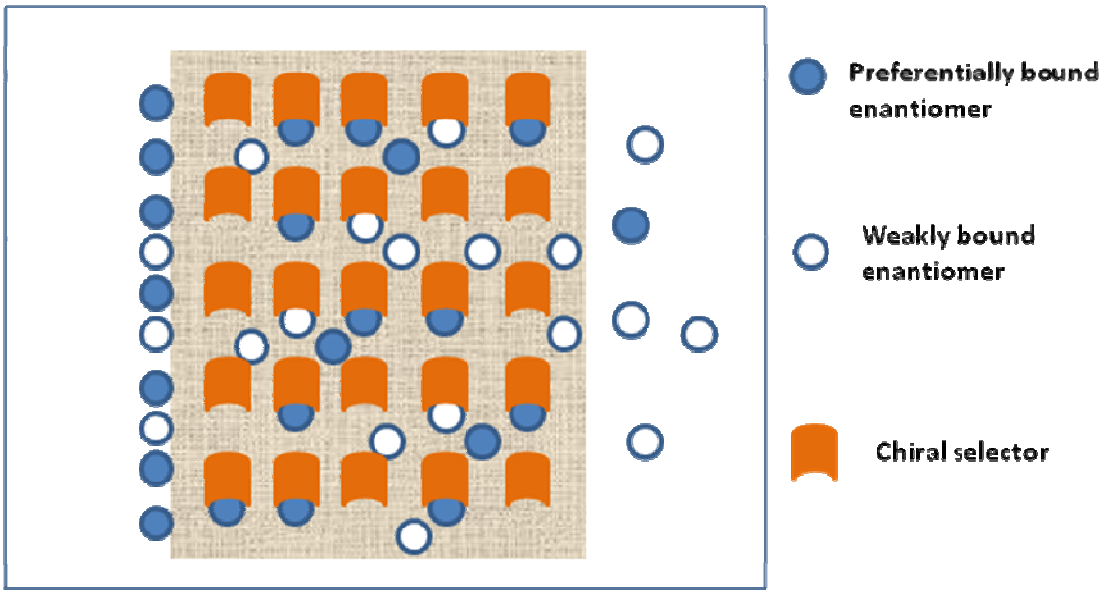

Figure 2.7. A schematic diagram of the transport of chiral molecules in a chiral selective membrane functionalized with chiral selectors.

However, the results will be otherwise if the chiral selector is not fixed in the membrane matrix but loosely bound inside the membrane pores. As shown by Lakshmi et al [20], the more strongly bound enantiomer actually permeated faster since the chiral selector is physically immobilized inside the pores and facilitates the transport of one of the

enantiomers. This is similar to the mechanism in a supported liquid membrane system, and a clear description of which is shown below.

A chiral selective supported liquid membrane system composed of three parts as shown in Figure 2.8, a feed chamber with the racemic mixture, a permeate chamber and a membrane, inside the pores of which containing the chiral selectors in a solvent that is immiscible with that of the feed and permeate. The racemic feed should be insoluble in the solvent in the membrane pores such that the only way for it to permeate through the membrane is by binding with the chiral selectors. In this case, the mechanism is different from the above: the enantiomer amount of enantiomer permeated through the membrane is directly related to the number of enantiomer-chiral selector complexes formed, and the transport resistances of both enantiomers are the same. Therefore, the chiral selector functions as a carrier and facilitates the transport of the more strongly bound enantiomer.

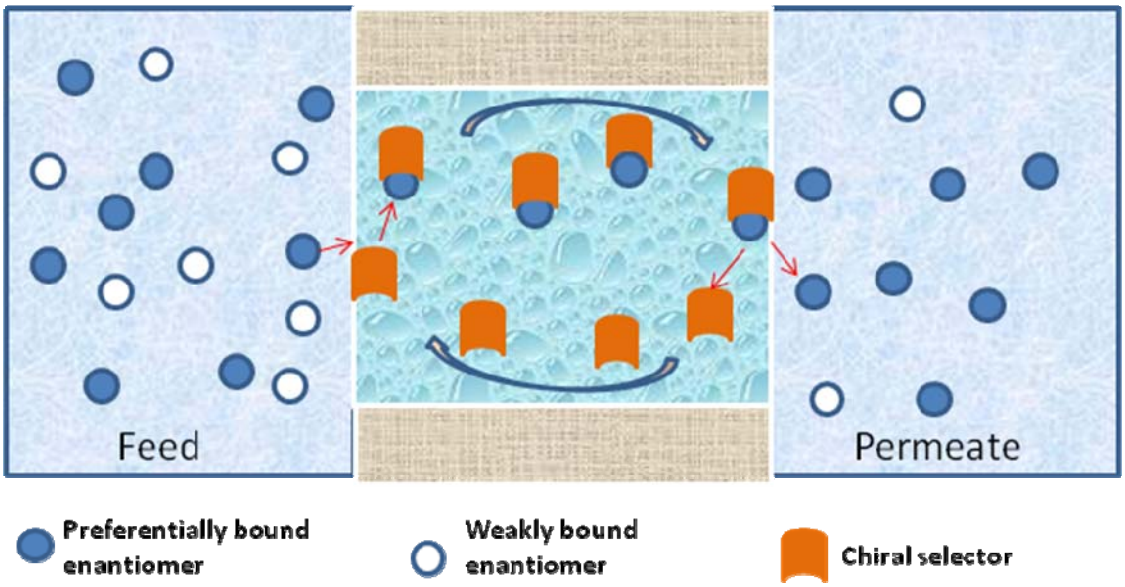

Figure 2.8. The separation mechanism in a supported liquid membrane.

2.2.3.2. Chiral separation with non-chirally selective membranes

In a system with a non-chiral selective membrane, the chiral selectors are usually injected in the feed solution to form complexes with the enantiomers. The complexes and the left-over free enantiomers are then separated with the membrane either by size exclusion or/and charge effect. A common example is the use of serum albumins by Higuchi et al [23] and Zydney et al [22]. And in parts of this study, serum albumins are used as the chiral selector for the resolution of tryptophan in systems with non-chirally selective membranes.

The separation mechanism in this case is straight forward: the more strongly bound enantiomer is retained in the feed solution and the more weakly bound enantiomer is collected in the permeate chamber. The separation efficiency greatly relies on the equilibrium binding constants of the chiral selector.

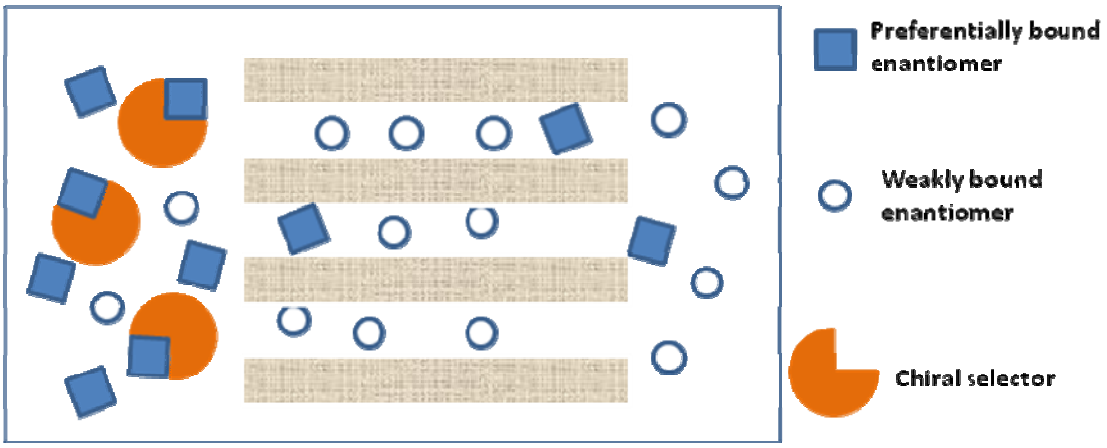

Figure 2.9. schematic diagram of the transport in a system using a non-chirally selective membrane

The separation mechanism is very different in a free flow isoelectric focusing (FFIEF) membrane system, and is discussed separated below.

Free flow isoelectric focusing (FFIEF)

FFIEF is a separation technique making use of the charges on the molecules under different pH environment. A molecule is positively charged in a buffer with pH lower than its pI value and negatively charged in buffer pH higher than its pI. In a series of buffer chambers partitioned by ion exchange membranes, an electric field is generated by setting the anode at the lower pH and the cathode at higher pH side. The positively charged molecules can migrate to the cathode side which is at higher pH, the molecule will become neutral in charge once it reaches the chamber with pH equal to its pI (iso-electric point); it will then stay in the chamber since the electric field has no force acting on a neutral molecule. The mechanism is similar for negatively charged molecules. Thus a mixture of molecules such as proteins (Figure 2.10) with different pIs can be separated efficiently in a FFIEF system [44-46].

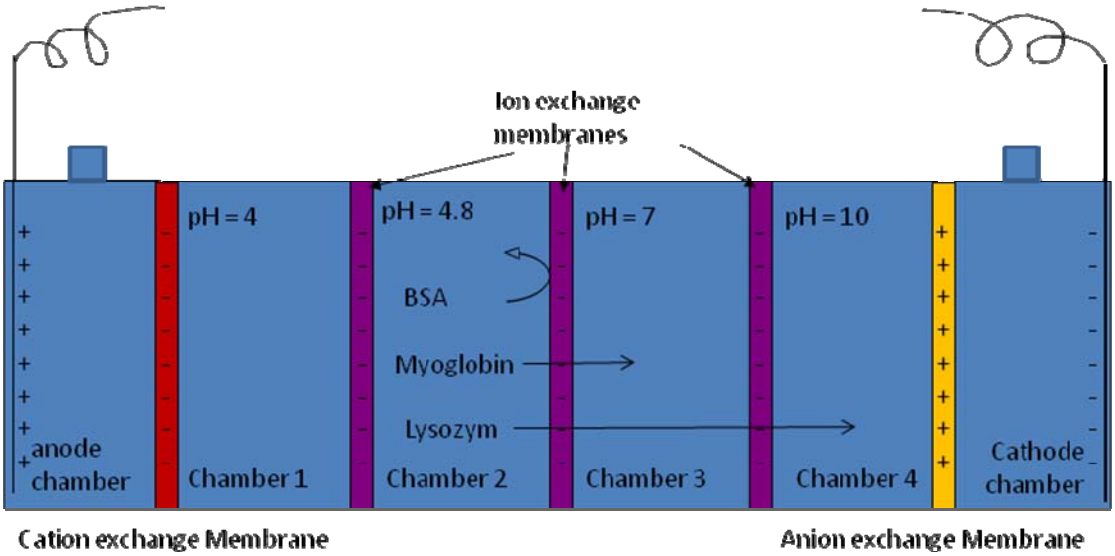

Figure 2.10. The schematic diagram of the application of FFIEF in protein separation.

In a solution with racemic feed and chiral selector, the complexes formed may have slightly different pI values. Although the difference can be as small as ~0.05, a separation using the FFIEF technique is still achieved [47] and high enantiomeric purity is obtained.

The separation mechanism is similar to that in protein separations above; the complexes with different pIs can be isolated in different chambers containing buffer solutions with a pH equivalent to the pI value of the complex.

In this study, a different approach is employed as our auto-titrating system is not able to control the pH in such a small range. The concept of iso-electric focusing is still employed.

2.3. Enantioselectivity of membranes [48]

The enantioselectivity of a membrane can be calculated the ratio between the permeability coefficients of the two enantiomers. The detailed calculations are shown below:

- ✓ A plot of enantiomer concentration in strip solution against time is plotted and the gradient G is calculated
- ✓ The permeability coefficient is then calculated by equation 1, while V is the strip volume, d the membrane thickness, A the membrane area, and C_F and C_P the concentration of feed and strip solutions respectively.

$$P = \frac{G \bullet V \bullet d}{A \bullet (C_F - C_p)} \tag{1}$$

- ✓ The selectivity is then calculated with equation 2, while P_D and P_L are the permeability coefficients of D- and L- enantiomer, respectively.

$$\alpha = \frac{P_D}{P_L} \tag{2}$$

2.4. Enantiomeric excess (ee%) [49]

Enantiomeric excess is defined as the absolute difference between the mole fractions of the enantiomers. The calculation is shown by equation 3, where C_D and C_L are the concentrations of the enantiomers, respectively.

$$ee\% = \frac{C_D - C_L}{C_D + C_L} \times 100\% \quad (3)$$

Chapter 3. Effects of spacer arm length and benzoation on enantioseparation performance of β-cyclodextrin immobilized cellulose membranes

3.1. Introduction

In a previous work published by our group, Xiao and Chung first studied the enantioseparation of tryptophan by immobilization of β-CD onto commercial cellulose membranes [48]; subsequently, Xiao et al. derivatized β-CD through acetylation and achieved enhanced selectivity in the separation of a racemic phenylalanine mixture [30]. A chiral layer model was developed to interpret the observed enantioselectivities. We report here the effects of chiral layer position on enantioselectivity, by comparing the tryptophan enantioselectivity of membranes immobilized with chiral selectors of different spacer arm lengths, and of chiral layer thickness by using membranes grafted with mixtures of spacer arms of different lengths. The spacer arm length is the distance from the membrane surface to the chiral selector, i.e., the length of the diamine linking the β-CDs to the cellulose membranes. The diamines were reacted first with a tossylated β-CD (Ts-β-CD) to form aminated-β-CD and the products are then grafted onto cellulose membranes via reductive amination. The enantioselectivity of the cellulose membranes was tested using a dialysis permeation cell with a concentration gradient as the only driving force.

Although native CDs often exhibit low enantioselectivity, higher selectivity can be realized by further derivatizing the CDs with various chemical moieties [50]. In this study, the hydroxyl groups on the CDs are substituted with benzoate groups which provide increased steric hindrance to the binding of guests within the CD cavity and a reduced

rotational freedom of these guests, in such a way that the enantioselectivity is notably enhanced.

3.2. Experimental

3.2.1. Materials

The cellulose dialysis membranes Spectra/Pro 7, MWCO (molecular weight cut-off) = 1000, membrane thickness = 0.002 inches) were purchased from Spectrum medical Industries, Inc. Beta-cyclodextrin (β-CD) and 6-O-(p-Toluenensulfonyl)-β-cyclodextrin (Ts-β-CD) from Cyclolab, DL-tryptophan from Alfa Aesar, ethylenediamine (EDA), diaminopropane (PDA), diaminobutane (BDA) and p-toluenesulfonyl chloride from Sigma Aldrich, were all reagent grade and used without further purification.

3.2.2. Synthesis of aminated cyclodextrins

The EDA-β-CD, PDA- β-CD and BDA- β-CD were synthesized by a method similar to that reported by Liu et al [51]. One gram of Ts-β-CD was reacted with 6ml of EDA, PDA and BDA respectively at 75°C for 4 hours. The mixture was added drop wise into 30-50ml of cold acetone after the reaction was completed; the precipitates were then dissolved with addition of 50:50 water-methanol mixtures after removal of acetone. This process was repeated 3 times to remove diamine impurities. The final product was obtained by drying the sample in a vacuum oven at 50°C for 3 days.

3.2.3. Immobilization of aminated cyclodextrins onto membranes

The cellulose membranes were immobilized with EDA- β-CD, PDA- β-CD and BDA- β-CD following a method similar to that reported previously by Xiao and Chung [48]. Before chemical modification, the membranes were first soaked in de-ionized water for 2 hours to remove residual storage chemicals; they were then partially oxidized by soaking in 1N $NaIO_4$ solution for 2 hours. After washing with de-ionized water, the membranes were soaked in phosphate buffers (0.5M, pH 6.0) containing 2mM of EDA- β-CD (or PDA- β-CD, BDA- β-CD) and 20mM $NaCNBH_3$ sequentially for 2 hours each to attach the chiral selectors via reductive amination. For the immobilization of a mixture of aminated β-CDs, the membranes were soaked in phosphate buffer containing equal molar concentrations of EDA- β-CD, PDA- β-CD and BDA- β-CD. All reactions in this process were carried out at room temperature. The modified membranes were stored in de-ionized water prior to the enantioseparation performance tests.

3.2.4. Benzoate derivatization at cyclodextrin

The cellulose membranes (EDA-β-CD modified) prepared in the previous stage were first immersed in repeatedly in fresh pyridine solvent for 1h at room temperature to remove residual water from the membranes. They were then reacted in a mixture consisting of 30ml pyridine, 20ml 3-picoline and 10g benzoic anhydride at 70°C for 10, 15, 30, 40 and 60 minutes. After the reactions were completed, the resulting membranes were washed repeatedly with de-ionized water and then soaked in de-ionized water for one day to remove residual pyridine. The reaction scheme is depicted in Figure 3.1.

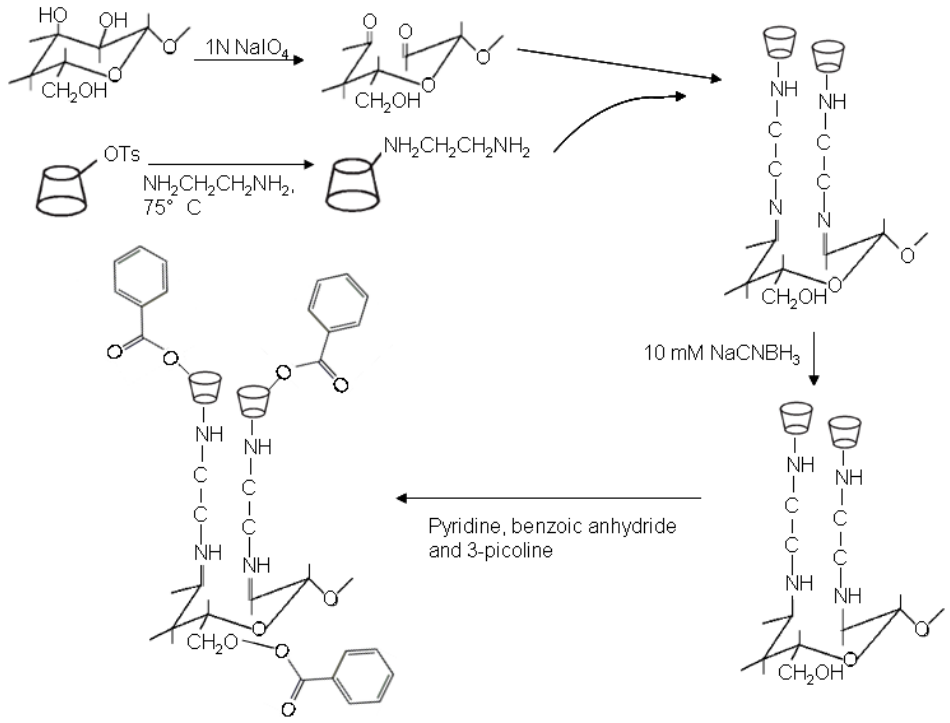

Figure 3.1: Preparation of EDA-β-CD immobilized membranes and further benzoation reaction. (The figures are schematic representation only and not drawn to scale)

3.2.5. Characterization of modified membranes

The elemental ratio on the membrane surface was measured by an AXIS His spectrometer (Kratos Analytical Ltd, England) using a monochromatized Al Kα X-ray source (1486.6 eV photon) at a constant dwell time of 100ns and a pass energy of 40 eV. The anode voltage and anode current were 15kV and 10mA respectively. The pressure in the analysis chamber was 5.0×10^{-8} Torr. The photoelectron takeoff angle with respect to the sample surface was 90°, and the X-ray penetration depth was about 5-7nm.

FTIR-transmission measurements were made on a Bio-Rad FTS-3500 ARX FTIR spectrometer with a scan range of 500-4000 cm^{-1}. Each sample was scanned 32 times after the sample chamber had been purged with nitrogen for 10 minutes.

3.2.6. Chiral separation performance test

The performance tests were carried out using a dialysis permeation cell as shown in Figure 3.2 [48]. The key units of the device were the two Teflon chambers, the feed and strip chambers, between which the modified membrane was clamped. The feed solution, with the initial tryptophan concentration of 0.1mM, was circulated between the feed chamber and a 1L reservoir; the solution volume in the feed chamber was maintained at 35ml. Different from the feed, 35ml of deionized water was used as a strip solution without external circulation. Both solutions were stirred by Teflon impellers connected to an overhead stirrer (CAT R18, M. Zipperer GmbH, Staufen, Germany) at 200 rpm. 200μL of samples were taken periodically and analyzed by Capillary Electrophoresis (P/ACE MDQ capillary electrophoresis system, Beckman). The buffer solution consisted of 20mM phosphate and 50mM α-cyclodextrin solution at pH = 2.2. Sample injection was 7.5s at 0.8 psi and the forward separating voltage was 25kV. The sample collection time ranged from 3 hours to 60 hours depending on the permeation flux of the membranes.

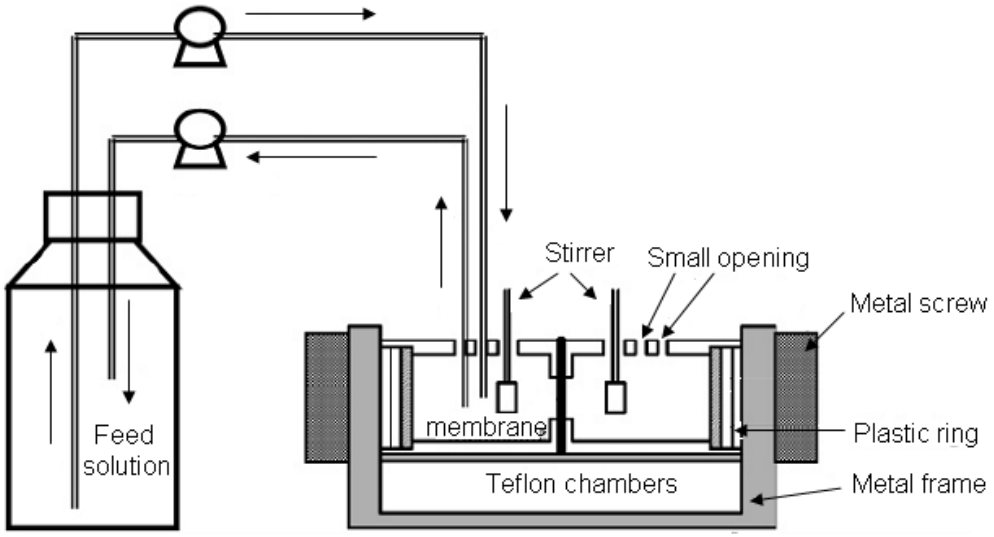

Figure 3.2: Permeation test set-up on immobilized membranes

3.2.7. Predicted binding energies and enantioselectivities

Calculations of complex formation energies were performed using the Material Studio 4.3 Visualizer software package from Accelrys Inc. All molecular structures were built using the builder visualizer and the complexes were formed by manually inserting the enantiomers into the chiral selector cavities. The structures were then optimized by the Discovery module and their minimized energies calculated. For all calculations, the pcff force field and ultra-fine iterations were applied.

Matlab 7.4.0 was used for the calculation of theoretical enantioselectivities of modified membranes. The function 'solve' was utilized to solve the series of mass balance and equilibrium equations.

3.3. Results and discussion

3.3.1. Characterization of modified membranes

The cellulose membrane used in this experiment had a molecular weight cut-off (MWCO) of 1000 Da; its effective pore size was about 1nm, comparable to the size of the aminated β-CDs (MW = 1177~1201 Da). Thus we assumed that the majority of the β-CDs were immobilized on the membrane surface and that only trace amounts penetrated the pores. This enabled the grafting efficiency of the β-CDs, proportional to the relative concentration of β-CDs immobilized on the membrane surface, to be investigated by XPS analysis, with the results shown in Table 3.1. Since only the aminated β-CDs contained nitrogen atoms, the atomic percentage of nitrogen was used to compare the β-CD concentrations on the surfaces of different membranes. The trace amount of nitrogen present in the unmodified membranes was from the residual storage chemical, sodium

azide, which suppressed bacteria growth. After reaction with β-CDs, an increase in nitrogen content was clearly observed, indicating the successful immobilization of β-CDs onto the membrane surface. The apparent nitrogen content decreased again following benzoation because of two factors related to the benzoate group: a shielding of the nitrogen atom in the bottom layers by this group, and a decrease in the percentage nitrogen content owing to the increase in carbon and oxygen atoms following benzoation. This observation also provided evidence for the successful benzoation of the EDA-β-CD.

Membranes	***O %***	***N %***	***C %***
Pristine	44.1 ± 0.3	0.2 ± 0.0	55.7 ± 0.3
EDA-BCD	42.3 ± 0.8	1.3 ± 0.1	56.4 ± 0.8
PDA-BCD	43.1 ± 0.4	1. 1 ± 0.1	55.8 ± 0.2
BDA-BCD	39.9 ± 0.3	1.0 ± 0.1	59.1 ± 0.5
Mix EPB	41.2 ± 0.1	1.2 ± 0.0	57.6 ± 0.1
Benzoated	40.2 ± 0.8	0.5 ± 0.0	59.3 ± 0.8

Table 3.1. Surface elemental analysis by XPS on membranes immobilized with various chiral selectors

The measured percentage atomic nitrogen decreased slightly with increasing spacer arm length, consistent with a higher grafting efficiency for EDA- β-CD than for the others, with the lowest grafting density for BDA- β-CD. This was due to their difference in reactivity in the reductive amination reaction. As this reaction was carried out in an aqueous solution, the amino end groups of the β-CDs could be protonated such that their nucleophilicity is reduced. Mehta and Zydney showed in their work that the charge on diamines with shorter chain lengths was smaller than that on longer diamines, and hence degree of protonation was lower [52]. We inferred from this work that the β-CDs with shorter diamine groups, especially EDA-β-CD, possessed the strongest nucleophilicity, and hence the highest grafting efficiency on the membranes.

FTIR spectrometry was also employed for surface characterization to confirm the benzoation sof the β-CD. Figure 3.3 shows the spectral changes for the membranes functionalized with benzoated β-CDs. The spectra for the unmodified and EDA-β-CD modified membranes were similar because both β-CD and cellulose consist of glucose building units. However, a new peak at wavenumber 1730 cm^{-1} was clearly observed in the spectra for the benzoated β-CDs. This wavenumber corresponds to the stretching vibration of the C=O in the benzoate group. Furthermore, the increment in absorption observed at a wavenumber of 1230 cm^{-1} can be attributed to the asymmetric stretching of the C-O bond in the ester group. Hence, the FTIR results further confirmed the successful benzoation of the β-CDs on the membrane surface. The analysis above provides qualitative comparisons only; methods for the precise quantification of the β-CD concentration on the membrane surface and the degree of substitution of hydroxyls on the β-CD by benzoate have not yet been fully realized.

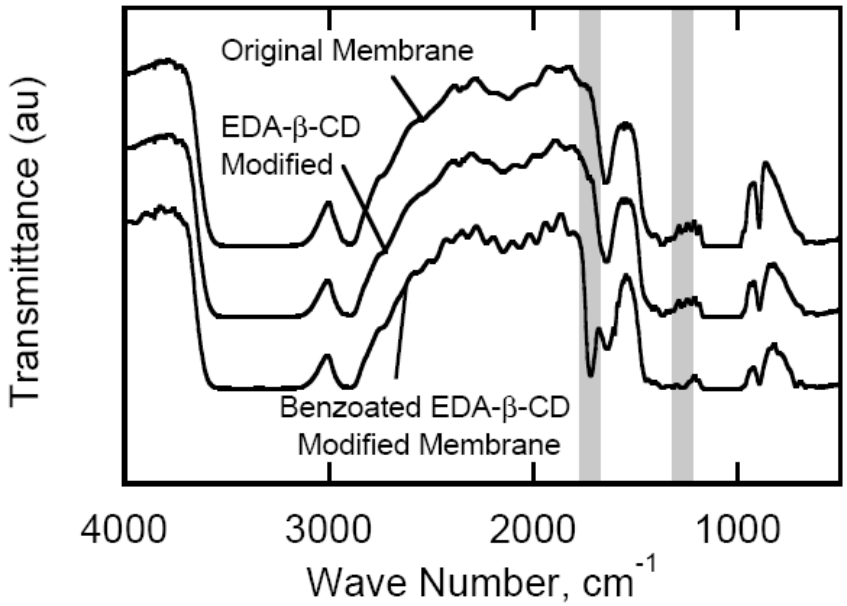

Figure 3.3: FTIR spectra of modified membranes

3.3.2. Enantioseparation performance of aminated CD modified membranes

With the concentration gradient as the only driving force, the permeation flux was relatively low such that the concentration of enantiomers in the stripping solution was only about a tenth of that in the feed by the end of experiment. Hence, the feed concentration was assumed to be constant at 0.1mM throughout. The plots of enantiomer concentration C_S (mM) in the stripping solution against time t (min) were therefore approximated by straight lines, the slopes ($\Delta C_S / \Delta t$) of which were utilized in the calculation of the flux J (mol/cm^2 min) via the equation:

$$J = \frac{V \Delta C_S}{A \Delta t} \tag{1}$$

where ΔC_S is the change in concentration, Δt is the permeation time, V is the stripping volume (35 ml) and A is the effective membrane area (1.77 cm^2). The permeability coefficient P (cm^2/s) is calculated as

$$P = \frac{Jd}{C_F - C_S} \tag{2}$$

where d is the membrane thickness (0.005cm) and C_F is the feed concentration (0.1mM). Finally, the enantioselectivity α was obtained as the ratio of the permeability coefficient of D-tryptophan to that of L-tryptophan:

$$\alpha = \frac{P_D}{P_L} \tag{3}$$

The permeability coefficients and enantioselectivity calculated from experimental results are tabulated in Table 3.2. The unmodified membranes, i.e., those with no β-CD immobilization, exhibited no selectivity for racemic tryptophan separation, and were used as a control to show that the enantioselectivity of our functionalized membranes was due to the attachment of the chiral selectors.

Membranes	*Permeability (10-7 cm2/s)*		*Average selectivity*
	L-tryp	*D-tryp*	
Unmodified	4.41	4.34	0.99
EDA-β-CD immobilized	3.05	3.66	1.19
PDA-β-CD immobilized	2.81	3.08	1.10
BDA-β-CD immobilized	2.54	2.71	1.07
Mix EPB immobilized	1.94	2.33	1.20

Table 3.2. Permeability and enantioselectivity in racemic tryptophan separation through membranes immobilized with various chiral selectors

Enantioselectivity was observed for all membranes immobilized with aminated β-CD chiral selectors. The β-CD exhibited a stronger interaction with L-tryptophan than with D-tryptophan such that more β-CD-L-tryptophan complexes were formed at the membrane surface, resulting in lower concentrations of free and mobile L-tryptophan there. Thus the concentration gradient of free L-tryptophan across the membrane was smaller than that of D-tryptophan. As this concentration gradient was the only driving force for transport across the membrane, and since the diffusion constants for both enantiomers were the same, a higher permeation flux of D-tryptophan through the membrane was observed, i.e., the membrane exhibited an enantioselectivity for D-tryptophan over L-tryptophan.

We also observed a decrease in enantioselectivity with increasing spacer arm length. This was partly due to the decrease on the membrane surface in β-CD concentration with the longer spacer arms. Through mathematical modeling as shown in equations 4-10, and with the assumption of thermodynamically equilibrated complex formation, we deduced that a higher chiral selector concentration resulted in a higher enantioselectivity. The results of these simulations, given in Figure 3.4 show a steady increase in enantioselectivity with increasing chiral selector concentration. This model was used to

estimate the β-CD concentration from experimental measurements of the membrane selectivity; the results in Table 3.3 show a decreasing chiral selector concentration can be responsible for an enantioselectivity decrease. These estimated concentrations did not correspond perfectly with those obtained by XPS analysis given in Table 3.1 and shown in Figure 5, although both showed similar trends. We inferred from Figure 3.5 that the decrease in β-CD concentration at membrane surface was not the only factor affecting the selectivity when the spacer arm length was increased.

$$[L]+[L.CD]=[L]_0 \tag{4}$$

$$[D]+[D.CD]=[D]_0 \tag{5}$$

$$[L]_0=[D]_0 \tag{6}$$

$$[L.CD]+[D.CD]+[CD]=[CD]_0 \tag{7}$$

$$K_L=\frac{[L.CD]}{[L][CD]}=0.043 \tag{8}$$

$$K_D=\frac{[D.CD]}{[D][CD]}=0.031 \tag{9}$$

$$\alpha=\frac{[D]}{[L]} \tag{10}$$

Membranes	***Selectivity***	***Calculated Conc/mM***
EDA-β-CD immobilized	1.19	31
PDA-β-CD immobilized	1.10	11
BDA-β-CD immobilized	1.07	7
Mix EPB immobilized	1.20	34.5

Table 3.3. Theoretical β-CD concentration on membrane surface calculated from measured selectivity

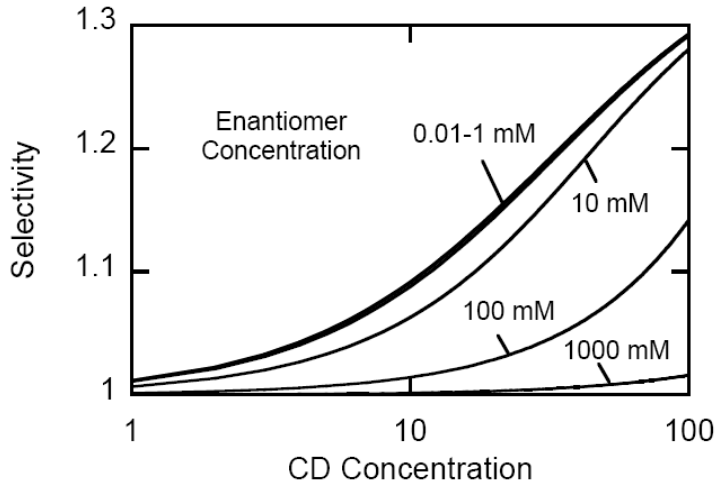

Figure 3.4: Theoretical calculation of enantioselectivity as a function of tryptophan and β-CD concentration

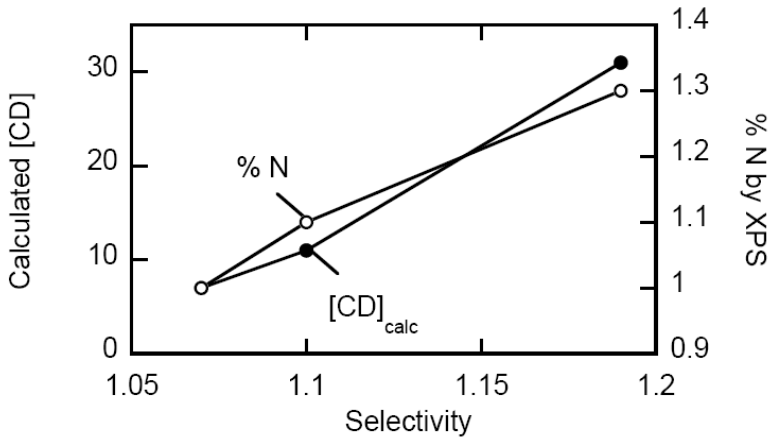

Figure 3.5: Comparison of CD concentrations by theoretical calculation and XPS results

Another cause of the lower selectivity with longer spacer arms was the presence of defects in the chiral layers. The chiral selectors with longer spacer arms had higher degrees of translational freedom than those with shorter arms such that defective spots form in the chiral layer through which the enantiomers could pass without interacting with the chiral selectors. The enantiomers reaching the membrane surface via the defective spots would off-set the enantioselectivity by decreasing the difference between

the driving forces for D-tryptophan and L-tryptophan diffusion across the membrane. For chiral selectors with shorter spacer arms, the probability of defect formation was smaller as the chiral selectors were much closer to the membrane surface. We therefore conclude that the enantioselectivity would be compromised if the chiral layer position were to be located too far from the membrane surface.

The selectivity was the highest when a mixture of chiral selectors was grafted onto the cellulose membrane surface. From the XPS results, the total β-CD concentration was slightly lower than that of the EDA-β-CD modified membrane mainly due to the lower grafting efficiency of the other two chiral selectors (PDA- β-CD and BDA- β-CD); this again indicated that the β-CD concentration, though important, was not the only factor determining enantioselectivity. The high selectivity associated with this membrane was due mainly to its chiral layer thickness. While the three previously-described modified membranes with only single chiral selector layers, these could be viewed as possessing three layers of chiral selectors. Thus the enantiomers experienced more stages of separation. Similar to the plate number concept in chromatography, a thicker chiral layer could be depicted as a micro scale chromatography column with a higher plate number. Hence, a thicker chiral layer could enhance enantioselectivity.

It is generally accepted that there is a trade-off between selectivity and permeability in membrane separations [53] but this trend is not observed in our studies in which permeability also decreased as the selectivity decreased with increasing spacer arm length, as shown in Table 3.2. This interesting phenomenon is due to the reduction in pore size

through two different effects as depicted in Figure 3.6. First, the opening of the pores was blocked partially by the chiral selectors with longer spacer arms due to their greater degree of translational freedom. Second, small amounts of the chiral selectors were immobilized within the membrane pores although the majority were on the membrane surface; the larger the size of chiral selectors, the severer the reduction in pore size. As the sizes of the selectors varied according to the ranking BDA- β-CD > PDA- β-CD > EDA- β-CD, the extent of the pore size reduction increased in the same order, and hence the permeability decreased with increasing spacer arm length. [This was evidenced in a recent study on the pure water permeation fluxes of the pristine membranes without functionalization (9.9 $Lm^2hr^{-1}bar^{-1}$), the membranes functionalized with BDA- β-CD (8.3 $Lm^2hr^{-1}bar^{-1}$) and EDA- β-CD (9.2 $Lm^2hr^{-1}bar^{-1}$), which agree well with our argument.] While the aminated β-CD concentration on the membrane surface was the highest for the EDA-β-CD functionalized membrane, and was thus expected to have a stronger retarding effect on enantiomer diffusion than the other, longer selectors, this effect was mitigated by the smaller pore size reduction with the shorter selectors. The lowest permeability was observed with the mixed EPA/PDA/BDA membrane owing to the greater thickness and density of the chiral layer in this case.

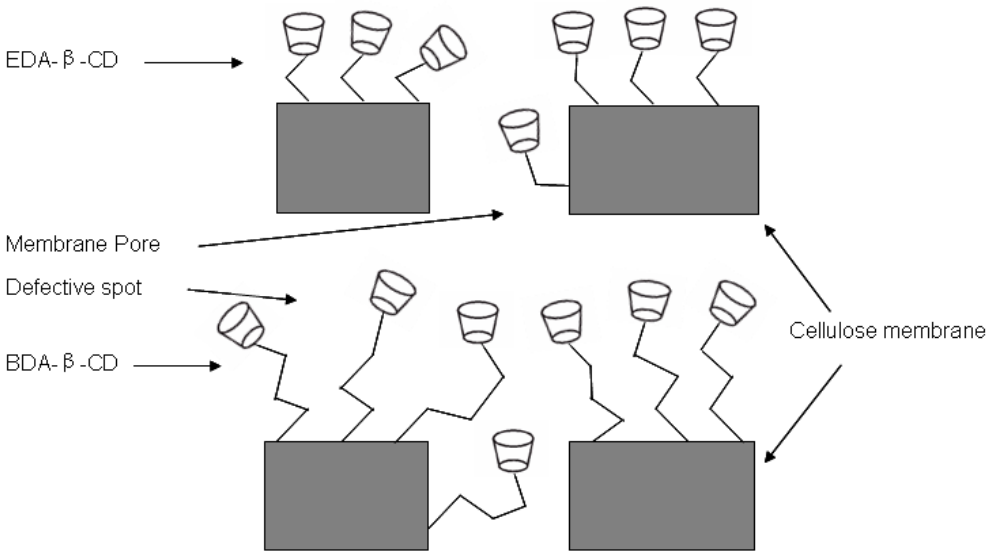

Figure 3.6: Graphical representation of pore size reduction by various chiral selectors

3.3.3. Enantioseparation performance of benzoated CD modified membranes

The enantioselectivity β-CD functionalized membranes increased after the immobilized chiral selectors were derivatized with benzoate groups as shown in Table 3.4. The rotational freedom of tryptophan in the β-CD cavity was greatly restricted following its distortion by the replacement of the secondary hydroxyl groups with the much bulkier benzoate groups. The binding between the enantiomers and the benzoated β-CD was more stereo-specific, i.e., the enantiomeric selectivity of the β-CD was enhanced by the attachment of the benzoate groups. We compared the binding energies between racemic tryptophan and EDA-β-CD against those of benzoated β-CD calculated using molecular modeling. The structures of L, D-tryptophan, chiral selectors and their respective binding complexes shown in Figure 3.7 were drawn with the visualizer, and their minimized energies were obtained using the discovery module. The complex formation energy was calculated by subtracting the minimized energies of the free compounds from those of the complexes. The relative differences between the calculated complex formation energies

of the two tryptophan isomers and the different selectors (ΔΔGs) were consistent with the relative differences in measured enantioselectivities for these selectors: the larger this difference, the higher the enantioselectivity. The results summarized in Table 3.5, indicate that the ΔΔG value increased after benzoation, consistent with a higher theoretical selectivity in agreement with the experimental results.

Reaction Time/min	*Permeability(10-7 m2/s)*		*Selectivity*
	L-tryp	*D-tryp*	
0	3.05	3.66	1.19
10	1.86	2.22	1.19
15	1.53	2.20	1.32
30	0.644	0.844	1.31
40	0.147	0.221	1.51
60	0.147	0.218	1.49

Table 3.4. Permeability and enantioselectivity in racemic tryptophan separation through benzoated EDA- β -CD immobilized membranes with various reaction times

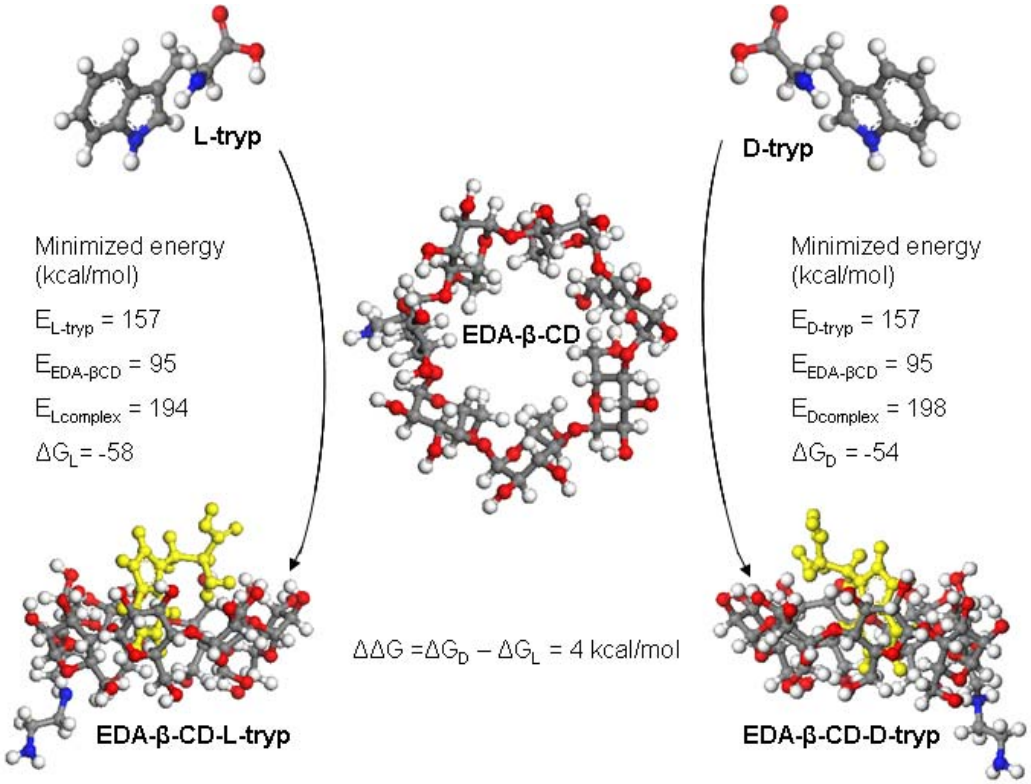

Figure 3.7: Computational analysis of complex formation energy between tryptophan and EDA-β-CD

Chiral selector	Δ GL (kcal/mol)	/Δ GD (kcal/mol)	/ΔΔ G / (kcal/mol)
EDA-β-CD	-58	-54	4
Partially benzoated EDA-β-CD	-52	-45	7
Fully benzoated EDA-β-CD	-27	-18	9

Table 3.5. Comparison of simulated complex formation energy before and after benzoation. Δ GL is complex formation energy of L-tryptophan with chiral selector, ΔGD is that of D-tryptophan and ΔΔG = ΔGD - Δ GL.

The experimental results in Table 3.4 also showed increased enantioselectivity with a longer benzoation reaction time, i.e., with a greater extent of benzoation of the EDA-β-CD. This increase in the concentration of the more efficient chiral selector on the membrane surface resulted in an enhancement in the enantioselectivity. Furthermore, the degree of substitution (DS) on each EDA-β-CD selector was higher for longer reaction times, which also played a role in enhancing enantioselectivity. The complex formation energies for partially (DS=7) and fully (DS=20) benzoated EDA-β-CD calculated using material studio are shown in Table 3.5, from which we can deduce that a higher degree of substitution should enhance the enantioselectivity since a larger ΔΔG was obtained for the fully benzoated EDA-β-CD than for the partially substituted selector.

Although benzoation of the EDA-β-CD allowed for an increased membrane enantioselectivity, the permeability decreased, especially with prolonged reaction time. In Table 3.4, a drop of 50% in L-tryptophan permeability was noted after 15 minutes reaction, while about a 20-fold drop was observed following a reaction time of one hour. The drop in permeability was primarily due to the reduction in pore size, since not only were the hydroxyl groups of EDA-β-CD benzoated, but also the hydroxyl groups of the cellulose membrane. As a result, the membrane pores were greatly reduced in size as the bulkier benzoate groups were attached to the pore walls. Also, the trace amount of EDA-

β-CD inside the pores grew in size with benzoation and further blocked passage of the enantiomers. All these factors led to a lower permeability which worsened with longer reaction times, the higher degree of benzoation intensified the pore size reduction and yielded even a lower permeability.

3.4. Conclusion

In this study, commercial cellulose membranes were first immobilized with chiral selectors of various spacer arm lengths and their enantioseparation performance was investigated and compared. Both higher permeability and higher selectivity were observed with chiral selector monolayers with shorter spacer arms. The enantioselectivity was highest (1.20) for thicker chiral layers formed by attaching a mixture of chiral selectors of varying spacer lengths to the membranes, although the permeability was lower. The membrane enantioselectivity further increased to ~1.3-1.5 following benzoation of the EDA-β-CD selector. The enhanced selectivity was interpreted in terms of the increase in estimated complex formation energy difference ($\Delta\Delta G$) determined from molecular modeling calculations. It was found that the degree of benzoation was critical to enantioseparation performance, which was enhanced with higher degrees of substitution.

3.5. Acknowledgement

We thank the Singapore-MIT Alliance and the National University of Singapore (Grant No.R-279-000-249-646) for funding this project. Thanks are also due to Professor Andrew Zydney and Professor Donald Paul for their invaluable suggestions.

Chapter 4. Novel Membrane Process for the Enantiomeric Resolution of Tryptophan by Selective Permeation Enhancements

4.1. Introduction

As discussed in section 2.2.3.2, different from the chiral selective membrane we prepared in chapter 3, another type of membrane chiral separation is carried out using non-chirally selective membranes coupled with affinity ultra-filtration concepts, where a specific chiral selector is introduced into the racemic feed solution to form complexes preferentially with one of the enantiomers [22-23, 54]. This mixture is then filtered under pressure by the non-chiral selective membrane with a suitable pore size and surface charge that retains the large complexes. A relatively high enantioseparation can be achieved. For example, chiral selectors such as bovine serum albumin (BSA) [23] and human serum albumin (HSA) [22, 55] have shown promising results in tryptophan separation. However, this pressure driven process is subject to higher operating costs, and the performance may deteriorate with membrane fouling. Also, extra post steps are required to separate the chiral selectors and enantiomers in the feed side.

A different approach to membrane-based chiral separations that combines the concepts of liquid membrane technology and affinity ultra-filtration is employed in this study where the chiral selectors are added to the *strip* solution instead of the racemic feed solution. In a normal diffusion process, the diffusion rate decelerates with time since the concentration gradient across the membrane decreases. With chiral selectors in the strip solution, the enantiomers permeating through the membrane bind to the chiral selectors to different extents depending on their relative association equilibrium constants. As a

consequence, not only do we compensate for the deceleration of permeation rate, but the deceleration rates themselves also become different, i.e. the permeation deceleration of the more strongly binding enantiomer is lower, resulting in a higher accumulated permeation flux. Enantioselectivity can hence be demonstrated by the selective permeation enhancement of the enantiomers. Moreover, this is also different from the normal extraction process by a liquid membrane system where two immiscible solvents are used in the feed and the strip [56]. As all solutions in this work are aqueous, and the chiral selectors are fully constrained to be inside the chamber by the small pore sizes of the membranes, the stability problems associated with ordinary liquid membrane systems can be averted.

The enantioseparation effectiveness of the newly developed selective permeation enhancement (SPE) approach is examined via three approaches in this study: single permeation cell, two permeation cells in series and the pre-addition of the racemic and chiral selectors to the strip solution. HSA and tryptophan are chosen as the chiral selector and enantiomer pair since the HSA has a high intrinsic selectivity for the resolution of a racemic tryptophan mixture. It has been reported that the L-tryptophan binds to the indol-benzodiazepine site of HSA with an affinity 100 times greater than that of D-tryptophan [34]. Following a demosntration of the feasibility of enantioseparation by the single permeation cell process, the separation performance is further improved by adding a racemic mixture to the strip solution as well; both the selectivity and enantiomeric excess are shown to increase with higher concentrations of racemic mixture pre-added to the strip solution. Finally, by connecting two permeation cells in series, we show that the

separation performance is greatly enhanced; a new design suitable for industrial application is proposed using hollow fiber membrane modules. Mathematical modeling was exploited to interpret and support the experimental data, through the solution of a set of ordinary differential equations representing the mass balances and reaction equilibria.

Overall, this is an original work that not only demonstrates the model designs of SPE for achieving high enantioselectivity, but may also open up new routes and stimulate new ideas for enantiomeric resolution.

4.2. Experimental

4.2.1. Materials

The cellulose dialysis membranes Spectro/Pro 7, (MWCO (molecular cut-off) = 1000, membrane thickness = 50μm) were purchased from Spectrum Medical Industries. Inc. Human serum albumin (HSA) and bovine serum albumin (BSA) from Sigma Aldrich, α-cyclodextrin from Cyclolab, DL-tryptophan from Alfa Aesar and sodium phosphates were all reagent grade and used without further purification.

4.2.2. Chiral separation by SPE in single permeation cell

The chiral separation test was carried out on a dialysis permeation cell setup as shown in Figure 4.1 [30]. The permeation cell was comprised of two Teflon chambers between which the dialysis membrane was clamped. The feed was a 35ml racemic tryptophan solution of 0.1mM and the strip chamber contained a 35ml HSA solution at various concentrations. The pH of each solution was maintained at 8.6 by 20mM phosphate buffer. Two Teflon impellers connected to an overhead stirrer (CAT R18, M. Zipperer GmbH, Staufen, Germany) operating at 200 rpm were used to stir the solutions. 200 μl of samples were taken from the feed solution periodically and analyzed by Capillary Electrophoresis (CE) (P/ACE MDQ capillary electrophoresis system, Beckman). The CE buffer was a 50mM α-cyclodextrin solution with pH maintained at 2.2 by a 20mM phosphate buffer. The sample injection time was 7.5s at 0.8 psi and the forward separating voltage was 25kV. The permeate concentrations were back calculated by subtracting the feed chamber concentration from the original feed solution.

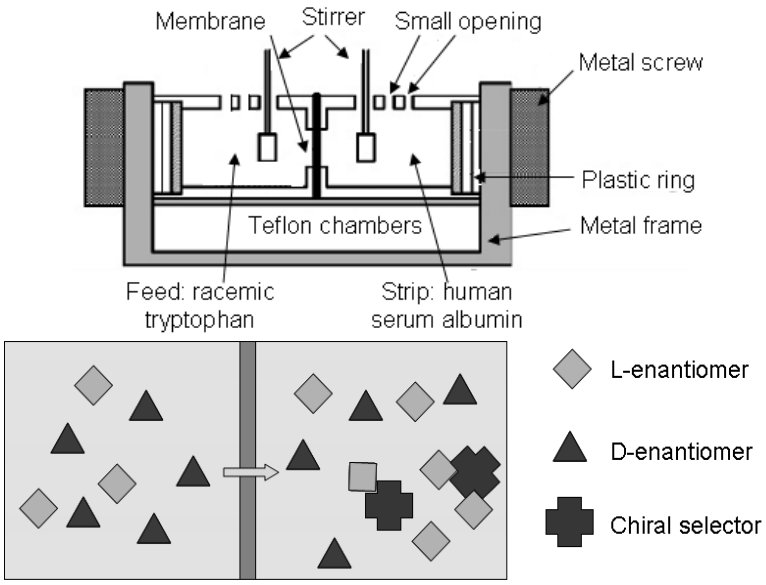

Figure 4.1. Schematic diagram of SPE with single cell

4.2.3. Chiral separation by SPE with pre-addition of feed

The experimental procedures were similar to those described in the previous section except that a racemic enantiomer mixture was added, with concentration varying up to that of the feed, together with the HSA, into the strip solution. The mixture in the strip solution was prepared 4 hours before permeation experiments to ensure equilibrium. The difference in the concentration gradients of the two enantiomers across the membrane could then be increased from the beginning of the experiment, and in such a way, products with higher enantiomeric excess were harvested from the feed chamber.

4.2.4. Chiral separation by SPE in two permeation cells in series

The setup consisted of two permeation cells in series as shown in Figure 4.2. The contents of cell 1 were similar to those used in the single cell test, while the two chambers of cell 2 contained HSA solution and phosphate buffer, respectively. The protein chambers of the two cells were connected with a circulating pump, such that the

solution concentrations of the two chambers could be assumed to be the same. Samples were withdrawn periodically from the strip side and analyzed by Capillary Electrophoresis.

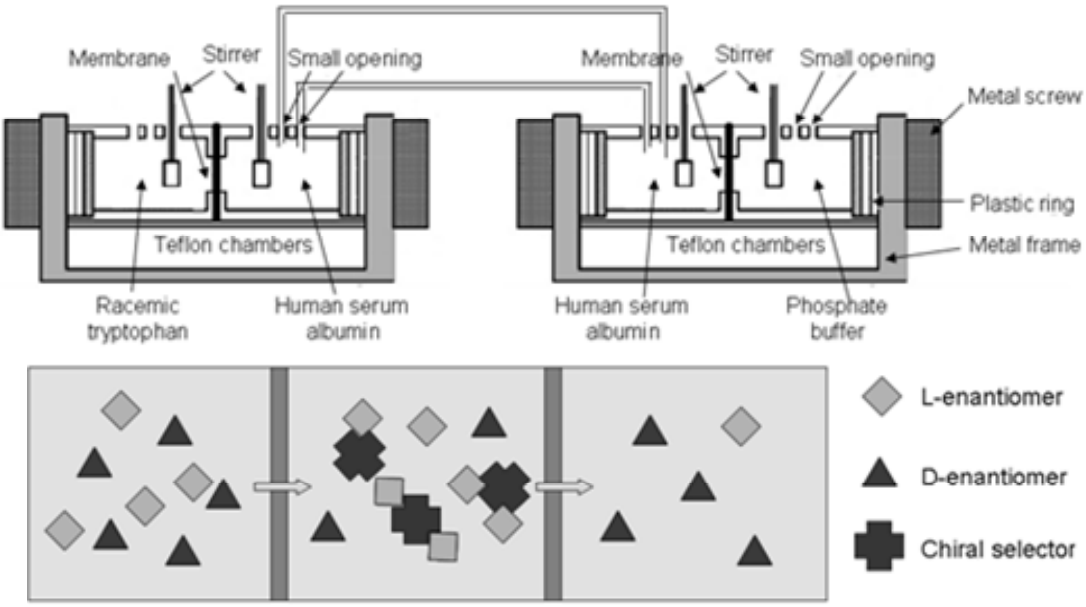

Figure 4.2. Schematic diagram of SPE with two cells in series

4.2.5. Control experiments of affinity ultra-filtration

In the affinity ultrafiltration control experiments, 10g/L HSA were added directly to the feed solution and formed complexes with enantiomers which were retained by the membrane. The permeation experiment was conducted 4 hours after solution preparation to ensure equilibrium. Samples were then taken from the strip solution and tested by Capillary Electrophoresis.

4.2.6. Mathematical modeling of permeation tests

Matlab 7.4.0 was used for the calculation of theoretical permeation results. The set of standard mass balance and equilibrium equations listed below was solved with the aid of the built in function ‘ode45’.

$$V_1 \frac{dC_{L1}}{dt} = -\frac{AD}{d}(C_{L1} - C_{L2}) \quad (1)$$

$$V_1 \frac{dC_{D1}}{dt} = -\frac{AD}{d}(C_{D1} - C_{D2}) \quad (2)$$

$$V_2 \frac{dC_{L2}}{dt} = \frac{AD}{d}(C_{L1} - 2C_{L2} + C_{L3}) - V_2(k_L C_{L2} P - k_L^{'} P_{CL}) \quad (3)$$

$$V_2 \frac{dC_{D2}}{dt} = \frac{AD}{d}(C_{D1} - 2C_{D2} + C_{D3}) - V_2(k_D C_{D2} P - k_D^{'} P_{CD}) \quad (4)$$

$$V_1 \frac{dC_{L3}}{dt} = \frac{AD}{d}(C_{L2} - C_{L3}) \quad (5)$$

$$V_1 \frac{dC_{D3}}{dt} = \frac{AD}{d}(C_{D2} - C_{D3}) \quad (6)$$

$$\frac{dP}{dt} = -(k_L C_{L2} P - k_L^{'} P_{CL}) - (k_D C_{D2} P - k_D^{'} P_{CD}) \quad (7)$$

$$\frac{dP_{CL}}{dt} = (k_L C_{L2} P - k_L^{'} P_{CL}) \quad (8)$$

$$\frac{dP_{CD}}{dt} = (k_D C_{D2} P - k_D^{'} P_{CD}) \quad (9)$$

where V, A, d, t and C represent the solution volume, membrane effective area, membrane thickness, permeation time and concentration, respectively, D denotes the apparent diffusion constant derived from experiments, and k_L, k_L', k_D and k_D' are association and dissociation constants between HSA and DL-tryptophan obtained from literature sources [35]. The subscripts 1, 2, 3 denote the feed chamber, HSA chambers and strip chamber, respectively, while subscripts *L, D, CL, CD* refer to the L-tryptophan, D-tryptophan, HSA, HSA-L-tryptophan complex and HSA-D-tryptophan, respectively.

4.3. Results and discussion

The concepts for the enhanced optical resolution of racemic mixtures proposed in this paper were tested experimentally using the membrane permeation cells described above. In this section, we discuss the overall performance of the three configurations and propose ways in which they might be employed industrially.

4.3.1. SPE performance by single cell permeation

As the concentration gradient was the only driving force in this experiment, the initial permeation rates of both enantiomers were similar. However, on formation of the HSA-tryptophan complexes on the permeate side according to the two equilibrium reactions

$$HSA + L - tryp \leftrightarrow HSA - L - tryp \quad \text{(A)}$$

$$HSA + D - tryp \leftrightarrow HSA - D - tryp \quad \text{(B)}$$

the free enantiomer concentrations in the strip solution were reduced. Since HSA is more selective to L-tryptophan, naturally more L-tryptophan was bound to form complexes and the free L-tryptophan concentration was reduced to a greater extent than was the D-tryptophan concentration. A higher concentration gradient of L-tryptophan across the membrane was therefore maintained, which resulted in a higher overall permeation flux of L-tryptophan, i.e. selectivity of L-tryptophan against D-tryptophan. This effect is clearly evident in the data shown in Figure 4.3, calculated using the equations

$$ee\% = \frac{C_D - C_L}{C_D + C_L} \times 100\% \quad (10)$$

$$\alpha = \frac{Q_L}{Q_D} = \frac{F_L - C_L}{F_D - C_D} \quad (11)$$

where ee% represents the enantiomeric excess of the retentate and α is the selectivity of the SPE system, defined as the ratio of the flux of L-tryptophan permeating through the

membrane to that of D-tryptophan, C_L, C_D, F_L and F_D are the L-tryptophan and D-tryptophan concentrations in the retentate and in the original feed solution, respectively, while Q_L and Q_D are the fluxes of enantiomers. It is also evident from Figure 4.3 that the separation performance increased with an increase in HSA concentration in the strip solution, consistent with expectations, because a high HSA concentration shifts the equilibrium concentrations in reactions A and B further to the right, such that the permeation fluxes of both enantiomers are enhanced. However, due to the stronger binding between HSA and L-tryptophan, a preferential concentration decrease of the free L-tryptophan prevailed, thus enhancing enantioselectivity.

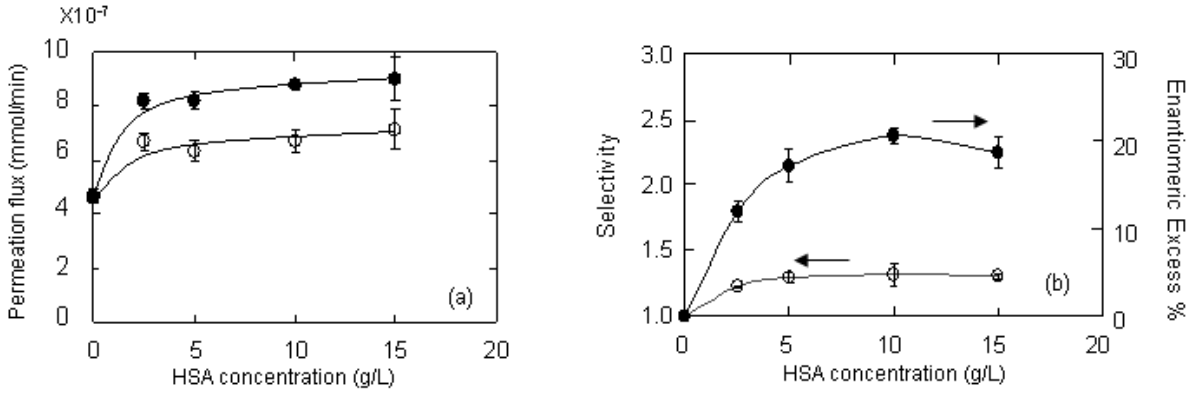

Figure 4.3. Enantioselectivity and ee% against HSA concentrations in strip with single cell SPE

It was also noted that the ee% and selectivity decreased when HSA concentration was too high as indicated by the results obtained with 15g/L of HSA. One possible reason could be that the binding of D-tryptophan is also greatly enhanced in too great an excess of HSA as reflected in the equilibria given in reactions A and B. As a result, the increment of D-tryptophan flux across the membrane was steadily maintained while the flux of L-tryptophan had almost reached its maximum since the free L-tryptophan concentration

was close to zero. Hence, we observed that both ee% and selectivity obtained using this approach were maximized at an intermediate value of HAS concentration, i.e., further improvements in separation performance cannot be achieved by simply increasing the HSA concentration. New approaches were designed and are presented in the following sections.

4.3.2. SPE performance by single cell permeation with pre-addition of feed

Although the enantiomers could be partitioned successfully in the experiments outlined above, one shortcoming was the low selectivity near the beginning of the experiment when both enantiomer concentrations in the permeate side were close to zero and their driving forces were similar. The overall selectivity was therefore compromised. A higher enantioselectivity would be possible if a difference in driving forces could be induced from the beginning of the experiments. Therefore in the subsequent experiments, while the HSA concentration in the permeate (or strip) side was maintained at 10g/L, certain concentrations of racemic enantiomer mixtures were also added to the permeate side prior to the permeation experiment. Under these conditions, the initial driving force (i.e., concentration gradient) for the L-tryptophan was higher than that for the D-tryptophan since the HSA/L-tryptophan complexes formed preferentially on the permeate side so that the actual concentration of free D-tryptophan was higher than the free L-tryptophan concentration in the strip solution, as depicted in Figure 4.4.

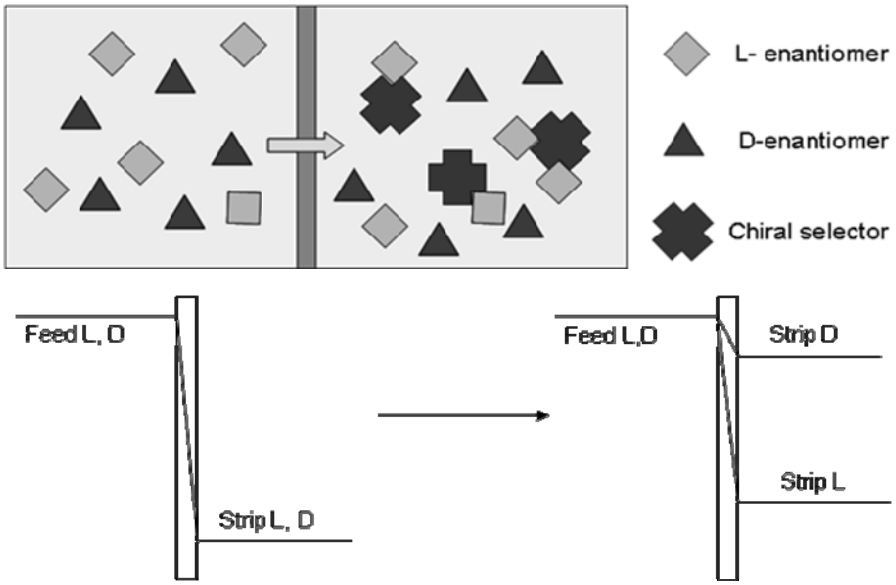

Figure 4.4. Schematic diagram of enantiomer separation with pre-feed addition (upper); schematic representation of change in concentration gradient by pre-feed addition (bottom).

The permeation results from such experiments are presented in Figure 4.5 (a) (b). It is evident that the results support our hypothesis very well as both ee% in the final feed solution and selectivity were improved, with a commensurately higher concentration of racemic tryptophan in the strip solution. With a higher free D-tryptophan than L-tryptophan concentration in the permeate side, the reduction in permeation flux of D-tryptophan was much stronger than that in the flux of L-tryptophan. This agreed well with Figure 5(a) which showed a greater increment in D-tryptophan yield from the feed chamber, as reflected in its steeper increase with increasing concentration of pre-added tryptophan. As a result, both the selectivity of L/D-tryptophan and the ee% of the retentate increased with an increase in the concentration of the racemic tryptophan mixture added to the permeate side.

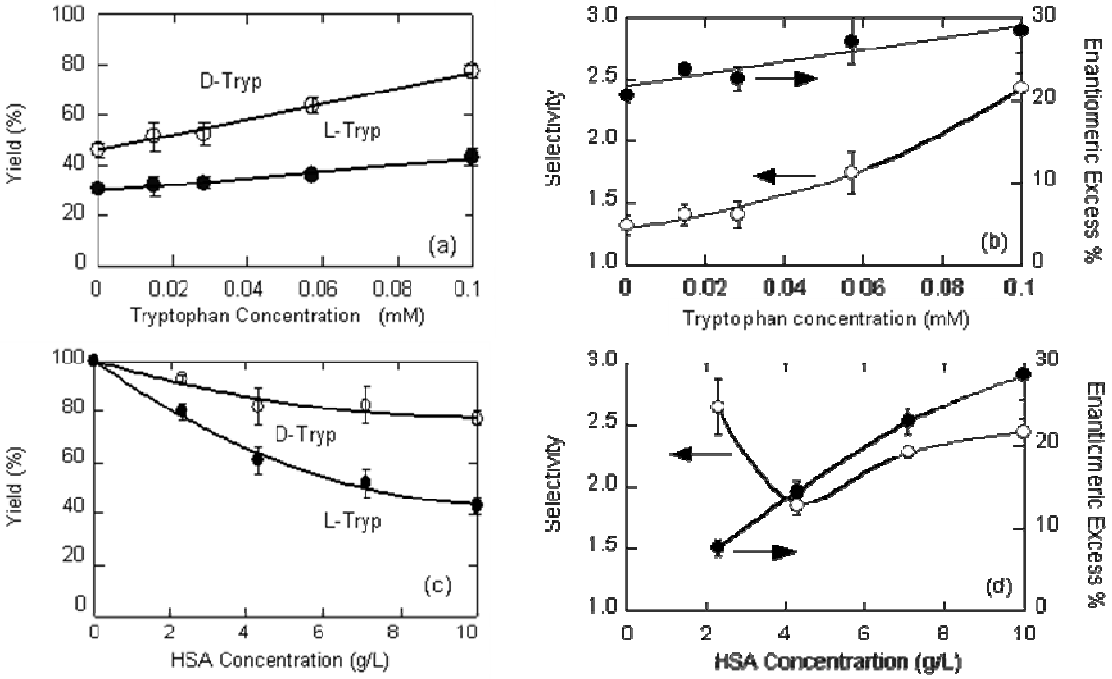

Figure 4.5. Trends of yield, enantioselectivity and enantiomeric excess (ee%) in single cell SPE process with pre-addition of racemic feed in strip. (a) yield of tryptophan from feed chamber in 22 hours vs.pre-added tryptophan concentration in strip; (b) selectivity & ee% vs. pre-added tryptophan concentration in strip; (c) yield of tryptophan from feed in 22 hours vs. HSA concentration in strip; (d) selectivity & ee% vs. HSA concentration in strip.

The effect of HSA concentration on enantioseparation performance was also studied by fixing the pre-added racemic tryptophan concentration at 0.1mM and varying the HSA concentration on the permeate side. The results in Figure 4.5 (c) (d) show a generally decreasing trend in tryptophan yield from the feed chamber but increasing trends in ee% in the final feed solutions and selectivity with HSA concentration, attributed primarily to the preferential permeation enhancement of L-tryptophan induced by the complex formation with HSA, as explained above. However, the selectivity at the lowest HSA concentration was higher than that at other HSA concentrations within the range of experiments. This interesting observation may be attributed to competitive binding between L-tryptophan and D-tryptophan with HSA in the strip side solution when the

HSA concentration (0.035mM) is lower than the pre-added racemic enantiomer concentration (0.1mM). Because of the selective binding of HSA with L-tryptophan, the permeation of D-tryptophan did not increase as much as that of L-tryptophan, resulting in a high selectivity in the L/D-tryptophan separation.

Overall, the effect of HSA addition to the strip solution was to increase the driving force for the permeation flux of enantiomers, with a significantly greater enhancement in the case of L-tryptophan. On the other hand, the effect of pre-addition of feed in the strip was to decrease the permeation flux of enantiomers but more so for D-tryptophan, which resulted cooperatively in higher enantioselectivities.

4.3.3. SPE performance by two permeation cells in series

Although fair enantioseparations were attained in the processes described above, they were considerably inferior to the optimized affinity ultra-filtration (AUF) systems reported by researchers such as Romero and Zydney [22] (selectivity ~ 7). In a typical AUF process, the complexes formed by incorporating a large enantioselective binding agent into a racemic feed solution can be retained by a membrane with a suitable pore size. Consequently, a higher transmembrane flux of the less strongly bound enantiomer is achieved, with good ee% in the filtrate and, after the removal of the binding agent, in the retentate. For comparison, both AUF and SPE processes were carried out using 10g/L of HSA and 0.1mM racemic tryptophan mixtures. The selectivity and ee% in the AUF approach can reach up to 3.01 and 62%, respectively, while the maximum selectivity and ee% are 1.3 and 20%, respectively, in the SPE approach.

To overcome this limitation, we have introduced a novel synergizing strategy by connecting an SPE and an AUF unit in series as depicted in Figure 4.2, which in turn provides an outstanding enantioseparation performance in comparison to that of each respective unit alone. The new approach can integrate the advantages of both SPE and AUF systems successfully. In the SPE unit on the left side, the enantiomers first diffuse from the feed chamber into the HSA chamber, with a higher permeation flux of L-tryptophan as discussed in the previous sections. Thus, while the total concentration of L-tryptophan in the HSA chamber was higher than that of D-tryptophan, the free L-tryptophan concentration was lower since most of the L-tryptophan was bound to HSA. This resulted in a higher concentration gradient of free D-tryptophan than of free L-tryptophan across the membrane in the AUF unit on the right side. Hence, the output strip solution of the AUF unit showed an enantiomeric excess of D-tryptophan, which was higher than that of the single SPE and AUF processes operating individually, as shown in Figure 4.6.

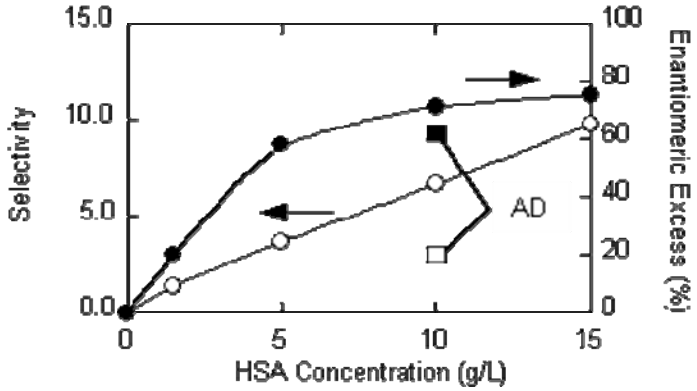

Figure 4.6. Enantioselectivity and enantiomeric excess with various HSA concentrations in central chambers. * AD = Affinity Dialysis

Since the free enantiomer concentrations in the HSA chamber were suppressed by the complex formation with HSA, the flux into the strip chamber of the AUF unit was relatively small; thus the permeate product concentration in the third chamber could be assumed to be linear with time, as shown by the straight lines in Figure 4.7. The permeability coefficients were therefore calculated from the slopes of these lines using the equation

$$P = \frac{GVd}{A(C_F - C_S)} \tag{12}$$

where G, V, d and A are the gradient, strip chamber volume, membrane thickness and membrane area, respectively. C_F and C_S are the corresponding enantiomer concentrations in the feed and strip chambers. The selectivity is the ratio of the enantiomer permeability coefficients, and since other parameter values were the same for both enantiomers, it was calculated from the ratio of gradients only.

$$\alpha = \frac{P_D}{P_L} = \frac{G_D}{G_L} \tag{13}$$

It should be noted that the ee% of the strip solution was calculated instead of that of the retentate in the feed chamber as done in the previous section, since the direct product from the setup was the strip solution, which had a higher ee%. Equation (10) was used by replacing the retentate concentration with the strip concentration.

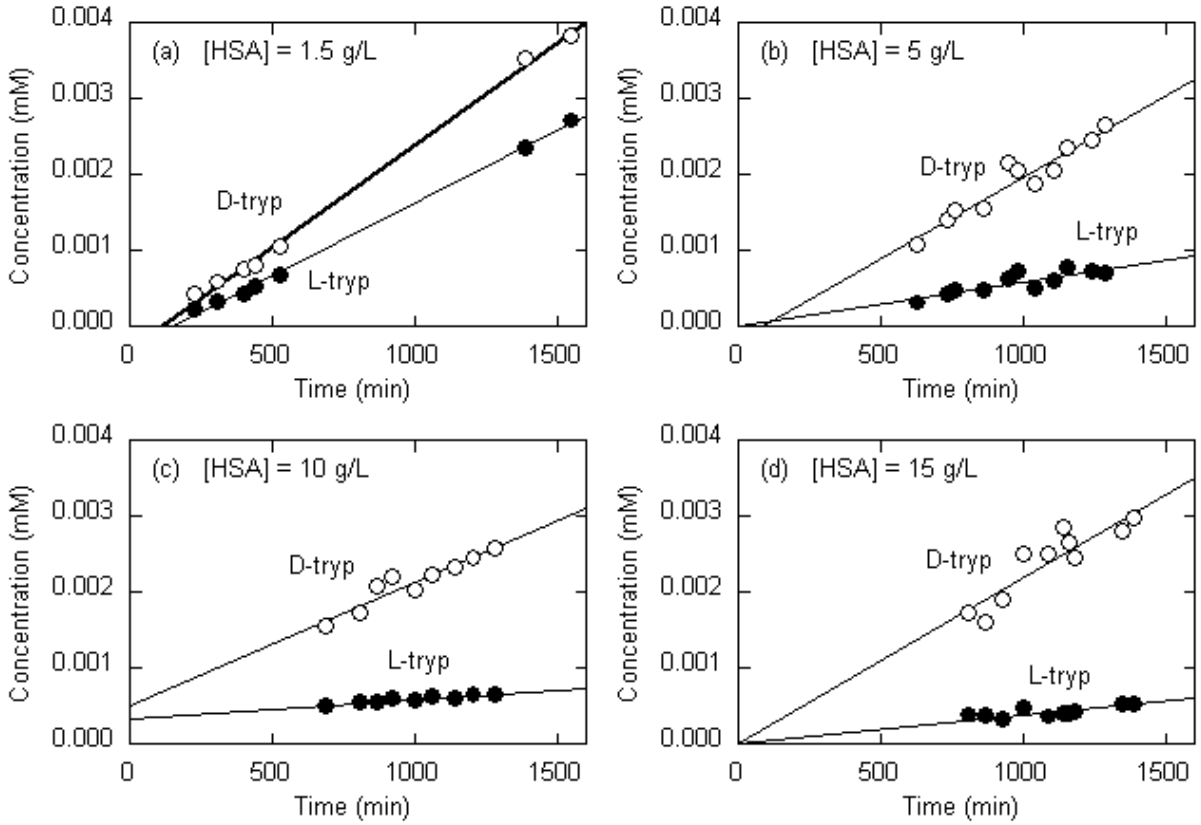

Figure 4.7. Graphs of tryptophan concentrations over time in the third chamber with the HSA concentrations in the central chamber being (a) 1.5 g/L; (b) 5 g/L; (c) 10 g/L; (d) 15 g/L.

It is expected that the separation performance of the SPE-AUF system would outperform the normal AUF system while keeping other conditions equal, as it was observed that higher selectivity and ee% of the product were obtained given the same HSA concentration of 10g/L. One possible explanation was the instantaneous high HSA to enantiomer ratio in the middle protein chamber. In our control AUF experiments, the ratio was around 3:2 (0.15mM: 0.1mM) and slowly increased as the enantiomers permeated through the membrane; however, this value was much larger in the SPE-AUF system. In the HSA chambers, the initial HSA concentration was also 0.15mM while the initial tryptophan concentration was zero and slowly increased with time, resulting in a

much higher overall HSA to tryptophan ratio. As a consequence, the free L-tryptophan concentration in the HSA chamber was maintained always at a very low level due to the formation of a complex with HSA. Thus, a high selectivity was achievable due to the low permeation of L-tryptophan.

A similar reasoning can be applied to explain the increasing trend in selectivity and ee% with higher HSA concentrations in the middle protein chambers. The increased HSA-to-enantiomer ratio with an increase in HSA concentration in the middle chamber decreased the free L-tryptophan concentration in the middle chamber to a greater extent, while the free D-tryptophan concentration was less affected due to its weaker complexation with the HSA. Hence, the permeation of L-tryptophan into the strip chamber was greatly reduced, resulting in a higher enantioselectivity of D-tryptophan over L-tryptophan.

Overall, the complete process can also be viewed as a liquid membrane system where the HSA chamber was the liquid membrane with chiral selectors immobilized in the bulk solution. However, this process exhibits much higher stability relative to common liquid membranes. In this newly proposed process, contamination of the product by the liquid membrane solvent was eliminated as DI water was employed as the sole solvent within the experiments. The cellulose membrane pore size was about 1 nm, much smaller than the size of HSA, and thus contamination by chiral selector leakage was highly unlikely as well.

4.3.4. Modeling of permeation processes

Since the concentration gradient was the only driving force for transport across the membranes, and the cellulose membrane was hydrophilic, membrane fouling was negligible in these experiments. The diffusion constant was calculated simply from the data of one control experiment. The initial conditions were 0.1mM racemic tryptophan in the feed chamber and phosphate buffer without HSA in the strip solution; samples from the feed and strip chambers were taken periodically and analysed by Capillary Electrophoresis. The set of equations (1) and (2), together with

$$V_2 \frac{dC_{L2}}{dt} = \frac{AD}{d}(C_{L1} - C_{L2}) \qquad (3')$$

$$V_2 \frac{dC_{D2}}{dt} = \frac{AD}{d}(C_{D1} - C_{D2}) \qquad (4')$$

was used to find D, with an initial D value calculated from the gradient of permeate concentration against time, and a built in function 'fminsearch', the diffusion constant was estimated to be 3.57×10^{-4} $cm^2 s^{-1}$.

The association and dissociation constants between HSA and L,D-tryptophan were obtained from the work of Yang and Hage [35]. The validity of these constants, together with the calculated diffusion constant, was supported by the close agreement of the *a priori* predictions with experimental results shown in Figure 4.8 for the control affinity ultra-filtration experiments.

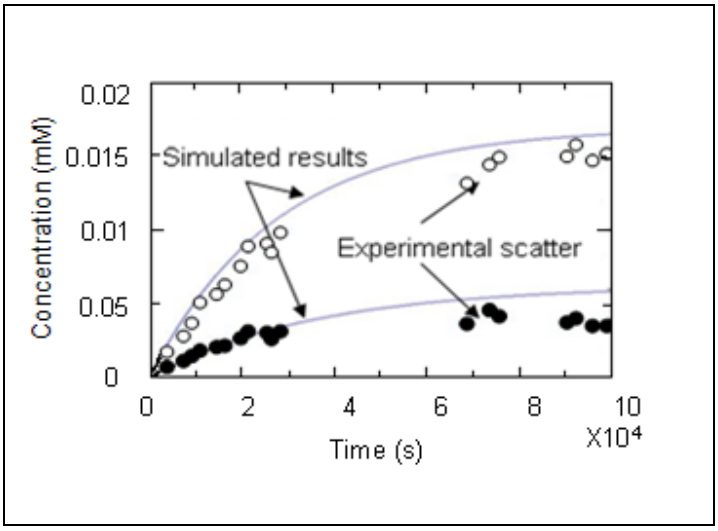

Figure 4.8. Simulated and experimental results of affinity dialysis with 10g/L HSA

A representative simulation of the SPE in series, with a protein concentration of 10g/L, is depicted in Figure 4.9, again showing good agreement between the experimental and modeling results. This result not only validates the model, but also, to a certain extent, the accuracy of the experimental data and the applicability of the SPE system. With this model, it would be possible theoretically to optimize the experimental conditions to achieve the desired separation performance for any pair of chiral selectors and enantiomers as long as their diffusion, association and dissociation constants were available.

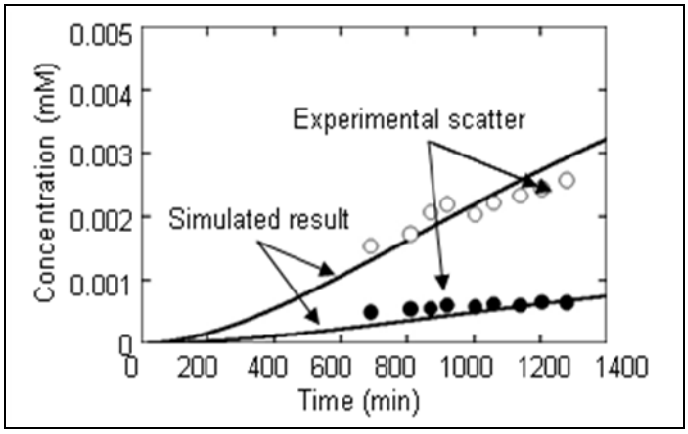

Figure 4.9. Simulated and experimental results of SPE with two cells in series at HSA concentration of 10g/L

4.3.5. Design for large scale applications

As the driving force for the two cells in series design was the concentration gradient only, and the effective membrane area in our experiments was small, the overall permeation flux was relatively low; thus a simple, direct scale-up would not be suitable for real industrial application despite its high enantioselectivity. Inspired by the module designs in other applications [57-60], we propose an improved design making use of hollow fiber membranes instead; the schematic diagram, which is a modification of that for an internally staged permeator [57], is shown in Figure 4.10. The racemic feed and the strip solution flow in the lumen side of each of the two separate bundles of hollow fiber membranes, while the stream containing the chiral selectors flows on the shell side. This design has at least two advantages in comparison to the current experimental setup that greatly increase the permeation flux of the enantiomers. First, the total effective membrane area of hollow fibers is much larger than that of the flat membranes. Second, the hollow fibers in which the feed and strip solutions flow can be closely packed such that the diffusion distance of the enantiomers is shortened. Hence this new design can lead to a much higher permeation flux while maintaining the enantioselectivity. Moreover,

the flow rate and concentration of each stream can be optimized with the aid of mathematical modeling by adopting mass balance equations for processes involving hollow fiber membranes.

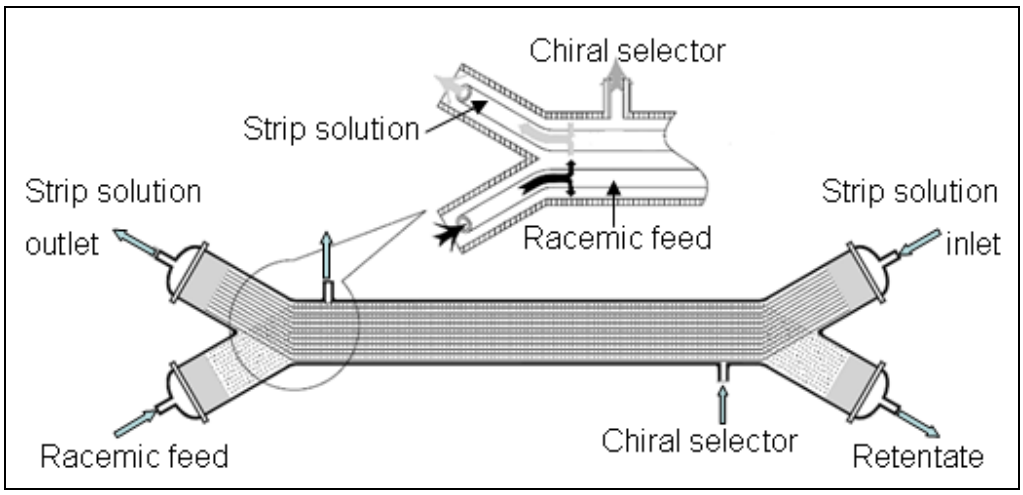

Figure 4.10. Schematic diagram of enantioseparation for industrial application (Modified from Li's work [25])

4.4. Conclusion

In our systematic search for efficient enantioseparation processes, we have studied the performance of a novel operation, SPE, using three different approaches: single cell permeation, pre-addition of feed, and two cells in series permeation. The feasibility of SPE was first demonstrated successfully in the single cell permeation system where trends in selectivity and ee% were elucidated, but limitations on the overall performance were also discovered. These limitations were overcome by the pre-addition of some of the feed solution to the strip solution; better performance was achieved and an increase in the selectivity and ee% with increasing pre-added feed solution was observed. The enantioseparation performance was further enhanced by exploiting the SPE concept using two cells in series to give selectivities of up to 9.76 and corresponding enantiomeric excesses of up to 75%. These performance metrics can be improved further by using a

more concentrated HSA solution. This impressive performance was also predicted by the simulation results. The overall rates of the enantiomeric separation were rather slow in the experimental systems studied because of the small membrane areas relative to the volumes being treated, this limitation can be readily overcome using hollow fiber membrane systems, with two bundles of fibers (for the feed and the stripping solutions) being separated by the chiral selector solution in the shell of the module; this new design should provide for a greatly increased throughput.

4.5. Acknowledgement

We thank the Singapore-MIT Alliance and the National University of Singapore (Grant No.R-279-000-249-646) for funding this project. Thanks are also due to Dr. Li Yi for his invaluable suggestions.

Chapter 5. Enantiomeric resolution of tryptophan via stereoselective binding in an ion-exchange membrane partitioned free flow isoelectric focusing system

5.1. Introduction

Apart from being employed for chiral separations by simple membrane processes as what we have presented in the previous chapters, membranes have also been coupled with other methods, either conceptually or practically, such as chromatography and electrophoresis for better separations. For instance, Wang et al. [61] achieved separation of racemic thiopental and tryptophan via membrane chromatography using a poly (vinylidene fluoride) (PVDF) membrane absorbed with BSA. Isoelectric focusing with the aid of ion exchange membranes is one prominent technology with the potential to produce enantiomeric drugs on a preparative scale. Currently, most research done using isoelectric focusing (IEF) is for protein separations [45-46, 62], by exploiting the different pI values (isoelectric points) of various types of proteins. With the ion exchange membranes separating the buffer chambers of various pHs, a charged biomolecule migrates under an external electric field until it reaches a buffer chamber of pH equivalent to its pI, and then becomes neutral in charge and isolates in this particular chamber. Following this theory, the first isoelectric focusing enantiomer separation was introduced by Righetti et al. [47] who used β–cyclodextrin as the chiral selector for the resolution of dansylated tryptophan and phenylalanine with a pI difference between the complexes of only 0.05. Glukhovskiy et al. [63] also demonstrated high separation efficiency during isoelectric focusing with immobiline membranes (membrane with a pH) in an IsoPrime multi-compartment electrolyzer. However, the high costs of both the immobiline membranes and the ampholyte buffer used in these works are significant

drawbacks that hinder the scale up of this process. Moreover, the immobiline membranes have poor mechanical strength and a short life span, unsuitable for industrial applications [64]. We overcome these limitations by developing a free flow isoelectric focusing (FFIEF) process making use of cheaper and stronger polymeric membranes and phosphate buffer.

In this work, the polymeric membranes were fabricated from sulfonated polyetherketone (SPEK) which carries a negative charge and the buffer used was sodium phosphate. Instead of using neutral chiral selectors such as cyclodextrins, human serum albumin (HSA) was mixed with the tryptophan in the feed chamber. The unbound tryptophan, which contained an enantiomeric excess of D-tryptophan, then migrated into the permeate chamber under the electric field, whereas the HSA-tryptophan complex remained in the feed chamber, in such a way that the enantio-resolution of tryptophan was achieved. Thus, different from the IEF processes presented by other researchers, this FFIEF process isolated not the HSA-L-tryptophan and HSA-D-tryptophan complexes, but the HSA-tryptophan complex and free tryptophan in the feed and permeation chambers, respectively.

The feasibility of this process was demonstrated, with a separation factor greater than 4 using a protein to tryptophan concentration ratio of 0.75. This performance is compared with and proven to be superior to other processes such as affinity dialysis (AD), affinity ultrafiltration (AUF) and separation permeation enhancement-affinity dialysis (SPE-AD) [65]. The separation behavior as affected by the number of buffer chambers and the chiral

selectors was investigated in this study. Overall, this new process is a potential candidate for chiral separations and worthy of further investigation.

5.2. Experimental

5.2.1. Materials

The NEOSEPTA ion exchange membranes used at the anode (CMB C-0346) and cathode chambers (AHA A-0182) were purchased from Astom Corp, Japan. Udel P3500NT polysulfone (Psf) was provided by Solvay, Germany. For synthesis of SPEK polymer, 2,2-Bis(4-hydroxy-3,5-dimethyl-phenyl) propane (TMBPA) and 4,4'-difluorobenzophenone (DFBP) from Tokyo Kasei Kogyo Co. Ltd. and the 50% fuming sulfuric acid, dimethylsulfoxide from Wako Junyaku Kogyo Co. Ltd. were used as received. Sodium hydroxide pellets, human serum albumin (HSA) and bovine serum albumin (BSA) from Sigma Aldrich, disodium hydrogen phosphate, monosodium hydrogen phosphate and N-methyl-2-pyrrolidone(NMP) from Merck, phosphoric acid and isopropanol (IPA) from TEDIA, α-cyclodextrin from Cyclolab and DL-tryptophan from Alfa Aesar, were all reagent grade and used without further purification. For high performance liquid chromatography (HPLC) and Capillary Electrophoresis (CE) tests, the HPLC grade ethanol from TEDIA and ultra pure water from a 'Milli-Q plus 185' pure water system were used.

5.2.2. Synthesis of SPEK polymer

The SPEK polymer was synthesized by Mitsui Chemicals using a method similar to that described by Xiao et al [66]. In a five-necked reactor equipped with a nitrogen-

introducing tube, a thermometer, a reflux condenser and a stirrer, a mixture containing 480g of DMSO, 120g of toluene, 37.16 g (0.088 mol) of 5,5'-carbonylbis(2-fluorobenzene sulfonic acid) sodium salt, 28.80 g (0.132 mol) of DFBP, 62.57 g (0.220 mol) of TMPBA and 36.49 g (0.264 mol) of potassium carbonate was charged, heated to, and maintained at 140 ℃ with stirring for 8 h under a nitrogen atmosphere to remove water generated by the system. The reaction mixture was then distilled for 2 h to remove toluene and diluted by 180 g of NMP after cooling to room temperature. The polymer powder was precipitated by discharging the solution into 2000 g of methanol, then filtered and washed with water. 109.1g (yield of 91%) of polymer product was collected after drying at 80℃ for 10 h and 150 ℃ for 8 h under nitrogen atmosphere. The inherent viscosity of the polymer in a solvent (NMP/DMSO) was 82 cm^3 g^{-1}, measured at a concentration of 0.005 g cm^{-3} at 35 ℃.

5.2.3. Membrane fabrication

A polymer solution was prepared by mixing 11.5 wt% SPEK and 11.5 wt% Psf in NMP. After degassing overnight, the solution was cast on a non-woven cloth with a casting knife of thickness 250 μm. The as-cast membranes were immersed immediately into a pure IPA coagulant bath for 15 min and then in pure water overnight. The prepared membranes were then post-treated with 0.5 M HCl and thoroughly rinsed with water before use.

5.2.4. Membrane characterization

The membrane morphology was observed with a JSM-6700F Field Emission Scanning Electron Microscope (FESEM) with a resolution of 1.0 nm at 5.0 kV. The membrane samples were dried in a freeze drier, fractured in the liquid nitrogen (the non-woven part was cut with a blade) and coated with platinum before the FESEM study.

The membrane pore size distribution was characterized by the solute rejection method [67]. A series of 200 ppm aqueous solutions were prepared from PEG of molecular weight 35 kD and PEO of molecular weights 100, 200 and 300 kD, respectively. Under a pressure of 4.0 bars, the concentrations of retentate (*Cf*) and permeate (*Cp*) were determined with a Shimadzu ASI-5000A total organic analyzer (TOC). The solute rejection (R) was calculated using the following equation:

$$R = \left(1 - Cp/Cf\right) \times 100 \tag{1}$$

A straight line was obtained from the log-normal probability plot of R against r_s (m), the Stokes radii of the solutes which were calculated based on the average molecular weights M (kg/mol) to be:

$$r_s = 16.73 \times 10^{-12} \times M^{0.557} \tag{2}$$

and $$r_s = 10.44 \times 10^{-12} \times M^{0.587} \tag{3}$$

for PEO and PEG, respectively. The mean effective pore radius μ_p was determined at R=50%, the geometric standard deviation σ_p was the ratio of r_s at R = 84.13% and 50% and the molecular weight cut off (MWCO) was obtained at R = 90%. The pore size (d_p) distribution curve was generated with the following probability density function based on the values of μ_p and σ_p:

$$\frac{dR(d_p)}{dd_p} = \frac{1}{d_p \ln \sigma_p \sqrt{2\pi}} \exp\left[-\frac{(\ln d_p - \ln \mu_p)^2}{2(\ln \sigma_p)^2} \right] \quad (4)$$

The membrane surface charge property was measured by a SurPASS electrokinetic analyzer from Anton Paar GmbH, Australia. The membrane was first immersed in a 1M NaCl solution overnight prior to the test, then its zeta potential was measured accordingly in the pH range of 2.2 ~ 9.7 by manual titration to cover the whole range of pH (4 ~ 8) in the FFIEF study.

The ion exchange capacity (IEC) and the degree of sulfonation (DS) were calculated from titration results. A piece of the SPEK membrane was first soaked in phosphoric acid for 24 h, after rinsing repeatedly with pure water, it was immersed in pure water for another 24 h to remove the residual acid. The membrane was then immersed into 25 ml of 0.01 M NaOH for 24 h; the remaining NaOH was titrated against phosphoric acid to calculate the amount of NaOH reacted with the membrane. The DS and IEC were then calculated with the following equations, modified from Guan et al [68]:

$$\mathrm{DS} = \frac{0.196\mathrm{M} \bullet \mathrm{V}}{\mathrm{W} - 0.08\mathrm{M} \bullet \mathrm{V}} \times 100\% \quad (5)$$

$$\mathrm{IEC} = \frac{1000 \times \mathrm{DS}}{196 + 81 \times \mathrm{DS}} \quad (6)$$

where W, M and V are the mass of SPEK (g), concentration of NaOH (mol/L) and volume of NaOH (ml) reacted with the SPEK, respectively; the 196 and 81 are the molecular weights of the PEK repeat unit and the -SO_3H, respectively.

The IEC values of the commercial anion exchange and cation membranes were estimated to be 88.9 meq/ m^2 and 55.6 meq/ m^2, respectively, by performing a similar experiment but applying a different equation as:

$$IEC = \frac{M \bullet V}{A} \quad (7)$$

where A is the membrane area (0.0009 m^2). It should be noted that the IECs of SPEK calculated with both equation 6 and 7 (by changing the area to sample mass) are the same.

5.2.5. Chiral separation in the FFIEF system

The enantio-resolution of racemic tryptophan was conducted using the four-chamber FFIEF system shown in Figure 5.1 & 5.2. The cathode chamber, bounded by an anion exchange membrane, was filled with 0.2 M NaOH and the anode chamber, isolated by an cation exchange membrane, was filled with 0.1 M H_3PO_4. The solution chambers 1 to 4, separated by the as-prepared SPEK ion exchange membranes, were injected with phosphate buffer solutions of 50 mM concentration and initial pH 4, 4.8, 5.8 and 7.5, respectively. The solutions were circulated using a cartridge pump (Masterflex® I/S model 7519-06). With the aid of a computer controlled Metrohm auto titrating system, the pH values were monitored and adjusted by titrating against the two chambers 1 and 4 with 0.3 M NaOH and 0.2 M phosphoric acid, respectively. A separation process in a two-chamber system was also carried out in a similar manner except that the titrants were injected directly to the feed and permeate chambers.

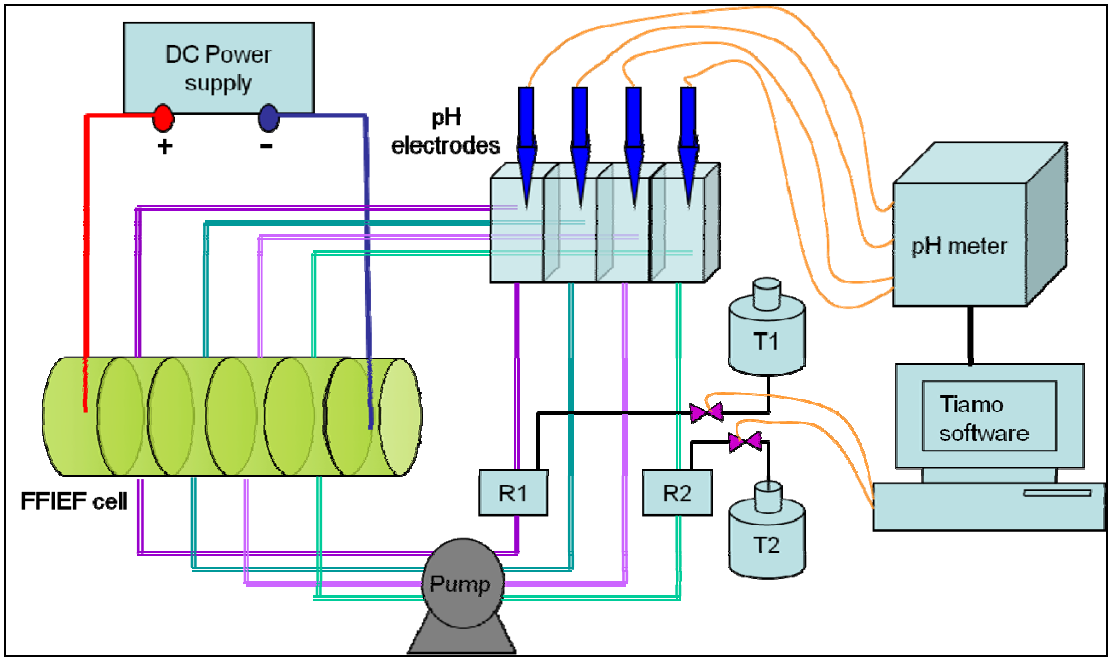

Figure 5.1. Schematic diagram of FFIEF setup

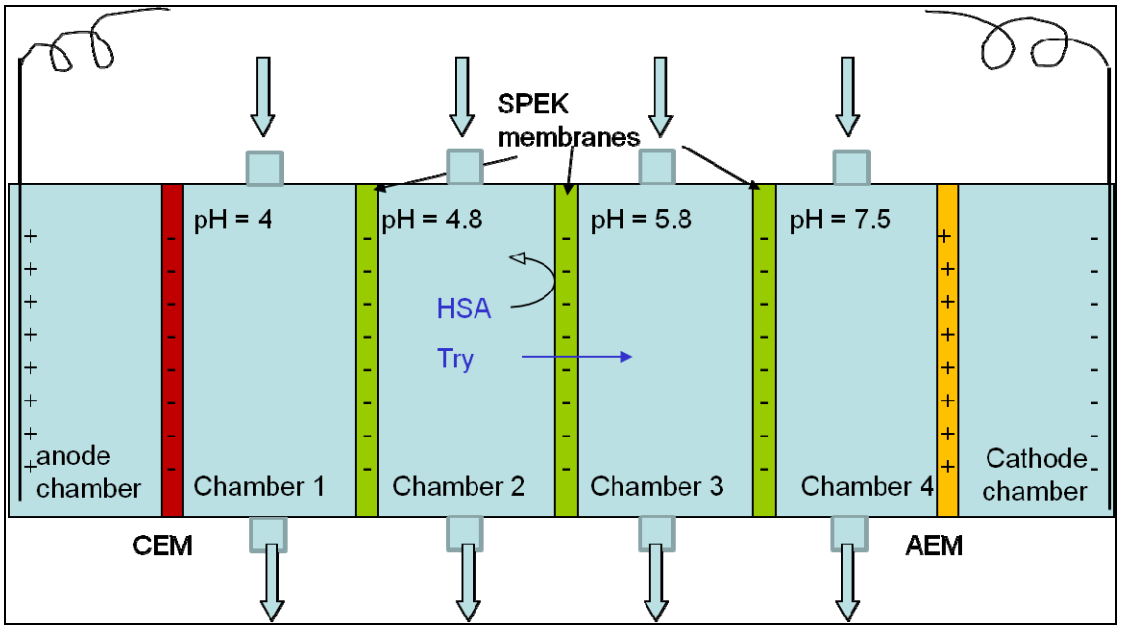

Figure 5.2. The detail representation of the FFIEF cell

The feed solution in chamber 2 was 0.1 mM racemic tryptophan mixed with a certain concentration of proteins (HSA & BSA). Under the electric fields generated by direct currents of various magnitudes, between the two circular electrodes made of nickel plates

located in the anode and cathode chambers, the free tryptophan migrated into chamber 3 across the SPEK membrane while the protein-tryptophan complexes were retained by the membrane due to both size and charge effects. A UV-Vis spectrometer was also employed to monitor the general concentration variation in the chamber 3. For the accurate measurement of concentrations of tryptophan, 200 μl of samples were taken from the feed solution periodically and analyzed by Capillary Electrophoresis (P/ACE MDQ capillary electrophoresis system, Beckman). The CE buffer was a 50 mM α-cyclodextrin solution of pH 2.2 generated with 20 mM phosphate. The sample injection time was 7.5 s at 0.8 psi (5516 Pa) and the forward separating voltage was 15 ~ 25 kV. An Agilent 1200 HPLC equipped with a Chirobiotic T from Astec Inc was also used for the measurement with the following analytical conditions: a 20:80 wt% ethanol:water mixture mobile phase at a flow rate of 0.8 ml/min, column temperature of 298 K and UV detection at 214 nm.

5.2.6. Control experiments of affinity dialysis & affinity ultrafiltration

In affinity dialysis, a mixture of tryptophan and protein was injected into the feed chamber of a dialysis cell similar to that presented in our previous work [69], while the permeate chamber was filled with buffer of the same concentration. Samples were withdrawn from the permeate chamber periodically and analyzed using HPLC. The SPE-AD experiment was performed in [65]: two dialysis cells were connected in series; the racemic feed and the HSA were injected into the first chamber and the middle chambers (2^{nd} & 3^{rd}), respectively. The tryptophan thus diffused through the protein chambers with different rates to the 4^{th} chamber, where samples were collected and analyzed in CE. For

affinity ultrafiltration, a trans-membrane pressure of 4 bars was employed as the driving force instead of just the concentration gradient as in dialysis. The schematic diagram of the setup is shown in Figure 3. The filtrate collected periodically from the outlet was analyzed with HPLC as well.

5.3. Result and discussion

5.3.1. Electric properties of the membranes

The DS and IEC values of the SPEK material are calculated to be 11.2% and 0.55 meq/g, respectively, suggesting the successful sulfonation of the PEK polymer, which is further proven by the zeta potential measurement of the fabricated SPEK membrane as shown in Figure 5.3, since the $–SO_3H$ group contributes the negative charges. By increasing the pH, more $–SO_3H$ groups are ionized to become $–SO_3^-$, hence a more negative zeta potential is measured. The curve reaches a plateau after pH 7 when the sulfonyl groups are almost fully ionized.

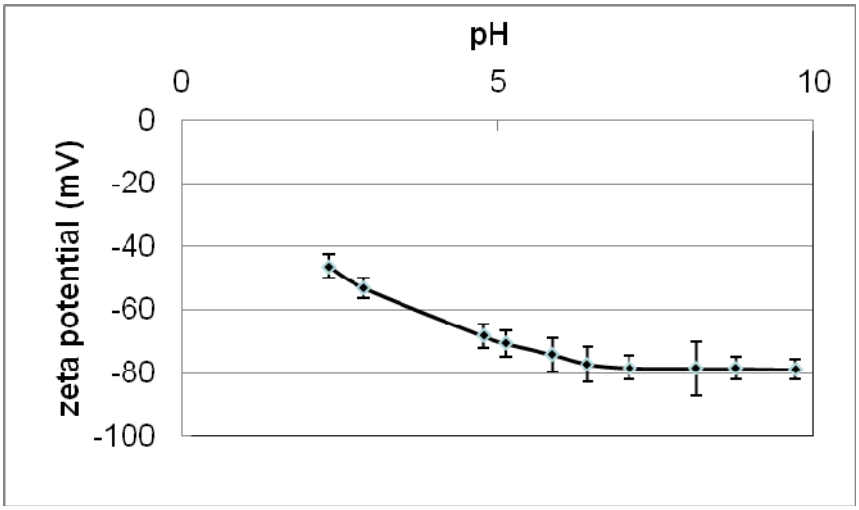

Figure 5.3. The zeta potential of the SPEK membranes

5.3.2. Comparison between FFIEF systems with two and four chambers

The pH stabilities of the two systems with two and four chambers are compared using the time dependent pH in the various chambers shown in Figure 5.4. Neither system shows perfectly horizontal straight lines; however, poorer pH stability in the two-chamber system was still observed, as evidenced by the significant decrease in the feed chamber pH. Two causes may account for this phenomenon. First, the influx of H^+ from the anode chamber reduced the pH, which overpowered the pH increment by the NaOH titrant for the two chamber system; this was solved by using more concentrated NaOH such that the H^+ from the anode chamber can be neutralized in time. Another factor was the time lag inherent in the system design: the titrant was injected into the reservoir (R1 in Figure 1) first before it reached the buffer chamber, such that the total time for thorough mixing was prolonged. This may have resulted in addition of either excess or insufficient titrant if the titrant was concentrated or dilute, respectively. Thus, coupled with auto-titration, manual adjustment was also employed occasionally in the subsequent runs.

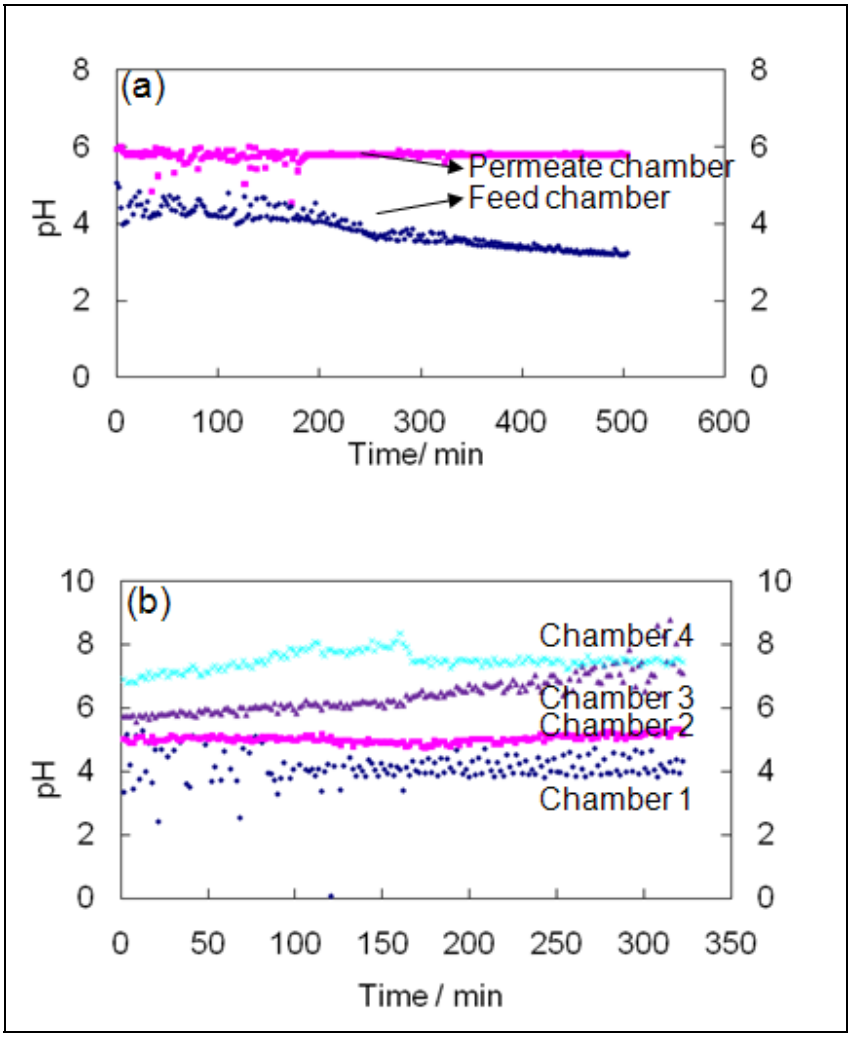

Figure 5.4. The pH changes with time in (a) the two chambers FFIEF and (b) the four chambers system

For results obtained with the four-chamber system shown in Figure 5.4(b), the pH of chamber 2 (feed chamber) was kept stable at around 4.8~5.0, and that of chamber 4 at 7.3~7.5; however, the pH in chamber 3 slowly increased and that of chamber 1 fluctuated with time. The instability in chamber 1 was mostly due to the limitation of the equipment as discussed above and the slight increment in pH in chamber 3 might have been due to the influx of small amount of hydroxide ions originating from the cathode chamber. Such

small disturbances in pH gradient can apparently be tolerated by the system since a steady trans-membrane flux of tryptophan was recorded by the UV spectroscopy.

The two-chamber system was not only poorer in pH stability, but also less productive as the tryptophan flux across the membrane was much lower compared to that in the four-chamber system. The L-tryptophan and D-tryptophan fluxes calculated using a method described in section 2.3 were 0.48 $\times 10^{-7}$ mol $cm^{-2}s^{-1}$ and 1.56×10^{-7} mol $cm^{-2}s^{-1}$, respectively, about 3 times lower than those obtained with the four-chamber system under the same driving force of 80mA operating current (Figure 5.5). The main factor responsible for the low fluxes was a decrease in electro-osmotic flow, as a result of increasing ionic strength in the feed chamber due to the continuous titration of the H^+ migrating from the anode chamber; such an effect has been observed in capillary electrophoresis (CE) [70-71], the transport characteristics of which are closely analogous to those of membrane pores. In the four-chamber system, the titrations were done in chambers 1 and 4 such that the ionic strengths of the solutions in the feed and permeate chambers were less affected, and thus so was the ionic strength in the pores of the membrane partitioning these two chambers. Hence, the four-chamber system resulted in higher fluxes and was used in the subsequent tests.

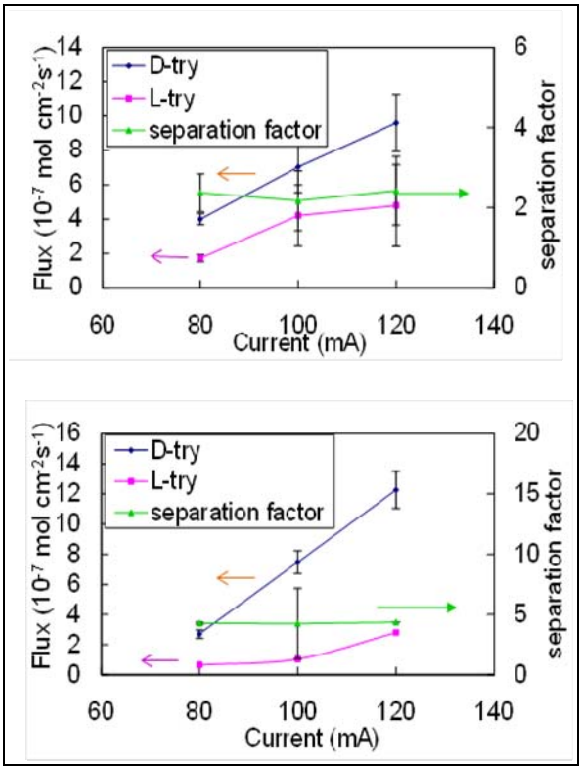

Figure 5.5. The variation of permeation fluxes and separation factors with operating current in FFIEF with HSA concentrations of 0.0375mM (top) and 0.075mM (bottom).

5.3.3. The separation behavior of FFIEF

The separation behavior of FFIEF was scrutinized in depth by investigating the enantio-resolution performance changes with varying operating current and protein:tryptophan ratio. The change in enantiomeric excess with time was also studied. The performance was characterized in terms of two metrics, permeation flux and separation factor, the calculation methods for which we presented in section 2.3 & 2.4.

The driving force is often an important factor determining the performance of a membrane system. Usually, a large driving force (concentration gradient, pressure, voltage, etc) gives higher permeability and lower selectivity. In this section, the effect of

the driving force in FFIEF, the operating current, on the separation of tryptophan were investigated. As expected, the permeation fluxes of both enantiomers increased with operating current as shown in Figure 5.5, in accordance with the transport behavior described by Ennis et al. [72] as captured by the following equation:

$$\frac{dC_i}{dt} = \frac{\mu I C_i}{V_A \lambda_p} \tag{8}$$

where C_i, μ, t, I, V_A and λ_p denote the tryptophan concentration in the feed, mobility, time, operating current, volume of feed chamber and conductivity of the fluid in membrane pores, respectively. It is clear that an operating current of high magnitude resulted in a more rapid change in tryptophan concentration, i.e. in a higher flux. According to this relationship, even higher fluxes would be achievable if the system operated with currents larger than 120mA. However, the joule heating effect, represented by Joule's first law $Q = I^2 \cdot R \cdot t$ (where Q, I, R, t are the heat, current, resistance and time, respectively), becomes significant with currents above 120mA resulting in an elevated buffer temperature above 300 K, which has two negative impacts on separation. First, as shown by Yang and Hage [35], decreasing trends in equilibrium constants are observed for the binding of HSA to both L-tryptophan and D-tryptophan with increasing temperature from 277 to 318 K, where the decrease for L-tryptophan binding constants is to a greater extent, such that the selectivity of HSA is reduced. Second, the protein may denature at these higher temperatures. Hence, the highest current applied in these experiments was 120mA.

It is interesting to note in Figure 5.5 that the separation factor is not affected by a high operating current and only the permeation fluxes are enhanced, due to the nature of this affinity separation process, which is different from processes using chiral selective

membranes. In such processes, the membrane achieves separation by either binding to one enantiomer or rejecting the other, a large driving force may decrease the separation factor by either disassociating the binding of the preferentially bound enantiomer or forcing the rejected enantiomer through the membrane. However, in the FFIEF system, the ratio of free L-tryptophan to D-tryptophan in the feed chamber is invariant with respect to the current applied, and the SPEK membrane shows no preferential interaction with either enantiomer, so that the ratio of L-tryptophan to D-tryptophan permeate through the membrane is unaffected. The separation factor is therefore almost constant with increasing current.

The effect of HSA:tryptophan concentration ratio was also determined in this system. It has been shown in our previous work [65] that the selectivity is enhanced by increasing the HSA concentration while keeping a constant tryptophan concentration. Similar behavior was also observed in the FFIEF process: the separation factor increased from about 2.3 to 4.3 when the HSA concentration doubled from 0.0375mM. With a higher concentration of HSA, more HSA-tryptophan complexes were formed according to the two equations below:

$$HSA + L_{tryp} \xleftrightarrow{K_1} HSA\text{-}L_{tryp} \quad (A)$$

$$HSA + D_{tryp} \xleftrightarrow{K_2} HSA\text{-}D_{tryp} \quad (B)$$

where K_1 and K_2 are the equilibrium constants and $K_1 > K_2$. Due to its preferential binding to HSA, the free L-tryptophan concentration in the feed chamber was reduced to a greater extent than was the D-tryptophan concentration. Hence, the trans-membrane flux of L-tryptophan was reduced with increasing HSA concentration, while that of D-

tryptophan was less affected, as shown in Figure 5.6. As a result, the separation factor was duly enhanced.

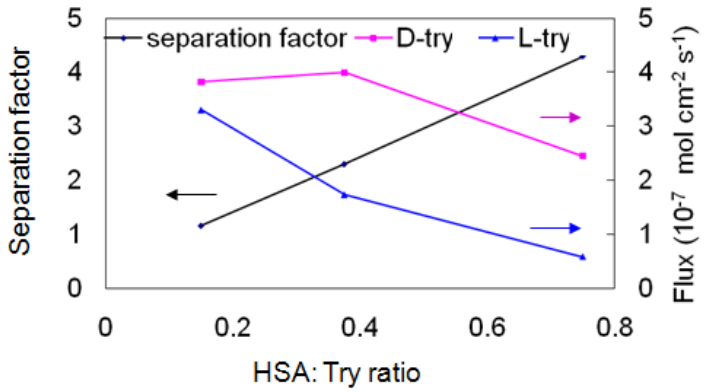

Figure 5.6. The changes of separation factor and flux with the HSA: tryptophan ratio.

Another noteworthy phenomenon observed in the FFIEF processes is the slow reduction, the degree to which varied in different experiments, in the enantiomeric excess of the permeated tryptophan with time as shown in Figure 5.7. This is partly due to adsorption of the biomolecules on the ion exchange membranes. It has been shown that the zwitterionic form of the amino acids interacts with the membrane and compromises its conductivity [73], as proven by the observation of an increase in voltage during the experiment while keeping a constant operating current. Effectively only trace amounts of L-tryptophan permeated through the membrane at the beginning. Another factor is the slow migration of the HSA-tryptophan complexes into the permeate chamber over long experimental times. As these complexes contain higher concentrations of L-tryptophan due to stronger binding, the overall enantiomeric excess of D-tryptophan is reduced. To solve this problem, ion exchange membranes with optimized pore sizes can be designed, which will be discussed in future work.

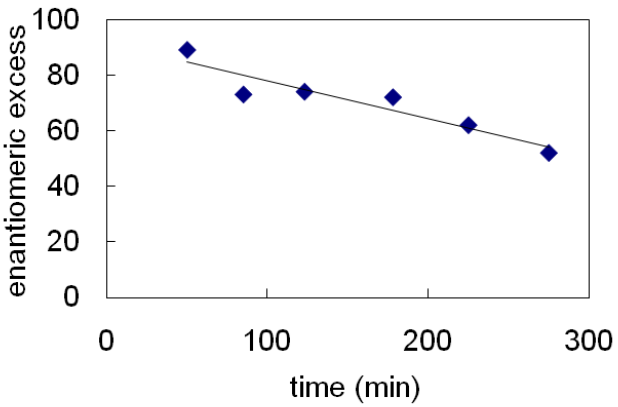

Figure 5.7. The change of ee% with time of one typical experiment conditions: feed solution of 0.075mM HSA and 0.1mM tryptophan, operating current of 80mA.

5.3.4. Separation performance of FFIEF compared to other processes

The enantio-resolution efficiency of the FFIEF process is compared with other processes in this section. Using the membranes prepared in the same batch and under exactly the same experimental conditions, chiral separation of tryptophan was carried out in FFIEF, AD and AUF. The experimental results, together with the values obtained from SPE-AD using the same protein concentration [65], are listed in Table 5.1 from which it is clear that the best performance is achieved by the FFIEF process.

Processes	Driving force	Flux (10^{-7} molcm^{-2}s^{-1})		Separation factor
		L-try	D-try	
SPE-AD	Concentration gradient	1.25	4.64	3.69
IEF	120mA	2.81	12.26	4.36
AD	Concentration gradient	7.56	8.38	1.11
AUF	4 bars	289	297	1.03

Table 5.1. Comparison of chiral separation performances of various membrane processes with the same protein concentration of 0.075mM.

Both AD and AUF give separation factors close to unity; these low values are mostly attributable to the lower intrinsic selectivity related to low buffer pH. This phenomenon has been reported by many researchers [35, 74]; the optimum separation performance was achieved at a high pH of 8.0 ~ 9.0, whereas the separation factor at pH lower than 5.0 approached unity. Moreover, the binding constants for both L-tryptophan and D-tryptophan to HSA are also small at lower pH. Thus relatively high concentrations of both free L-tryptophan and D-tryptophan are present in the feed chamber, resulting in the lower separation factors and higher permeation fluxes observed in AD and AUF. The high flux of AUF was mainly due to the direct transport of feed solution across the membrane with poor retention under high pressure, different from the diffusion mechanism in AD. Moreover, as the hydrodynamic radius of HSA (7-8nm) [75] was smaller than some of the membrane pores, the distribution of which is plotted in Figure 5.8, the protein was not rejected efficiently in this process; Figure 5.9(a) shows that a high concentration of HSA was detected in the permeate chamber. This further decreased the enantiomeric excess of D-tryptophan in the permeate chamber, and an even lower separation factor than that for AD was obtained.

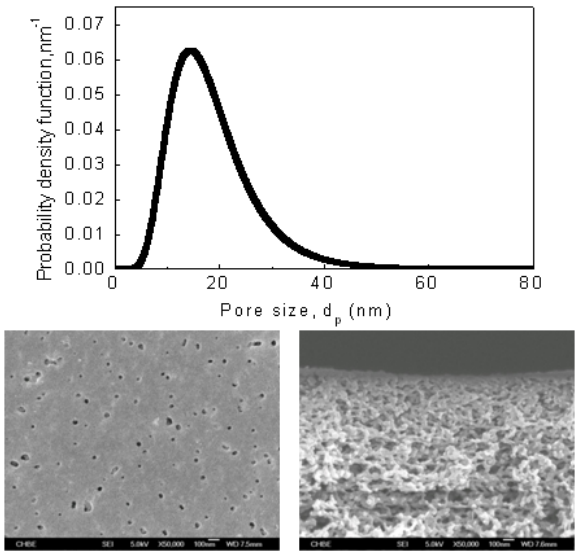

Figure 5.8. (top) Pore size probability density plot of the SPEK membrane; (bottom) FESEM images of the ion exchange membrane: top surface (left) and cross section (right).

The permeation fluxes in the FFIEF process were more than double those observed in SPE-AD. This was to be expected as the transport of the tryptophan was enhanced under an electric field. Moreover, the FFIEF even demonstrated a slightly higher separation factor than SPE-AD, despite the fact that the latter operates at a much higher pH of 8.6 and by right should yield better separation results. This is mainly due to the penetration and adsorption of the HSA inside the membranes driven by the electric field. Through a second stage binding between the tryptophan and HSA in a confined space (membrane pores in this case), such that the L-tryptophan is preferentially bound inside the membrane and experiences a larger transport resistance, the enantioselectivity can be greatly enhanced, as discussed by Wang et al. [55]. Another possibility is that the unfolding of the HSA at low pH that loosened the stereo structure at the binding site may be intervened by the electric field. However, the detailed mechanism is still unknown and need further investigations.

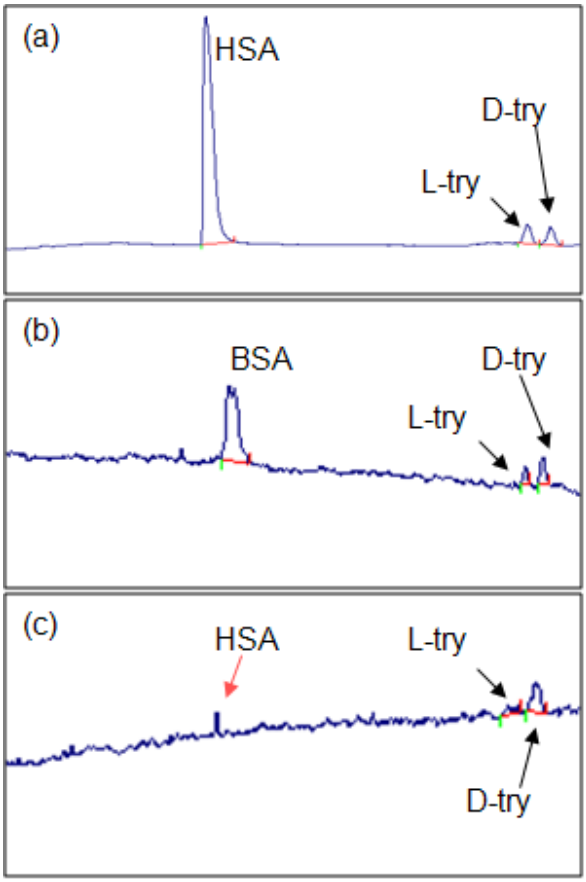

Figure 9. The electropherograms of the permeate solutions from (a) AUF at 10 minutes; (b) FFIEF with 0.0375mM BSA at 5 hours and (c) FFIEF with 0.0375 HSA at 5 hours.

Hence, the FFIEF process outperforms other processes as it demonstrates the highest selectivity with the same concentration of chiral selectors used, and is the most tolerant to relatively larger pore sizes.

5.3.5. Comparison of separation performance using HSA and BSA

It would be desirable to substitute bovine serum albumin (BSA) for HSA in this FFIEF process since it has the same amino acid sequence but much lower cost, provided it did not adversely affect the separation performance. However, the resolution efficiency on racemic tryptophan using BSA was unsatisfactory; higher fluxes but lower separation

factors in comparison with the results of HSA were obtained as shown in Table 5.2. One factor accounting for this poor separation efficiency with BSA is its lower intrinsic selectivity [76], which resulted in higher concentrations of free tryptophan present in the feed chamber with a smaller ratio of free D-tryptophan to L-tryptophan than when HSA was used as the chiral selector, such that the fluxes were enhanced but the separation factor of D-tryptophan over L-tryptophan was compromised.

Current	Protein conc /mM	Tryp conc /mM	Flux (10^{-7} molcm^{-2}s^{-1})		Separation factor
			L-try	D-try	
80mA	0.0375(BSA)	0.1	5.86	11.3	1.9
	0.0375	0.1	1.52	4.31	2.8
100mA	0.0375(BSA)	0.1	4.87	9.76	2.0
	0.0375	0.1	1.33	4.81	3.6
	0.075(BSA)	0.1	8.3	12.0	1.4
	0.075	0.1	1.04	7.47	7.1

Table 5.2. The chiral separation performance of BSA and HSA.

Another important factor is the smaller hydrodynamic radius of BSA compared to that of HSA. As briefly mentioned in previous sections, the protein-tryptophan complexes can pass through the membranes under high pressures. It was also found that the protein complexes, though mostly retained by the negatively charged membranes, do leak slowly across the membrane after some hours under the electric field since both the hydrodynamic radii of BSA (4-5nm) [77] and HSA (7-8nm) [75] are smaller than the membrane pores. With a smaller radius, a larger number of BSA complexes passed into the permeate chamber as evidenced by the larger peak for BSA in Figure 5.9 (b) and (c) and the enantiomeric excess of D-tryptophan was more strongly compromised.

5.4. Conclusion

The FFIEF process using SPEK membranes has been applied in the enantio-resolution of racemic tryptophan. A four-chamber system was used to investigate the chiral separation behavior of FFIEF with HSA as the chiral selector. The separation data are encouraging, and are superior to those obtained for processes such as AD, AUF and SPE-AD with key parameters unvaried, i.e. using the same concentrations of chiral selectors. Although a few drawbacks such as long term stability have surfaced, this process is nonetheless a potential new candidate for membrane chiral separation as these issues can be resolved by optimizing the experimental parameters through fabricating new membranes and changing buffer concentrations and chiral selectors, etc, which will be discussed in future works.

5.5. Acknowledgements

We thank the Singapore-MIT Alliance and the National University of Singapore (Grant No.R-279-000-249-646) for funding this project. Special thanks are also due to Dr. Natalia Widjojo for her invaluable help.

Chapter 6. The exploration of the nature of the driving forces on the enantiomer resolution performance

6. 1. Introduction

Cellulose acetate (CA) is the first material for membrane fabrication by phase inversion technology in 1960s [78], and has wide application in water treatment and purification via various membrane processes, i.e. ultrafiltration, nanofiltration, reverse osmosis and forward osmosis [79-82], etc. And with suitable functionalization [83] and molecular imprinting [84] treatment, it has also been used for chiral separation. In this work, instead of using chiral recognition molecules such as proteins or cyclodextrins, a common polymer, chitosan (CS) which shows enantioselective absorption of amino acid resolution [39-40], is for the first time employed in the functionalization of the cellulose acetate membranes. This replacement brings the advantages of low material cost, low toxicity comparing with crown ether for instance, and better stability considering the denaturation involved in biomolecules such as enzymes and albumin proteins.

The enantiomeric resolution of tryptophan using the CS functionalized CA membranes have been carried out in three systems utilizing different driving forces, namely electric field, concentration gradient and hydraulic pressure. The highest enantiomeric excess (ee%) above 90% is obtained in the concentration driven process and interestingly, a permeating solution with a reversed ee% (L-trp rich) of -19% is resulted in the electric field driven process. Similar behavior is also observed in the resolution of phenylalanine. The effects of membrane fabrication protocols, functionalization and other experimental conditions are also investigated in this study. Overall, we have proven the feasibility of the as-prepared membrane in enantiomeric resolution and understand its different

separation behaviors under various driving forces, which can contribute significantly to the current chiral separation studies.

6.2. Experimental

6.2.1. Materials

The dense ion exchange membranes used at the anode and cathode chambers were purchased from Astom, Japan. The cellulose acetate (CA-389-30) and chitosan (CS) polymer were purchased from Eastman Chemical Company and Sigma, respectively. Sodium hydroxide pellet and glutaraldehyde from Sigma Aldrich, disodium hydrogen phosphate, monosodium hydrogen phosphate, and formamide from Merck, acetone, phosphoric acid and acetic acid from TEDIA, cyanuric chloride from Tokyo Kasei Kogyo Co. Ltd and DL-tryptophan from Alfa Aesar were all reagent grade and used without further purification. For analysis done with the high performance liquid chromatography (HPLC), the HPLC grade ethanol from TEDIA and ultra pure water from a 'Milli-Q plus 185' pure water system were used.

6.2.2. Membrane fabrication

A polymer dope solution was prepared by dissolving 23 wt% CA in pure acetone. It was then cast on a non-woven cloth with a casting knife of thickness 250 μm after degassing overnight. The as-cast membrane was allowed for solvent evaporation for a short time before immersing into the pure water coagulation bath. The membrane was then washed several times with and stored in pure water before further post-treatments.

6.2.3. Membrane functionalization

The CA membrane was immersed in a 3 wt% cyanuric chloride solution (solvent is 50:50 xylene-dioxane) for 40 minutes and then in 2.5wt% chitosan aqueous solution for 20 hours. After rinsing with a 0.1M acetic acid solution, the grafted chitosan was then crosslinked with a 2.5% glutaraldehyde solution. All reactions were carried out at room temperature.

6.2.4. Membrane characterization

The element ratio on the membrane surface was analyzed by an X-ray photoelectron spectrometer (AXIS His spectrometer from Kratos Analytical Ltd, England) using a monochromatized Al Kα X-ray source (1486.6 eV photon) at a constant dwell time of 100ns and a pass energy of 40 eV. The anode voltage and current were 15kV and 10mA respectively while the pressure in the analysis chamber was kept lower than 5.0e-8 Torr. The photoelectron takeoff angle was 90° with respect to sample surface and the X-ray penetration depth was about 5-7nm.

The surface morphology of the membranes was analyzed in a Nanoscope IIIa AFM from the Digital Instruments Inc. For each membrane, an area of 1 μm × 1 μm was scanned using the tapping mode at a rate of 1 Hz. The membrane morphology was also observed with a JEOL JSM-5600LV Scanning Electron Microscope (SEM) prior to which the membrane samples were first dried in a freeze drier, fractured in the liquid nitrogen (the non-woven part was cut with a blade) and then coated with platinum using a JEOL JFC-1300 Platinum coater.

6.2.5. Enantiomer resolution tests

The enantiomeric resolution of tryptophan was carried out in three setups with different driving forces, namely pressure driven, concentration gradient driven and electric field driven processes. In the pressure driven mode, a dead-end static permeation cell as shown in Figure 6.1 was employed. A pressure of 8 bars was supplied from a compressed air cylinder to drive the racemic mixture of tryptophan in the feed chamber across the membrane located at the bottom of the cell; the permeate solution at the outlet was collected and analyzed in an Agilent 1200 HPLC. A Chirobiotic T HPLC column from Astec Inc was used in the measurement with the following analytical conditions: a mobile phase containing 20:80 wt% ethanol:water mixture at a flow rate of 0.8ml/min, a column temperature of 298K and the UV detection at 214nm.

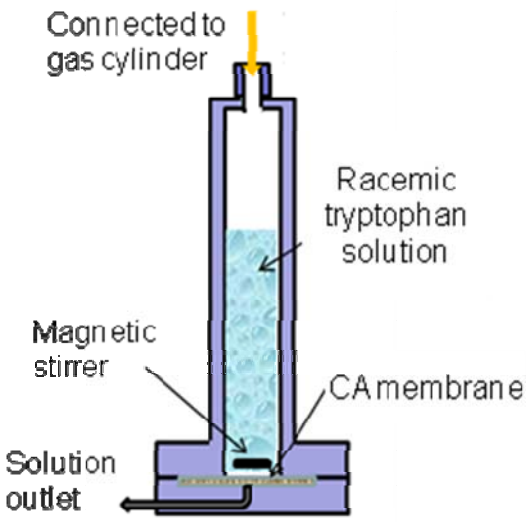

Figure 6.1. the schematic diagram of the pressure driven process.

For the concentration gradient driven process, the racemic tryptophan feed and a buffer of the same concentration were injected into the feed and permeate chambers of a permeation cell shown in [69]. Solutions in both chambers were stirred with Teflon

impellers connected to an overhead stirrer (CAT R18, M. Zipperer GmbH, Staufen, Germany) at 200 rpm. Samples of 100 μl were withdrawn from the permeate chamber periodically and analyzed in HPLC as well.

A free flow iso-electric focusing (FFIEF) system as shown in Figure 2 was employed in the performance test of the electric driven process. The anode chamber and cathode chambers were filled with 0.1M H_3PO_4 and 0.2M NaOH solutions, respectively; while the solution chambers 1 and 2, separated by the functionalized cellulose acetate membranes with the non-woven surface facing the cathode, were filled with 50 mM phosphate buffer solutions with the initial pHs of 3 and 8 respectively. The racemic tryptophan feed was injected in the chamber 1. Both buffer solutions were circulated with a cartridge pump (Masterflex® I/S model 7519-06) and the positively charged molecules were driven by the electric field generated with a Bio-Rad power Pac HV 5000. The solution pH values were monitored and adjusted with the aid of a computer controlled Metrohm auto titrating system with a 0.3M NaOH and a 0.2M phosphoric acid as the titrants, respectively. Samples were collected from the chamber 2 periodically and analyzed in HPLC as well. The permeation fluxes j, separation factor SP and enantiomeric excess ee% were calculated using the following equations:

$$j_i = \frac{C_i V}{A\,t} \tag{1}$$

$$Sp = j_D / j_L \tag{2}$$

$$ee\% = \frac{(C_D - C_L)}{(C_D + C_L)} \tag{3}$$

where the C, V, A and t denote the concentrations in the product, volume of the permeate chamber, membrane effective area and experimental time, and the substrate $_D$ and $_L$ denote the D-trp and L-trp.

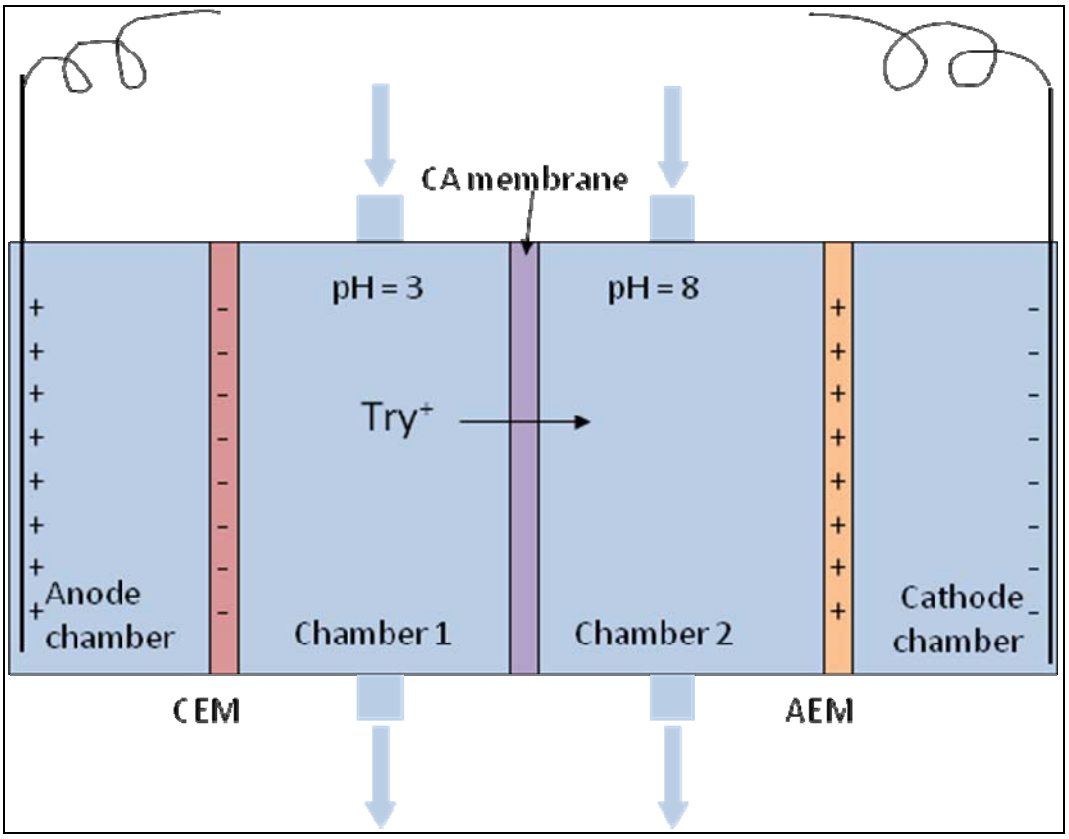

Figure 6.2. the schematic diagram of the electric driven process. * CEM: cation exchange membrane; AEM: anion exchange membrane

6.2.6. Computer experiments

The total minimized energy of each molecular structure was calculated with the aid of the Material Studio 4.3 Visualizer software package from Accelrys Inc. First, the tryptophan molecules, the copper complexes and the chitosan polymer chains were constructed with the builder visualizer directly and optimized by the Discovery module with the pcff force field to get the equilibrium state structures at minimized energies. Second, an amorphous cell comprising of chitosan polymer chains and free tryptophan molecules were generated

using the Amorphous module to simulate the interactions between L,D-tryptophan and chitosan; the minimized energies were then calculated by Discovery module in pcff force field.

6.3. Result and discussion

6.3.1. Membrane characterization

The functionalization of chitosan on the cellulose acetate membrane surface is proven by the XPS analysis and the results are tabulated in Table 6.1. The nitrogen atomic percentage content of the unmodified CA membrane analyzed by XPS is 0 since there is not any nitrogen atom in the CA polymer chain. However, the atomic percentage ratio increases to 0.5 after the membrane reacts with cyanuric chloride, the molecular structure of which has three nitrogen atoms in its aromatic ring. This increment in nitrogen content shows that the cyanuric chloride has been attached to the membrane surface. Further increase in nitrogen content to 0.9 has been observed on the membranes after chitosan functionalization, indicating the successful grafting of chitosan polymers onto the membrane surface as the chitosan also contains nitrogen atom. The increase in carbon and the decrease in oxygen contents are mainly due to the glutaraldehyde in the post treatment which has a high carbon to oxygen ratio.

Membrane	C%	O%	N%
CA23- unmodified	65.1	34.9	0
CA23- *CC activated	65.9	33.6	0.5
CA23- chitosan modified	72.6	26.5	0.9

Table 6.1. The element ratio on the membrane surface by XPS analysis.
*CC = cyanuric chloride

The changes in the membrane morphology have been demonstrated by the AFM observation shown in Figure 6.3. The membrane surface becomes rougher after reaction with cyanuric chloride and regular nodules are observed after chitosan functionalization. Thus the thickness of the chitosan layer covering the membrane surface is not uniform throughout, which is shown more clearly by a larger picture from the SEM observation in Figure 6.3 (d). It can be concluded from these observations that the chitosan aggregates function more as an absorber to tryptophan than a uniform membrane that controls both the adsorption and diffusion of the tryptophan. Thus the enantiomeric separation is mainly achieved by the higher absorption of the more strongly bound enantiomer (L-trp) at the membrane surface, which results in the decrease in the free L-trp concentration in the feed chamber and therefore the lower transmembrane flux of L-trp than that of D-trp.

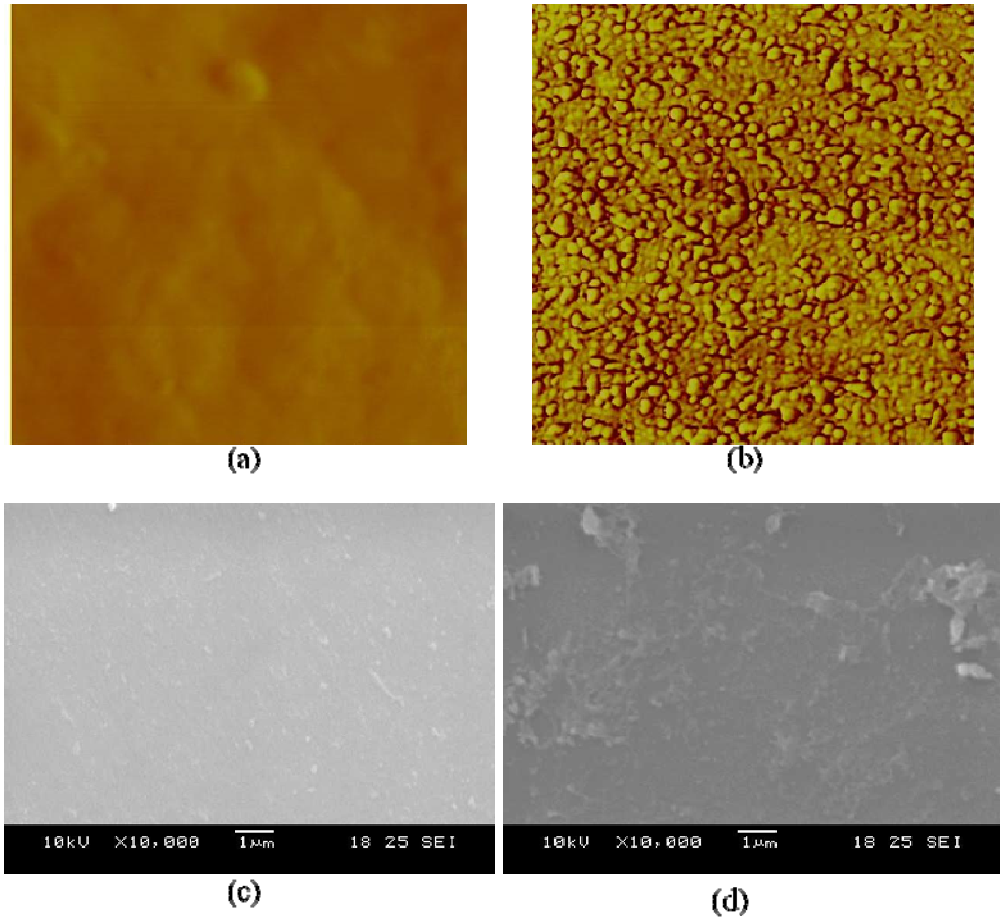

Figure 6.3. The membrane surface morphology analysis by AFM (a) and (b) cellulose acetate membrane before and after chitosan functionalization, respectively; (c) and (d) SEM picture of membranes before and after chitosan functionalization, respectively

6.3.2. The comparison of different driving forces in enantiomeric separation

The representative results by the separation processes employing various driving forces are depicted in Figure 6.4. Significant differences in L-trp and D-trp concentrations in the permeate solution are observed in both the pressure and concentration gradient driven processes. The most interesting phenomenon observed is the reversed selectivity: the permeate solutions are D-trp rich for the pressure driven and concentration gradient driven processes, but L-trp rich in electric field driven process. It has been discussed in literature [40] that the chitosan selectively binds to L-trp, such that the concentration of

L-trp near the membrane surface is suppressed by binding with chitosan and results in an enantiomeric excess of D-trp diffusing through the cellulose acetate membrane. Thus the permeate solution should be rich in D-trp and a positive enantiomeric excess value should be obtained for all the three processes. However, the negative enantiomeric excess obtained in the electric field driven process suggests a more complicated situation in this process.

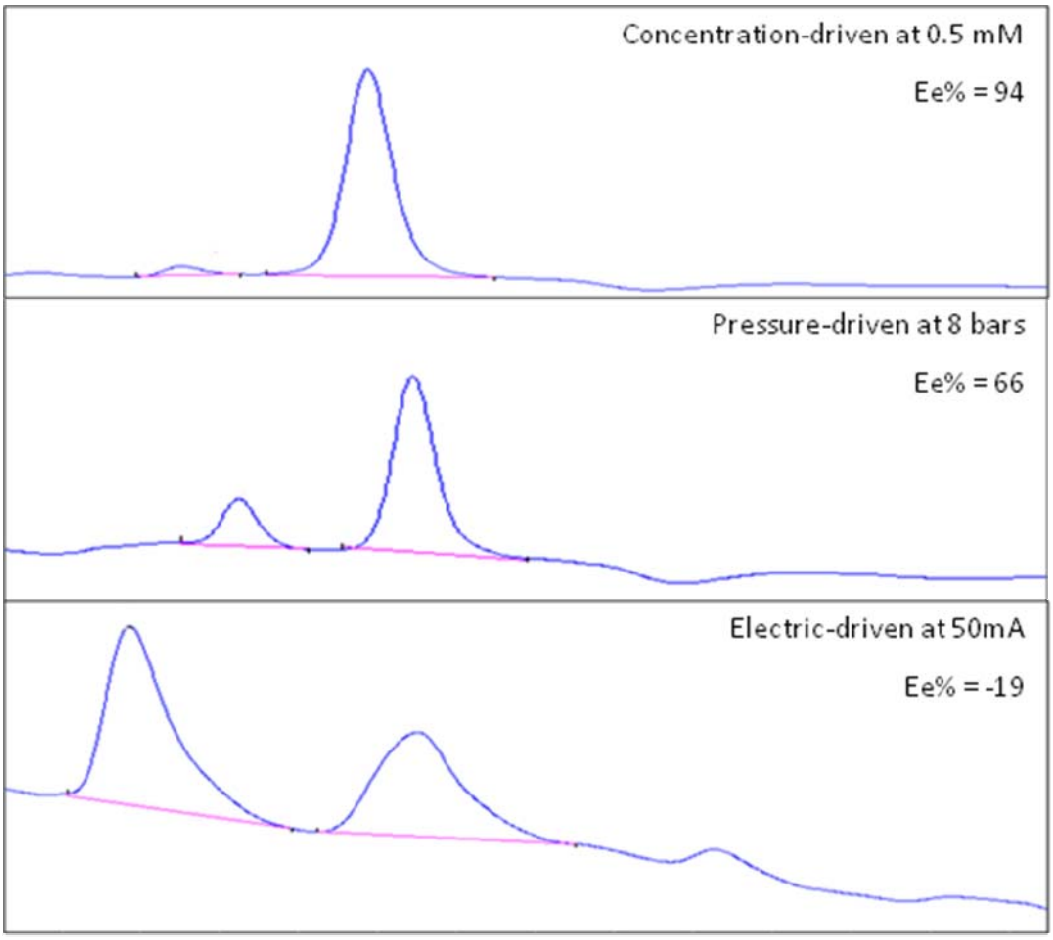

Figure 6.4. The chromatograms of the permeate solution collected in processes utilizing various driving forces. Membranes used are CA23-0.5 with feed concentrations of 0.5 mM racemic tryptophan.

Molecular simulations using material studio are employed to explain this phenomenon. First, two cells comprising of the chitosan polymer chain and the single L-trp and D-trp

and the tryptophan are generated using the inbuilt module 'amorphous cell', the equilibrium state are then calculated by simulating the minimized energy. The energies calculated correspond to the bonding between the chitosan and tryptophan: the lower the value, the stronger the interactions and the larger tendency to be retained by the membrane. As shown in Table 6.2, the minimized energy of L-trp with chitosan is lower, indicating the selective interaction between L-trp and chitosan, hence L-trp is more likely to be retained by the membrane, resulting in a D-trp rich (positive ee %) permeate in the pressure driven and concentration driven processes. However, in the electric field driven process, the tryptophan molecules also experience the electric field, other than the interaction with the chitosan polymer chains. As discussed by Bielski and Tencer [29], a force is thus exerted on and tends to align the tryptophan molecules in the direction of the electric field, with the amino end pointing towards the cathode. The interaction between the chitosan and the tryptophan is therefore disturbed by the electric field. Instead of directly simulate this effect (due to the limitation of our current software), we investigated the extreme case where the electric field is strong enough to align the tryptophan molecules completely by setting the amino end of the tryptophan in the amorphous cells in one direction and calculate the minimized energies. Comparable minimized energies for L-trp and D-trp are obtained, suggesting the electric field can decrease the L-trp binding selectivity of the chitosan polymer, since the enantiomers are no longer in their most appropriate positions for interaction with chitosan. Fig. 6.5 shows the simulated amorphous cells of D-trp with chitosan without external disturbance (left) and with the D-trp oriented in the extreme case (right).

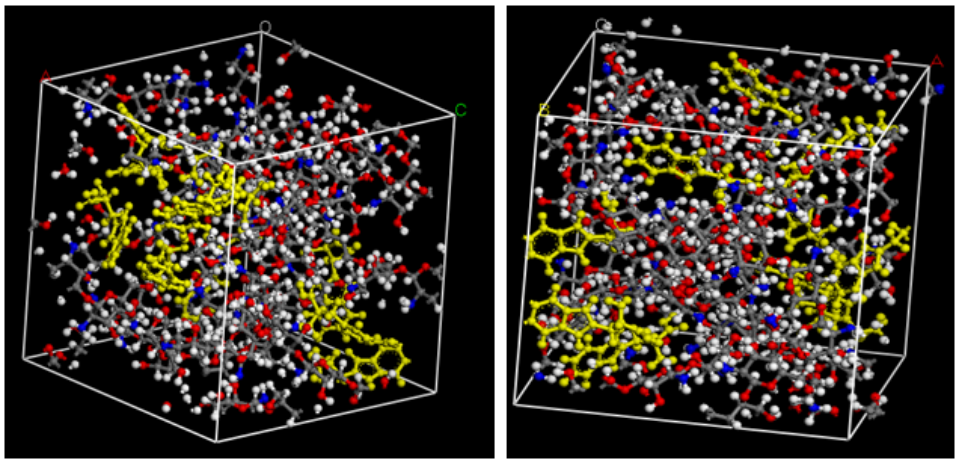

Figure 6.5. The amorphous cell structures of chitosan polymer chains with randomly oriented D-trp (left) and oriented D-trp (right) in Material Studio.

Complex	Total energy (kcal/mol)	Complex	Total energy (kcal/mol)
CS-D-trp (random)	2879	CS-D-trp (oriented)	1267
CS-L-trp (random)	2226	CS-L-trp (oriented)	1278

Table 6.2. The simulated total energy of chitosan-tryptophan amorphous cells and copper complexes.

Another factor that can possibly affect the selectivity is the trace amount of copper ions present in the buffer chambers that originated from the electrolysis of the copper at the electrode connections. Wang et al [39] investigated the stability of the complexes formed by the copper ions and tryptophan and found the stability is in the order of Cu-D-trp < Cu-L-trp < Cu-DL-trp. It is argued in [39] that at high copper ion concentrations, the most stable complex Cu-DL-trp is formed and the enantioselectivity is not affected; however, at low copper ion concentrations, the Cu-L-trp is more preferentially formed. The initial copper ion concentration is zero and slowly builds up with time, and thus the majority of the complexes present in the feed chamber is Cu-L-trp in the first few hours

of the experiment. As this complex carries higher positive charge and is subjected to a larger electric driving force, higher diffusion rate of L-trp is resulted so that the permeate solution becomes L-trp rich. Hence, a negative ee% is obtained in the electric field driving process, different from the other two processes.

We also calculated the minimized energies of the copper complexes and the chitosan polymer, using the similar simulation method described above, where the tryptophan molecules are changed to their complexes respectively. The minimized energy of CS-Cu-L-trp is found to be 6163 kcal/mol, lower than that of CS-Cu-D-trp which is 6845 kcal/mol, this founding further substantiate [39] that Cu-L-trp complexes is preferentially formed inside the polymeric membranes.

One point to note in the electric field driven process is that the separation factor slowly decreases with experimental time as shown in Figure 6.6. This is mainly due to two reasons. The first is migration of the racemic tryptophan, though the rate is slower than the complexes, from the feed chamber across the membrane. With longer experimental time, an increasing amount of free racemic tryptophan is present in the permeation chamber such that the ee% of product is reduced with time. Second, the buildup of copper ions in the feed chamber due to electrolysis favors the Cu-DL-trp complex formation at higher copper concentrations. The critical copper sulfate concentration for the selectivity reverse is discovered by Wang et al to be 0.16g/L when the initial tryptophan concentration is 5mM. In this particular experiment, the copper ion concentration build up rate in the feed is estimated, with the aid of capillary electrophoresis, to be 0.014g/ (L·h) and the initial tryptophan concentration is 0.5mM. So

the racemic complex formation starts after approximately one hour and decreases the separation factor, which approaches unity after about 5 hours.

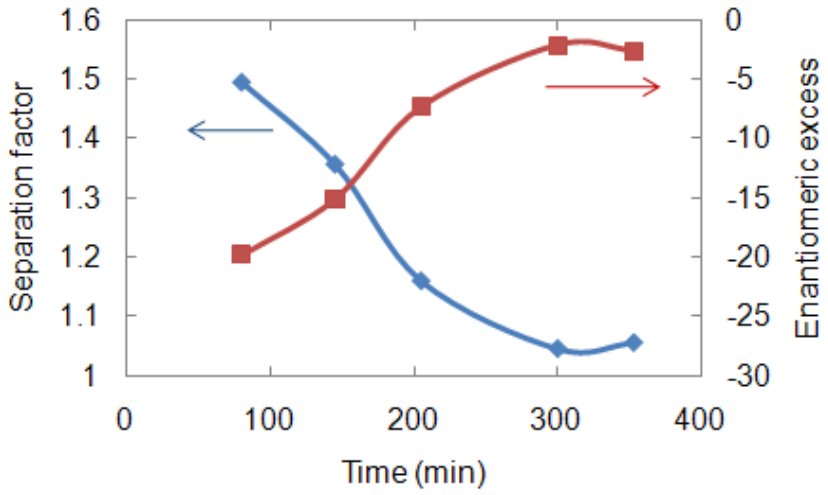

Figure 6.6. The changes in separation factor and enantiomeric excess with time in the electric driven process. The functionalized membrane is CA23-3 and operating current is 50mA.

It is also noteworthy that the enantiomeric separation performance of the concentration gradient driven processes is higher than that of the pressure driven process. This is expected since a large driving force usually results in poorer selectivity [83]. More efficient interaction between the chitosan and the tryptophan molecules is possible when the process is only driven by the concentration gradient and no extra forces are involved. For the tryptophan solution driven through the membrane under a hydraulic pressure, there may not be enough time for an efficient bonding to be established for all the tryptophan molecules. Hence a better selectivity is achieved by the concentration gradient driven process.

6.3.3. The effect of experimental conditions on separation performance

A control membrane without any chemical modification is tested in the electric driven process and insignificant selectivity was observed, in comparison with that obtained by the functionalized membrane (Table 6.3). It shows that the pristine cellulose acetate has poor enantioselectivity towards tryptophan which, is in accordance with the literature [83] that only functionalized cellulose membranes exhibit enantioselectivity to amino acids despite the chiral centers in its polymer chains. Similar result has also been generated in the pressure driven process where an enantiomeric excess of 5% is obtained with the unmodified membrane.

Membrane	Modified	I (mA)	Feed Conc (mM)	Flux (10^{-7} mmolcm^{-2}s^{-1})		ee%
				L-try	D-try	
CA23-0.5	no	50	0.5	8.4 ± 0.8	8.5 ± 0.9	0 ± 1
CA23-0.5	yes	50	0.5	6.2 ± 1.5	5.2 ± 1.9	-12 ± 6
CA23-0.5	yes	80	0.5	8.2 ± 1.8	6.5 ± 1.8	-12 ± 1
CA23-0.5	yes	50	0.1	0.64 ± 0.07	0.45 ± 0.05	-17 ± 2

Table 6.3. The separation performance of electric field driven process under various conditions. *CA23-0.5 means the dope concentration is 23% and evaporation time is 0.5minute.

The enantioselectivity is not significantly affected by increasing the operating current but the permeation fluxes are enhanced as shown in Table 6.3. The molecules in the buffer chambers experience a higher electric driving force when the operating current is increased; the transport rate and hence the permeation fluxes are therefore enhanced. Also, similar to the argument for the difference between concentration driven and pressure driven process in the previous section, the binding of the tryptophan molecules

to the chitosan is compromised; however, this only renders the L-trp sorption selectivity of the membrane that decreases the preferential absorption of L-trp which, is actually a positive contribution to the overall separation in the electric driven process, where the transport of L-trp through the membrane is favorable. Furthermore, the formation of copper complexes in the buffer chamber is less affected, so that the enantioselectivity is comparable to the process operating with a lower current.

The effect of the racemic feed concentration is also investigated (Table 6.3). Lower permeation fluxes are observed as expected, moreover, a slightly higher enantiomeric excess is also obtained with a diluted feed. At a lower feed concentration, the amount of uncomplexed tryptophan is also less such that the migration of the free tryptophan across the membrane, which compromises the enantiomeric purity in the permeation chamber as discussed in the precious section, is at a much slower rate. Thus a larger enantiomeric excess is maintained by a decreased feed concentration.

Similar trends in the effect of the feed concentration are observed in the pressure driven and concentration driven processes as well, as shown in Figure 6.7, but with different reasons. The enantiomeric excesses of both processes show decreasing trends with increasing feed concentrations. For both process, the selectivity is closely related to the ratio of free D-trp to L-trp concentrations in the feed chamber, i.e.

$$SP \rightarrow \frac{C_{DF}}{C_{LF}} = \frac{0.5C_F - C_{CS-L}}{0.5C_F - C_{CS-D}} \tag{4}$$

$$CS + L\text{-}trp \Leftrightarrow CS\text{-}L\text{-}trp \tag{5}$$

$$CS + D\text{-}trp \Leftrightarrow CS\text{-}D\text{-}trp \tag{6}$$

where the substrate $_{F}$, $_{CS\text{-}L}$ and $_{CS\text{-}D}$ represent the feed, L-tryp and D-tryp complexes with chitosan, respectively. For the same concentration of chitosan, a more concentrated feed

results in higher concentrations of both free enantiomers in the solution where the increment of L-trp concentration is to a greater extent since there is insufficient mount of chitosan for preferentially binding. Mathematical modeling for similar concentration gradient driven separation processes has also been carried out in our earlier studies [48], and the enantioselectivity is found to decrease with increasing feed concentrations for all concentrations of grafted chiral selector. Moreover, as discussed in the above section, Figure 6.7 also shows that the separation performance of the concentration driven process is generally higher than the pressure driven process which reinforces our previous argument.

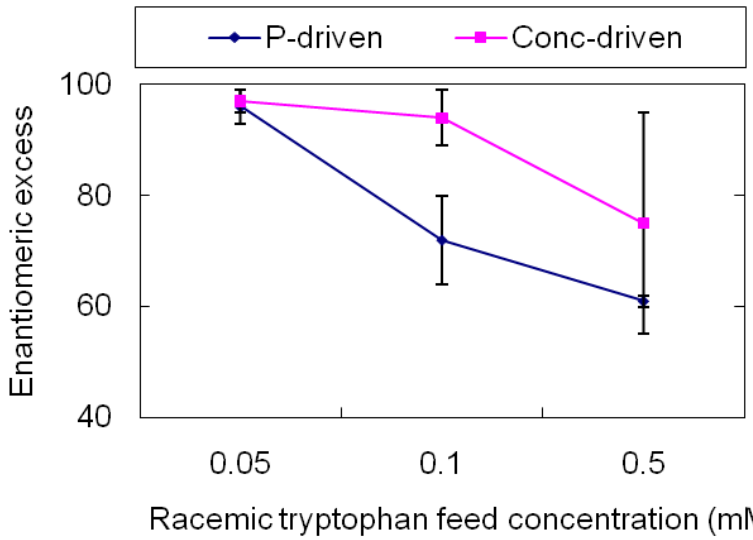

Figure 6.7. The enantiomeric resolution performance changes with concentration of feed in both pressure and concentration driven processes. Membrane used is CA23-0.5.

Another crucial factor for better selectivity is the solvent evaporation time during the membrane fabrication process. It is clear from Figure 6.8 that the separation factor of a membrane without evaporation is close to unity, much poorer than that obtained with membranes undergone solvent evaporation. As the solvent in the dope is acetone, which is very volatile and evaporates fast in ambient conditions, the cellulose acetate

concentration at the membrane surface after evaporation increases, resulting in the formation of a denser surface with smaller pores, evidenced by the approximately 40 times lower solution permeation flux associated with a membrane undergone 3 minutes evaporation (0.016 L $m^{-2}h^{-1}bar^{-1}$ compared with 0.64 L $m^{-2}h^{-1}bar^{-1}$). The low selectivity is mainly due to the insufficient binding between the tryptophan and the chitosan which is accounted from two angles. First, the bonding cannot be fully established as the time of interaction is insufficient given the much higher permeation flux. Second, due to the larger pore sizes, the tryptophan molecules can pass through the membrane without any interaction with the chitosan, and no bonds are established; this is also supported by our previous studies [48, 69]. A shorter evaporation time of 0.5 minutes during the membrane fabrication process has also been tried and the separation performance is similar as shown in Figure 6.8 while the permeation fluxes are slightly increased, suggesting that an evaporation time of 0.5 minute is sufficient for a good selectivity. Similar results are also obtained in the pressure driven process. The membrane prepared without evaporation shows a separation factor of 1.1 and ee% of 6.5, however, the separation factor and ee% increases to 5.5 ± 0.9 and 68 ± 5, respectively, if the membrane undergoes 0.5 minute of evaporation.

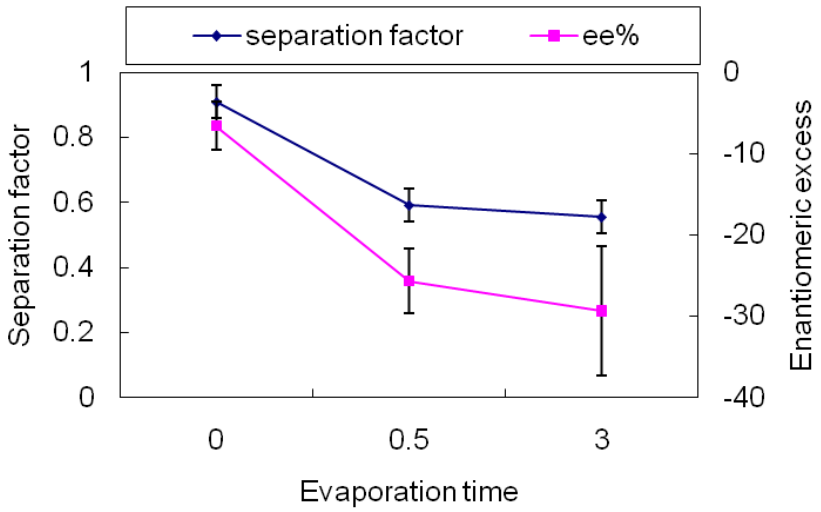

Figure 6.8. Enantiomeric resolution performance with respect to evaporation time in electric field driven separation. membrane used is CA23-0.5.

6.3.4. Enantiomeric separation performance of phenylalanine

Chiral separation tests have also been performed using phenylalanine and the characteristics of the separation performance shown in Table 6.4 is similar to that of tryptophan. While the enantiomeric excess of pressure and concentration driven processes is positive, negative enantiomeric excess is observed for electric driven separation process, suggesting more L-phe passing through the membrane under the electric field. Also, the highest ee% is obtained in the concentration driven process, similar to the results obtained using tryptophan. This suggests that the phenomenon observed is not limited to tryptophan, and possibly has broader applications.

Processes	Driving force	Flux (10^{-7} mmol $cm^{-2}s^{-1}$)		ee%
		L-Phe	D-Phe	
electric field	50 mA	2.42	0.42	-70
concentration gradient	0.5 mM	1.15	2.55	38
pressure	8 bars	0.9	1.6	28

Table 6.4. Separation of phenylalanine with the membrane CA23-0.5 in various processes.

6.4. Conclusion

The current study demonstrates the enantioseparation performance of the chitosan functionalized cellulose acetate membrane in processes utilizing various driving forces, including concentration gradient, hydraulic pressure and electric field. Due to the preferential absorption of L-trp to the chitosan, high enantiomeric excess of D-trp over L-trp above 90% are obtained in the concentration driven process and that achieved by the pressure driven process is 60-70%; interestingly, a negative ee%, indicating preferential permeation of L-trp, is resulted in the electric driven process, mainly due to the preferential permeation of the charged L-trp complexes formed with copper ions under the electric field and the orienting force generated by the electric field that disturbs the selective absorption of the chitosan. Moreover, similar behavior is also observed in the resolution of racemic phenylalanine, suggesting a wider impact of this phenomenon. Hence, the further works will be focused on the more accurate control of the copper ion concentrations by modifying the electrical parts and inject known amount of copper sulfate in the anode and feed chambers. Also, the integration of the pressure and electric driven processes may yield better separation results.

Besides, both the solvent evaporation before coagulation and chitosan functionalization are proven essential for good selectivity by comparing performance against the control membranes without the respective preparation procedures. The separation factors of all the three processes decrease with increasing racemic feed concentrations due to different mechanisms. It is also discovered that in the electric driven process, the operating current has less effect on the separation factor but the permeation fluxes, while the accumulation of copper ion with experimental time can decrease the separation factor.

6.5. Acknowledgement

We thank the Singapore-MIT Alliance and the National University of Singapore (Grant No.R-279-000-249-646) for funding this project.

Chapter 7. Conclusion & recommendation

Through the intensive studies on chiral separations by preparing and functionalizing various chiral selective membranes and designing innovative membrane systems, a more in-depth understanding of the chiral separation understanding is obtained, such as the effects of the position, location and concentrations of chiral selector on the separation efficiency, the change in selectivity with various driving force, the integrations of different systems, etc. Overall, we can draw a few conclusions from this study:

1. Membranes with superior selectivity are fabricated by functionalization with chiral selector and its derivatives (chapter 3), or chiral selective polymer materials (chapter 6); also, innovative membrane systems such as SPE (chapter 4) & FFIEF (chapter 5) are designed and proved to perform better than the existing processes such as AD and AUF. Hence, we have successfully met the objectives of this project.
2. The membrane functionalized with a chiral selector can exhibit chiral selectivity as shown in chapter 3 and 6.
3. Chapter 3: the position of the chiral selector at the membrane surface, which is controlled by the spacer arm length, affects the chiral separation efficiency. The longer the spacer, the further the chiral selector from the membrane surface, the more difficult to form a defect free chiral selector layer and hence the lower the separation factor.
4. Chapter 3: the selectivity of a chiral selector can be increased by strengthening the one or more of its interaction with the chiral molecules, e.g. by deirivatization that enhances the steric hindrance effect.

5. Chapter 4: the location of the chiral selector in a membrane system also plays an important role. By injecting the chiral selector in the permeate chamber instead of mixing with the racemic feed, chiral selectivity is still realized with enhanced permeation.
6. Chapter 4: the integration of two membrane systems may yield better results just as the case in the SPE-AD setup. (chapter 4)
7. Chapter 5: the utilization of a FFIEF system opens new windows in chiral separation and shows better separation performance than other systems such as AD and AUF under similar conditions.
8. Chapter 6: the type of driving forces not only affects the permeation flux, but also the selectivity in some of the processes. The example in chapter 6, that shows a reverse in selectivity by switching the driving force from pressure to electric field, suggests that a thorough understanding and control of all the process parameters is essential for a good separation performance.

However, despite the achievement above, we have also realized a few difficulties of chiral separation with membrane processes and thus present a few suggestions and recommendations for future endeavours.

1. The membrane processes are still low in selectivity in general and not suitable for commercial application in the near future. This difficulty is partially embedded in the nature of the membrane process, in comparison to HPLC process for example, the theoretical number of separation stages of a membrane process is much

smaller as it may only contain a very thin layer of chiral selective material whereas the HPLC columns are a few orders longer.

2. Because of the above, the selectivity of the chiral selector is very important in membrane processes. One of the research directions in membrane separation will be to search, synthesize and modify chiral selectors with superior selectivity.
3. It has also been observed that the membrane structure does play an important role in chiral separations. Only membranes with a suitable pore size can demonstrate the optimum separation. Thus techniques that can better control the membrane pore sizes shall also be investigated.
4. It has also been noticed in this study that the separation factor may deteriorate with time due to factors such as the saturation of binding with chiral selectors in the membranes. Two suggestions are hence proposed: a membrane system with chiral selectors that rejects one of the enantiomers rather than binding the other may be favourable as it circumvents the saturation problem; membrane systems that facilitate the transport of one enantiomer such as the supported liquid membrane should receive more attention for long term performance.
5. The FFIEF system that makes use of the difference in pI values of the enantiomer-chiral selector complexes can be one of the promising preparative technique in chiral separation, provided if we can have more accurate and precise engineering tools such as the auto-titrating system, better ion exchange membrane design and chiral selectors that can result in larger difference in pIs.

References

[1] http://web99.arc.nasa.gov/~astrochm/chirality.jpg

[2] N. M. Maier, P. Franco, W. Linder, Separation of enantiomers: needs, challenges, perspectives, *J. Chromatogr. A*. 906 (2001) 3

[3] RI technologies, Chiral Chemicals, March 2008.

[4] W. D. Lubell, M. Kitamura and R. Noyori, Enantioselective Synthesis of p-Amino Acids Based on BINAP-Ruthenium(II) Catalyzed Hydrogenation. *Tetrahedron: Asymmetry,* 1991, 2, 543.

[5] H. Pellissier, Dynamic kinetic resolution, Tetrahedron 59 (2003) 8291-8327.

[6] A. Ghanem, H. Y. Aboul-Enein, Lipase-mediated chiral resolution of racemates in organic solvents, Tetrahedron: Asymmetry 15 (2004) 3331-3351.

[7] K. Koch, R. J. F. van den Berg, P. J. Nieuwland, R. Wijtmans, M. G. Wubbolts, H. E. Schoemaker, F. P. J. T. Rutjes, J. C. M. van Hest, Enzymatic synthesis of optically pure cyanohydrins in microchannels using a crude cell lysate, Chem. Eng. J. 135S (2008) S89-S92.

[8] T. Akiyama, J. Itho, K. Yokota and K. Fuchibe, Enantioselective Mannich-Type Reaction Catalyzed by a Chiral Bronsted Acid. Angew. Chem, Int. Ed., 2004, 43, 1566.

[9] B. Weiner, W. Szymanski, D. B. Janssen, A. J. Minnaarda B. L. Feringa. Recent advances in the catalytic asymmetric synthesis of b-amino acids. Chem. Soc. Rev., 2010, 39, 1656–1691

[10] G. Subramanian, Chiral separation techniques: a practical approach

[11] J.Z. Li, D.J.W. Grant, Relationship between physical properties and crystal structures of chiral drugs, J. Pharm. Sci. 86 (1997) 1073.

[12] A. Ghanem, H. Y. Aboul-Enein. Lipase-mediated chiral resolution of racemates in organic solvents. Tetrahedron: Asymmetry 15 (2004) 3331 – 3351.

[13] C. Ravelet, E. Peyrin, Recent developments in the HPLC enantiomeric separation using chiral selectors identified by a combinatorial strategy, J. Sep. Sci. 29 (2006) 1322.

[14] E. R. Francotte, P. Richert, Applications of simulated moving-bed chromatography to the separation of the enantiomers of chiral drugs, J. Chromatogr. A 769 (1997) 101-107

[15] Y. Xie, Y-M. Koo, N-H. L. Wang, Preparative chromatographic separation: simulated moving bed and modified chromatography methods, Biotechnol. Bioprocess Eng. 6 (2001) 363-375

[16] D. Wistuba, V. Schurig, Enantiomer separation of chiral pharmaceuticals by capillary electrochromatography, J. Chromatogr. A 875 (2000) 255

[17] B. Tao, S. K. Wiedmer, M. Riekkola, Phospholipid-lysozyme coating for chiral separation in capillary electrophoresis, Electrophoresis 25 (2004) 1784

[18] A. Yudiato, E. Dewi, T. Kokugan, Separation of isomers by ultrafiltration using modified cyclodextrins, Sep. Purif. Tech. 19 (2000) 103.

[19] T. Kakuchi, T. Takaoka, K. Yokota, Polymeric chiral crown ether 6 optical resolution of alpha-amino-acid by polymers incorporating 1,3-4,6-di-O-benzylidene-D-mannitol residues, Polym. J. 22 (1990) 199

[20] B.B. Lakshmi, C. R. Martin, Enantioseparation using apoenzymes immobilized in a porous polymeric membrane, Nature 388 (1997) 758

[21] Z. Jiang, Y. Yu, H, Wu, Preparation of CS/GPTMS hybrid molecularly imprinted membrane for efficient chiral resolution of phenylalanine isomers, J. Membr. Sci 280 (2006) 876

[22] J. Romero, A.L. Zydney, Chiral separation using ultrafiltration with a stereoselective binding agent, Sep. Sci. Tech. 36 (2001) 1575.

[23] A. Higuchi, M. Hara, T. Horiuchi, T. Nakagawa, Optical resolution of amino acids by ultrafiltration membranes containing serum albumin, J. Membr. Sci 93 (1994) 157

[24] J. Romero, A. L. Zydney, Staging of affinity ultrafiltration processes for chiral separation, J. Membr. Sci. 209 (2002) 107-119.

[25] G. Zenoni, F. Quattrini, M. Mazzotti, C. Fuganti, M. Morbidelli. Scale-up of analytical chromatography to the simulated moving bed separation of the enantiomers of the flavour norterpenoids α-ionone and α-damascone. Flavour Fragr J. 17 (2002) 195-202.

[26] M. Mulder, Basic principles of membrane technology, Dordrecht, Kluwer Academic Publishers (1996)

[27] R. E. Kesting, Synthetic Polymer Membranes, New York, McGraw Hill (1985)

[28] M. A. Frommer, D. Lancet, H. K. Lonsdale, H.E. Podall, Reverse osmosis membrane research, New York, Pelnum Press. (1972)

[29] R. Bielski, M. Tencer, Concept of absolute enantioselective separation, J. Fluorine Chem. 131 (2010) 487-49.

[30] Y. Xiao, H. M. Lim, T. S. Chung, R. Raj, Acetylation of β-cyclodextrin surface-functionalized cellulose dialysis membranes with enhanced chiral separation, Langmuir 23 (2007) 12990

[31] A. Higuchi, Y. Higuchi, K. Furuta, B. O. Yoon, M. Hara, S. Maniwa, M. Saitoh, K. Sanui, Chiral separation of phenylalanine by ultrafiltration through immobilized DNA membranes, J. Membr Sci 221 (2003) 207-218

[32] E. Schneiderman, A. M. Stalcup, Cyclodextrins: a versatile tool in separation science, J. Chromatogr. B 745 (2000) 83

[33] J. W. Hawkins, A.Dugaiczyk, The human serum albumin gene: structure of a unique locus". Gene 19 (1982) 55–8.

[34] R. H. Mcmenamy, J. L. Oncley, The specific binding of L-tryptophan to serum albumin, J. Biol. Chem. 233 (1958) 1436-1447

[35] J. Yang, D. S. Hage, Role of binding capacity versus binding strength in the separation of chiral compounds on protein-based high-performance liquid chromatography columns interaction of D- and L-tryptophan with human serum albumin, J. Chromatogr. A. 725 (1996) 273-285.

[36] D. C. Carter, J. X. Ho, Structure of Serum Albumin. Adv. Protein Chem. 45 (1994) 153-203

[37] U. Bohme, U. Scheler. Effective charge of bovine serum albumin determined by electrophoresis NMR. Chem Phys Lett. 435 (2007) 342 – 345.

[38] A. I. Luik, Y. N. Naboka, S. E. Mogilevich, T. O. Hushcha, N. I. Mischenko. Study of human serum albumin structure by dynamic light scattering: two types of reaction under different pH and interaction with physiologically active compounds. Spectrochim Acta A. 54 (1998) 1503 – 1507.

[39] H. D. Wang. R. Xie, C. H. Niu, H. Song, M. Yang, S. Liu, L.Y. Chu, Chitosan chiral ligand exchange membranes for sorption resolution of amino acids, Chem. Eng. Sci. 64 (2009) 1462-1473.

[40] H. D. Wang, L. Y. Chu, H. Song, J. P. Yang, R. Xie, M. Yang, Preparation and enantiomer separation characteristics of chirosan/β-cyclodextrin composite membranes, J. Membr. Sci. 297 (2007) 262-270.

[41] S-M. Xie, W-F. Wang, P. Ai, M. Yang, L-M. Yuan, chiral separation of (R.S)-2-phenyl-1-propanol through cellulose acetate butyrate membranes, J. Membr,.Sci 321 (2008) 293-298

[42] N. H. Lee, C. W. Frank, Separation of chiral molecules using polypeptide-modified poly(vinylidene fluoride) membranes, Polymer 43 (2002) 6255-6262

[43] E. Yashima, K. Maeda, Chirality-responsive helical polymers, Macromelecules 41 (2008) 3-12

[44] P. Wenger, P. Javet, Isoelectric focusing using non-amphoteric buffers in free solution: I. Determination of stable concentration profiles. J. Biochem. Bioph. Meth. 13 (1986) 259-273.

[45] P. Wenger, P. Javet, Isoelectric focusing using non-amphoteric buffers in free solution: II. Apparatus and measure of pH stability. J. Biochem. Bioph. Meth. 13 (1986) 275-287.

[46] J. H. Cheng, Y. Li, T. S. Chung, S. B. Chen, W. B. Krantz, High performance protein separation by ion exchange membrane partitioned free-flow isoelectric focusing system. Chem. Eng. Sci. 63 (2008) 2241-2251.

[47] P. G. Righetti, C. Ettori, P. Chafey, J. P. Wahrmann, Enantiomer resolution in immobilized pH gradient gel via inclusion of a chiral discriminator. Electrophoresis 11 (1990) 1-4.

[48] Y. Xiao, T. S. Chung, Functionalization of cellulose dialysis membranes for chiral separation using beta-cyclodextrin immobilization, J. Membr. Sci 290 (2007) 78-85.

[49] A. D. McNaught and A. Wilkinson. Compendium of Chemical Terminology, 2nd ed. Blackwell Scientific Publications, Oxford (1997)

[50] L. Zhang, Y. Wong, L. Chen, C. B. Ching, S. Ng, A Facile immobilization approach for perfunctionalized cyclodextrin onto silica via the Staudinger reaction, Tetrahedron Lett 40 (1999) 1815

[51] Y. Liu, X. Fan, Y. Zhao, Synthesis and characterization of a poly (N-isopropylacrylamide) with β-cyclodextrin as pendant groups, J. Polym. Sci 43 (2005) 3516

[52] A. Mehta, A. L. Zydney, Effect of spacer arm length on the performance of charge-modified ultrafiltration membrane, J. Membr. Sci 313 (2008) 304

[53] B. D. Freeman, Basis of permeability/selectivity tradeoff relations in polymeric gas separation membranes, Macromolecules 32 (1999) 375

[54] F. Garnier, J. Randon, J. L. Rocca, Enantiomeric separation by ultrafiltration: complexation mechanism of tryptophan analogs to bovine serum albumin, Sep. Purif. Tech. 16 (1999) 243-250

[55] H. Wang, Y. Li, T. S. Chung, A fine match between the stereoselective ligands and membrane pore size for enhanced chiral separation, AICHE J. 55 (2009) 2284-2291

[56] K. Tang, Y. Chen, K. Huang, J. Liu, Enantioselective resolution of chiral aromatic acids by biphasic recognition chiral extraction, Tetraheron Asymm. 18 (2007) 2399-2408

[57] D. Li, R. Wang, T. S. Chung, Fabrication of lab-scale hollow fiber membrane modules with high packing density, Sep. Purif. Tech. 40 (2004) 15-30

[58] B. Liu, G. G. Lipscomb, J. Jensvold, A comparison of optimal internally staged permeator and external two-staged module designs for O2 enrichment from air, Sep. Sci. Technol. 36 (2001) 2385-2409

[59] M. Sidhoum, A. Sengupta, K. K. Sirkar, Asymmetric cellulose acetate hollow fibers: studies in gas permeation, AIChE J. 34 (1988) 417-425

[60] K. Li, D. R. Acharya, R. Hughes, Simulation of gas separation in an internally staged permeator, Chem. Eng. Res. Design. 69 (1991) 35-42

[61] P. C. Wang, J. Gao, C. S. Lee, High-resolution chiral separation using microfluidics-based membrane chromatography. J. Chromatogr. A 942 (2002) 115-122.

[62] J. H. Cheng, T. S. Chung, S. H. Neo, Investigation of mass transfer in the ion-exchange membrane partitioned free-flow isoelectric focusing system (IEM-FFIEF) for protein separation. Electrophoresis 30 (2009) 2600-2612.

[63] P. Glukhovskiy, T. A. Landers, G. Vigh, Preparative-scale isoelectric focusing separation of enantiomers using a multicompartment electrolyzer with isoelectric membranes. Electrophoresis 21 (2000) 762-766.

[64] M. Creitich, G. Pirri, G. Carrea, M. Chiari. Separation of proteins in a multicompartment electrolyzer with chambers defined by a bed of gel beads. Electrophoresis. 24 (2003) 577-581.

[65] Z. Zhou, Y. Xiao, T. S. Chung, T. A. Hatton, Enantiomeric resolution of tryptophan via selective permeation enhancement with the aid of human serum albumin. AIChE Journal 57 (2011) 1154-1162.

[66] Y. Xiao, M. L. Chng, T. S. Chung, M. Toriida, S. Tamai, H. Chen, Y. C. J. Jean, Asymmetric structure and enhanced gas separation performance induced by in situ growth of silver nanoparticles in carbon membranes, Carbon 48 (2010) 409-416.

[67] Q. Yang, T. S. Chung, M. Weber, Microscopic behavior of polyvinylpyrrolidone hydrophilizing agents on phase inversion polyethersulfone hollow fiber membranes for hemofiltration. J. Membr. Sci. 326 (2009) 322-331.

[68] R. Guan, H. Zou, D. Lu, C. Gong, Y. Liu, Polyethersulfone sulfonated by chlorosulfonic acid and its membrane characteristics, Eur. Polym. J. 41 (2005) 1554-1560

[69] Z. Zhou, Y. Xiao, T. S. Chung, T. A. Hatton, Effects of spacer arm length and benzoation on enantioseparation performance of β-cyclodextrin functionalized cellulose membranes, J. Membr. Sci 339 (2009) 21-27.

[70] S. S. Bahga, M. Bercovici, J. G. Santiago, Ionic strength effects on electrophoretic focusing and separations. Electrophoresis 31 (2010) 901-919.

[71] W. Thormann, C. X. Zhang, J. Caslavska, P. Gebauer, R. A. Mosher, Modeling of the impact of ionic strength on the electroosmotic flow in capillary electrophoresis with uniform and discontinuous buffer systems. Anal. Chem. 70 (1998) 549-562.

[72] J. Ennis, H. Zhang, G. Stevens, J. Perera, P. Scales, S. Carnie, Mobility of protein through a porous membrane. J. Membr. Sci. 119 (1996) 47-58.

[73] P.I. Kulintsov, O. V. Bobreshova, I. V. Aristov, I. V. Novikova, L. A. Khrykina, Electrotransport mechanisms in the ion-exchange membrean-amino acid solution systems. Russian Journal of Electrochemistry 36 (2000) 365-368.

[74] J. Romero, A. L. Zydney. pH and salt effects on chiral separations using affinity ultrafiltration. Desalination 148 (2002) 159-164.

[75] A. I. Luik, Y. N. Naboka, S. E. Mogilevich, T. O. Hushcha, N. I. Mischenko. Study of human serum albumin structure by dynamic light scattering: two types of reaction under different pH and interaction with physiologically active compounds. Spectrochim Acta A. 54 (1998) 1503 – 1507.

[76] C. Lagercrantz, T. Larsson, I. Denfors. Stereoselective binding of the enantiomers of warfarin and tryptophan to serum-albumin for some different species studied by affinity-chromatography on columns of immobilized serum-albumin. Comp. Biochem. Physio. C.69 (1981) 375-378.

[77] U. Bohme, U. Scheler. Effective charge of bovine serum albumin determined by electrophoresis NMR. Chem Phys Lett. 435 (2007) 342 – 345.

[78] S. Loeb, S. Sourirajan, Advances in Chemistry, Series No. 38, 1963.

[79] S. Zhang, K. Y. Wang, T. S. Chung, H. Chen, Y. C. Jean, G. Amy, Well-constructed cellulose acetate membranes for forwards osmosis: minimized internal concentration polarization with an ultra-thin selective layer, J. Membr. Sci 360 (2010) 522-535.

[80] J. Su, Q. Yang, J. F. Teo, T. S. Chung, Cellulose acetate nanofiltration hollow fiber membranes for forward osmosis processes, J. Membr. Sci 355(2010) 36-44.

[81] S. P. Sun, K. Y. Wang, N. Peng, T. A. Hatton, T. S. Chung, Novel polyamide-imide/cellulose acetate dual layer hollow fiber membranes for nanofiltration, J. Membr. Sci. 363 (2010) 232-242.

[82] A. G. Boricha, Z. V. P. Murthy, Preparation of N,O-carboxymethyl chitosan/cellulose acetate blend nanofiltration membrane and testing its performance in treating industrial wastewater, Chem. Eng. J. 157 (2010) 393-400

[83] S. Tone, T. Masawaki, T. Hamada, The optical resolution of amino acids by ultrafiltration membranes fixed with plasma polymerized l-menthol, J. Membr. Sci 103 (1995) 57-63.

[84] Y. Sueyoshi, C. Fukushima, M. Yoshikawa, Molecularly imprinted nanofiber membranes from cellulose acetate aimed for chiral separation, J. Membr. Sci. 357 (2010) 90-97.

Appendix

List of publications

1. Z. Zhou, Y. Xiao, T. S. Chung, T. A. Hatton, Effects of spacer arm length and benzoation on enantioseparation performance of β-cyclodextrin functionalized cellulose membranes*, J. Membr. Sci* 339 (2009) 21-27

2. Z. Zhou, Y. Xiao, T. S. Chung, T. A. Hatton, Enantiomeric resolution of tryptophan via selective permeation enhancement with the aid of human serum albumin. *AIChE Journal* 57 (2011) 1154- 1162

3. Z. Zhou, J. H. Cheng, T. S. Chung, T. A. Hatton, M. Toriida, K. Nishiura, S. Tamai, Enantiomeric resolution of Tryptophan via stereoselective binding in an ion-exchange membrane partitioned free flow isoelectric focusing system. *Chem. Eng. J. 174 (2011) 522-529*

4. Z. Zhou, J. H. Cheng, T. S. Chung, T. A. Hatton, The investigation of reversed enantioselectivity of a chitosan functionalized cellulose acetate membrane in processes with different driving forces. *J. Membr. Sci* 389 (2012) 372-379

Conferences and presentations

1. Membrane Science and Technology (MST) 2011, Singapore, Oral presentation, 24-25 Aug 2011

2. AIChE Annual Meeting 2009, Nashville, USA, Oral presentation, 8-13 Nov 2009

3. SMA Anniversary Symposium 2009, Singapore, Oral and Poster presentations, 21 Jan 2009

4. SMA Anniversary Symposium 2009, Singapore, Oral presentations, 19 Jan 2010

5. SMA Anniversary Symposium 2009, Singapore, Oral presentations, 12 Jan 2011